IDENTIFICATION OF PARAMETERS FOR PREDICTING LONG-RUNOUT LANDSLIDES IN THE WESTERN UNITED STATES

by

Russell A. Lockyear

A thesis submitted to the Faculty and the Board of Trustees of the Colorado School of Mines in partial fulfillment of the requirements for the degree of Masters of Science (Geological Engineering).

Golden, Colorado

Date _____

Signed: _____
Russell A. Lockyear

Signed: _____
Dr. Paul M. Santi
Thesis Advisor

Golden, Colorado

Date _____

Signed: _____
Dr. M. Stephen Enders
Professor and Department Head
Department of Geology and Geological Engineering

ABSTRACT

No existing research provides an integrated analysis of the key parameters that contribute to long-runout landslides in the Western United States. This study begins the task by assembling a dataset of geological, topographical, and hydrological parameters for landslides from eight study areas. Six measures of mobility were analyzed and two (landslide height drop to runout length ratio, H/L and landslide runout length, L) were selected for further use. Analysis of the correlations of the measured parameters with H/L and L was performed to quantify how well they predict these two mobility measures. The initial slope angle was found to match H/L for small landslides that did not experience a break in slope. Landslides in concave topography, landslides on previously moved material, and landslides in confined topography were found to possess lower H/L values, indicating higher mobility. Finally, landslides occurring on previously moved material and landslides in confined topography were found to possess larger values of L.

TABLE OF CONTENTS

LIST OF FIGURES

LIST OF TABLES

CHAPTER 1

INTRODUCTION

Landslides pose a serious threat to life and property both in the United States and around the world. The USGS estimates that property damage due to landslides in the United States alone exceeds a billion dollars per year (Landslides 101, 2018), a figure that does not include the cost of human life. In 1985, the National Research Council's Committee on Ground Failure Hazards estimated that there were between 25 and 50 fatalities due to landslides in the United States annually (Committee on Ground Failure Hazards, 1985), and the threat has only grown since then. Increased urbanization in landslide prone areas, continued deforestation, and the effects of global climate change are all factors that are contributing to the danger posed to human life and property by landslide activity (Schuster et al., 1996).

While most of these events are responsible for only a few fatalities, some events lead to a much larger loss of life. For example, the Oso landslide in Washington destroyed an entire neighborhood killing 43 people (Iverson, 2016). Other events outside the United States have caused hundreds or even thousands of fatalities (Schuster et al., 1996). Of these, the most deadly and destructive are frequently characterized by longer than expected runout. Such events affect disproportionately large areas during failure, and therefore have increased potential to encounter people and structures.

Because of the economic and human costs associated with long-runout landslides, it is critical to improve our ability to understand their processes, assess their degree of hazard, and predict their occurrence. As a result, a comprehensive account of the triggers, conditions, and mechanisms of these events is necessary. However, this challenge is not a simple one. The problem has typically been deconstructed into smaller and more manageable parts: papers are

frequently limited to addressing a specific contributing factor that has been correlated to mobility under equally specific conditions (a few examples include, Iverson et al. (2000), Wang and Sassa (2003), Jeong et al. (2017), and Montgomery et al. (2000)). No research provides an integrative view of the key parameters that predict these events, distinguishing which parameters hold more universal applicability and which are too tightly constrained by specific circumstances to be of general use. The goal of this research is to begin this process by identifying common characteristics of long-runout landslides in a number of separate locations across the Western United States.

CHAPTER 2

RESEARCH OBJECTIVES

The goal of the proposed research is to begin the process of identifying parameters that predict the mobility of translational and rotational landslides in soil materials in the Western United States. Completely characterizing prediction-related parameters is beyond the scope of this project. However, a complete characterization is needed, and the current research is the first step towards this need.

Parameters associated with an increase in landslide mobility have been collected such as parameters related to pore water pressure, topography, geology, vegetation, and the presence of previous movement. To relate these parameters to mobility, six mobility indexes for measuring the degree of mobility are evaluated to identify those that best describe translational and rotational landslides and can be used in a predictive capacity.

Finally, to consider the influence of specific parameters on mobility it is necessary to approach the investigation from two scales. First, investigations are conducted on local groups of landslides where many parameters are held constant. This allows for statistical problems associated with combining study areas to be minimized. It also provides a more geographically detailed picture of correlations between various parameters and mobility. Second, a cumulative dataset composed of all landslide data from the individual study areas is evaluated. This will give a more general picture of the key parameters that influence landslide mobility across the Western United States. This dataset will serve as a means of providing a tentative and quantitative assessment of the effects of various parameters on mobility, in the cases where it is found to reflect a general trend found in the individual study areas. In the case where the

conclusion of the cumulative dataset is not generally supported by the individual study areas, the cumulative dataset results will not be used.

The end result of this work is an understanding of the relationships between various parameters and landslide mobility, including both the conclusions of previous studies as well as new, statistical analysis of the available data. The research identifies the parameters that have the greatest contribution to landslide mobility and quantified their effects.

This project goal is broken down into five objectives.

- .. Selection of eight study areas containing groups of landslides where many parameters relevant to landslide mobility are the same within each group,
- .. Collection of additional data that is required and is not already provided in technical publications,
- .. Identification of the mobility measures to be used in the current research,
- .. Statistical analysis of data to quantify the local and regional influence of parameters on the selected mobility measures, and
- .. Synthesis of the results from previous studies with the results of the statistical analysis to identify the most significant parameters in contributing to landslide mobility

CHAPTER 3

TYPE OF LANDSLIDES TO BE STUDIED

The meaning of the term "landslide" varies considerably between studies. Some authors define a landslide as "the movement of a mass of rock, earth or debris down a slope" (Cruden, 1991). Others exclude all mass movements except those with a "shear failure at the base" (Chandler, 1972). To avoid confusion, the broader definition of Cruden (1991) is used. Additionally, the terms "mobile" and "long-runout" are used as synonyms for the purposes of this study. Having established the terminology, the type of landslides studied in this research needs to be specified.

Ideally, an account of landslide mobility in the Western United States will cover all types of movement. However, various types of landslides may attain high mobility under different initial conditions and by diverse processes and mechanisms. To simplify the problem of predicting landslide mobility, only translational, rotational, and complex failures involving a combination of both translation and rotation is the focus of this research. Landslides that move primarily by falling, toppling, spreading, or flowing have been excluded.

Additionally, preference is given to landslides involving soil. Landslides visibly occurring in locations where the surface material is rocky have been excluded. However, no further requirements related to material type are used for the landslide inventory. The main reason for this is that an accurate determination of material type is not feasible without a detailed subsurface investigation. Additionally, material type is frequently unknown prior to failure because of its dependence upon both the depth of the failure surface and the depth of bedrock. Therefore, making material type a condition for the application of a predictive model undermines the usability of that model.

There are other parameters that could be used to narrow down the subclass of landslides to be studied, including triggering mechanisms and climate. For this research, landslides triggered by water-related processes are the focus, however such a triggering mechanism is not required for inclusion in this study. This is for two reasons. First, when assembling an inventory of landslides the triggering mechanism will frequently be unknown for a given event. Second, landslide triggers are not very useful for prediction of landslide mobility. This is because, unlike current water conditions, the triggering mechanism cannot be guaranteed before an event occurs. Even if the triggering mechanism is known, the mobility of a landslide may be controlled by water conditions irrespective of the kind of trigger.

Climate could also be used in narrowing down the scope of landslides to be considered for this research. However, the narrower the climactic regime the smaller the area over which the results are applicable. To maximize applicability, while allowing for some limitation in climactic variability, study areas are restricted to the Western United States. An additional benefit of this broader scope is that climactic differences between study areas can be considered, leading to potentially useful insights regarding mobility prediction.

CHAPTER 4

PREVIOUSLY USED MEASURES OF LANDSLIDE MOBILITY

No single measure of landslide mobility is universally agreed upon, nor is there a consensus regarding the threshold between long-runout events and non-long-runout events. Therefore, a survey of the main perspectives in the literature has been prepared.

4.1 H/L and the Angle of Reach:

The most commonly used measure of landslide mobility is H/L, or the total drop height over the total runout distance. The total drop height is defined as the vertical distance between the distal margin of the landslide toe and the highest point where the failing material originated. Similarly, the total runout distance is the horizontal distance between these same points. This measure, proposed by Heim and others (as reported in Corominas, 1996), is depicted in Figure 1. It characterizes runout based upon the assumption that it corresponds to the coefficient of kinetic friction where the entire mass is simplified as a sliding block on an inclined plane. Given this assumption, Coulomb's law of sliding friction states that $H/L = \tan \alpha$, where $\tan \alpha$ was called the "equivalent" coefficient of friction by Hsu (1975) and the "effective" coefficient of friction by others (for example Howard, 1973). An equivalent measure, the angle of reach, α, is the inverse tangent of H/L (Figure 1). Other terms used to describe the angle of reach are "fahrboschung angle" (Hsu, 1975) and "travel angle" (Schuster et al., 1996).

4.2 H_{CM}/L_{CM}:

Legros (2002) challenged these measures of runout on the basis that the dimensions used in the calculation of runout should correspond to those of the center of mass of the landslide in order for it to accurately approximate the angle of friction. Otherwise, L is often significantly overestimated and there is danger of underestimating the apparent friction coefficient. The ratio of H_{CM} to L_{CM} is an alternative, where H_{CM} is the change in height of the center of mass and L_{CM}

is the horizontal displacement of the center of mass (Figure 1). However, there are limitations to this approach for landslides that spread significantly during movement (Legros, 2002). Nevertheless, the ratio of H_{CM} to L_{CM} has received support as a more physically significant measure of mobility than H/L (Iverson et al., 2016).

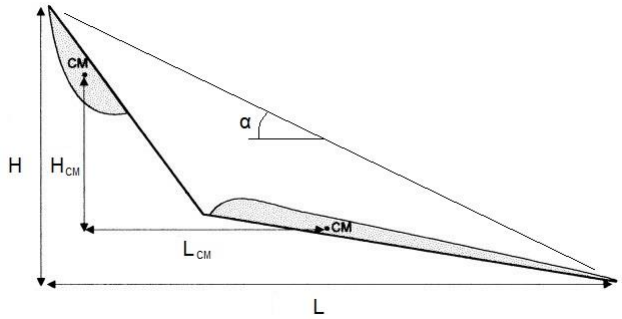

Figure 4-1: Standard mobility measures H/L and H_{CM}/L_{CM}. The angle of reach, (α), is also shown. Figure modified from Legros (2002).

4.3 Excess Travel Distance and Related Measures:

A third alternative, excessive travel distance, L_e, is the horizontal distance that a landslide extends beyond the horizontal distance that a sliding block which drops from the same height, H, would travel assuming a normal coefficient of friction for rock of 32°. Namely, $L_e = L - H/\tan(32°)$. This method, however, over-represents large landslides. For example, a small landslide with a very low angle of reach might have the same excess travel distance, L_e, as a very large landslide that only slightly exceeds the expected travel distance, H/tan(32°).

Hsu defended L_e on the grounds that small landslides are not sufficiently mobile to exhibit a positive value for L_e (Hsu, 1975). Corominas, however, contends that "most small landslides exhibit significant excess travel distance" (Corominas, 1996). In support of his contention, Corominas invokes another measure of runout which he terms L_r, or relative excess travel distance. Where, $L_r = L_e/(H/\tan 32°)$ (Corominas, 1996). This measure is simply the ratio of the excess travel distance to the expected travel distance. It has the advantage of weighting

both small and large landslides equally. Similarly, Nicoletti (1991) uses L_e/L as a mobility measure.

4.4 Other Measures of Mobility:

Several other measures of landslide mobility have been proposed. One measure defines a mobility coefficient by relating the planimetric area, A, to the volume, V, where the mobility coefficient = $A/(V^{2/3})$. For most rock and debris avalanches, as well as debris flows, the mobility coefficient is around 20. For the relatively mobile Oso Landslide, the mobility coefficient was closer to 30 (Iverson et al., 2015). One concern with this measure is that the volume is difficult to ascertain, and the most common way of estimating the volume is by multiplying the mapped area by a constant thickness (Legros, 2002). Another concern is that this measure completely ignores the height of the landslide (Iverson et al., 2015). Regardless, this measure has gained some support (Legros, 2002). Another mobility measure relates the potential energy of the slide to its area (Dade, 1998). A highly mobile landslide is one where the area is relatively large given its potential energy. This measure has also gained some support (Iverson et al., 2015).

CHAPTER 5

PREVIOUS RESEARCH IN LANDSLIDE MOBILITY

Research was conducted into a broad range of landslide types for the literature review for two reasons. First, many landslides are complex and do not fall into a simple classification category. While the current study in concerned with translational and rotational landslides specifically, other movement types may be involved at a location. Second, insights gained in the assessment of one landslide type may be applicable for other landslide types as well.

Topics discussed in the landslide mobility literature generally fall into four categories. First, there are parameters that trigger landslides. Research here focuses on identifying whether a given trigger correlates with greater mobility. Second, there are antecedent conditions which, when met, would facilitate a long-runout landslide once initiated. These parameters are important for prediction because they are identifiable at a given location before an event occurs. Third, there are mechanisms by which long-runout landslides achieve their unexpected degree of mobility. As certain conditions are required for a given mechanism to work, knowing the mechanism of failure improves knowledge of the conditions that facilitate mobility. Fourth, there are characteristics of long-runout landslides that can only be known post-failure. These characteristics are chiefly of interest because of the insight they give in understanding the nature of long-runout events. In some circumstances, these characteristics can be estimated prior to failure and are therefore useful for prediction. For ease, these four categories will be referred to as: triggers, antecedent conditions, mobility mechanisms, and post-failure parameters, respectively.

5.1 Triggers:

Schuster et al., (1996) defines a trigger as an "external stimulus… that causes a near-immediate response in the form of a landslide by rapidly increasing the stresses or by reducing the strength of slope materials" (Schuster et al., 1996). He goes on to detail five major triggers for landslides: "intense rainfall, rapid snowmelt, water-level change, volcanic eruption, and earthquake shaking" (Schuster et al., 1996). This list is not comprehensive, however, and several other triggers are mentioned, such as storm waves and rapid erosion caused by streams. The cases of rainfall and earthquake triggered landslides are considered below. Other triggers are worth considering, but little work has been done on their relation to mobility, and as such, they are not discussed below.

5.1.1 Rainfall:

Landslides are commonly triggered by rainfall (Jeong et al., 2017). Sometimes long-runout events that result from rainfall are attributed to the fluidization of the failing material. For example, in one experiment an artificial rainfall on a natural slope successfully induced a "fluidized landslide… [that] moved rapidly and traveled long" (Sassa, 2005). This has been observed in natural conditions as well. The long-runout of the Oso landslide is attributed to fluidization of colluvium as a result of rainfall and undrained loading (Stark et al., 2017). Indeed, such cases are not uncommon. "Most landslides that mobilize to form subaerial debris flows are triggered by increased pore water pressures associated with rainfall, snowmelt, or groundwater inflow from adjacent areas" (Iverson, 1997).

In other cases, long-runout events are triggered by rainfall without the saturation of the failing material. The West Salt Creek landslide, for example, was triggered by rainfall and snowmelt; however, increased pore water pressures probably did not play a major role in the high mobility of this event (White et al., 2015). In contrast, the high mobility of the rain-

triggered Hiegaesi landslide was likely due to excess pore water pressures along the sliding plane (Wang et al., 2002). Despite this, a study by Gou et al. found no relation between mobility and water-triggered landslides (Gou et al., 2016).

5.1.2 Earthquake:

It has been proposed that landslides triggered by earthquakes will have greater mobility than non-earthquake triggered landslides. McSaveney (1978) speculated that the Sherman Glacier rock avalanche might have been fluidized by the 3 to 4 minute ground shaking during that the Great Alaska earthquake. Similarly, a study of 635 landslides triggered by the magnitude 5.9 earthquake in Minxian, China, found that the average angle of reach was approximately 20° (or H/L = .363). The authors also speculated that earthquakes with larger magnitudes will produce landslides with greater aspect ratios (i.e. L/W) (Tian et al., 2017). The influence of earthquakes on mobility is further substantiated by the study of 66 rock avalanches in China triggered by the magnitude 7.9 Wenchuan earthquake in 2008 (Qi et al., 2011). These movements had an average angle of reach of only 15°. The mobility, however, may reflect the type of movement (i.e. rock avalanches) rather than the triggering mechanism (Tian et al., 2017). There has also been some evidence that earthquake-induced landslides in loess can have significantly greater than expected mobility. This has been explained as a result of earthquake-induced elevated pore water pressures, which decrease the effective stress and shear resistance of the soil (Zhang et al., 2007). In spite of these findings, some research has found no relation between mobility and earthquake-triggered landslides (Gou et al., 2016).

5.2 Antecedent Conditions:

Antecedent conditions are useful for prediction of landslide mobility but may be difficult to determine without intensive site investigation. Ideal antecedent conditions for this research

are those that can be determined with accurately with ease. Several antecedent conditions are reviewed below.

5.2.1 Initial Soil Porosity:

Iverson et al. (2000) tested loamy sand inclined at 31° and found that small differences in the initial soil porosity led to large differences in "landslide" failure velocity. Tests with initial porosities in excess of .5 accelerated to 1m/s within 1 second. Tests with porosities between .44 and .41 underwent slow and episodic slumping. Finally, a test with initial porosity of .39 did not move at all. This result is explained in relation to critical state porosities. In a loose soil the porosity is greater than the critical state porosity, and therefore the grain structure contracts during shearing, causing increased pore water pressures and reducing friction between the grains. Soils with porosities greater than the critical state porosity will liquefy when sheared resulting in longer runout (Iverson et al., 2016). In a dense soil, the porosity is less than the critical state porosity. This causes dilation of the grain structure reducing the pore water pressure, which increases the effective normal stress in the soil and thereby increases the friction between the grains, slowing or halting the failure (Iverson et al., 2000). Iverson et al. (2016) restates the same results in terms of the related concept of void ratio. Such differences in initial soil porosity or void ratio are nevertheless difficult to ascertain in the field (Iverson et al., 2000).

5.2.2 Grain Size:

Wang and Sassa (2003) performed flume tests on silica sand inclined at 30° to simulate rainfall-induced landslides. Finer grained sands had a median diameter of .05 mm (D_{50} = .05mm), while the coarser sands had a median diameter of .13mm (D_{50} = .13mm). The coarser grained sands moved slower because the increased permeability of these sands lowered the values for the maximum pore pressure. Additionally, the mode of failure also varied between the two sand sizes. The mode of failure for the finer grained sands was a rapidly accelerating

flowslide, whereas the mode of failure of the coarser sands was a series of slow retrogressive slides. Wang and Sassa (2003) also compared flumes prepared with different proportions of loam added to the finer grained sand. The samples with the higher proportions of loam were found to travel farther and at higher velocities (Wang and Sassa, 2003).

5.2.3 Initial Slope Angle:

The initial slope angle has been correlated to landslide initiation. For example, for 150 rainfall-triggered landslides in Umyeonsan, South Korea, "landslides [were] initiated at slope angles ranging from 16 to 44° and some 60% of all landslides occurred at slope angles greater than 30[°]" (Jeong et al., 2017). Other sources have found similar correlations (Dai, 2002).

Steep slopes have further been correlated to high mobility landslides. Iverson et al. (2015) claimed that highly mobile flows initiate on slopes that are greater than 20°. Iverson et al. (1997) added that debris flows usually initiate from landslides at slope angles between 25° and 45°. Similarly, Keefer concluded that long-distance transport of rock avalanches occurs only when H is greater than 150 m and the slope is steeper than 25° (Keefer, 1984). This result was further substantiated by the rock avalanches triggered by the 2008 Wenchuan earthquake in China, where it was found that of the 66 rock avalanches studied, 56 of them were formed on slopes steeper "than 25[°] and higher than 150 m" (Qi, 2011).

5.2.4 Topographic Obstacles:

It is widely assumed that obstructive topographic features can affect the mobility of landslides. Corminas (1996) compared obstructed and unobstructed landslides for rockfalls, translational landslides, debris flows, earthflows and mudflows. He noted that the presence of obstacles caused scatter in plots of Volume vs H/L. While rockfalls displayed the clearest reduction in mobility due to obstacles, translational landslides also obeyed this trend. Large translational landslides were the most dramatically affected, having the same H/L values that

would be expected for landslides "three to four orders of magnitude smaller" (Corominas, 1996). Finally, debris flows had the greatest mobility when unobstructed or channelized (Corominas, 1996).

5.2.5 Forests and Deforestation:

Initiation of landslides has been correlated to land cover. Montgomery et al. (2000) found that in the Pacific Northwest landslide initiation rates increase during the decade following deforestation by timber harvesting. Landslides occur because the loss of root strength over time causes a decrease in the apparent cohesion of the soil. Mature forests along the Oregon coast have an apparent cohesion that exceeds 10 kPa, while cut stumps and smaller vegetation generally have an apparent cohesion between 2 kPa and 4 kPa. This leaves deforested regions vulnerable to shallow soil landslides during intense and prolonged rainfall events, especially for "storms with 24 [hour] rainfall recurrence rates of less than 4 [years]" (Montgomery et al., 2000).

Corominas (1996) found that the presence of forests obstructed the movement of landslides. This reduced the angle of reach for events that would otherwise be expected to have high mobility due to their volume. This effect is especially prominent for smaller landslides under volumes of 1×10^6 m^3.

5.2.6 Previous Failures:

Previous movement at a location that is reactivated can result in long-runout landslides because of the difference between peak and residual strength. Skempton (1964) described the loss of strength of an over-consolidated clay soil after it has undergone shear displacement. The peak strength of the soil represents the maximum resistance to shearing of the soil can generate for a given effective stress. If displacement occurs after this point the shear strength of the soil diminishes until it plateaus out at a lower value known as the residual strength. In such material, only a few inches of displacement are needed for the shear strength to approximate the residual

strength. Coulomb-Terzaghi's law can be used to express the peak strength ($\tau = c' + \sigma'\tan\varphi$) and residual strength ($\tau_r = c_r' + \sigma'\tan\varphi_r$), where

τ – peak shear strength

τ_r – residual shear strength

c' – effective cohesion

c_r' – residual effective cohesion

σ' – effective stress normal to the failure plane

φ – peak friction angle

φ_r – residual friction angle

Skempton (1964) further argues that c_r' is approximately 0 for most overconsolidated clays. Additionally, the friction angle decreases such that: $\varphi > \varphi_r$. By consequence, a failure plane that has already moved enough to reach its residual strength will have less capacity to resist movement at a given effective stress (Skempton, 1964). With less frictional resistance and near-zero cohesion, landslides that have already moved will flow farther than those that have not.

5.3 Mobility Mechanisms

Numerous mechanisms have been proposed to explain the long-runout of various landslides. However, no mechanisms can explain all long-runout events. For this reason, a summary of the main mechanisms proposed in the literature has been provided.

5.3.1 Air Fluidization:

Kent (1966) proposed that catastrophic rockfalls attain very high degrees of mobility as a result of the fluidization of the entire mass of debris by entrapped air. He supports his claim with accounts of the Frank slide as well as a handful of other slides in the United States and Iran. His case is based on six lines of evidence: 1) the lack of sorting of blocks by gravity, 2) the limited abrasion of rocks during transport, 3) the fluidity at emplacement, 4) the thinness of the final

deposit, 5) the high velocities of modern slides, and 6) the evidence of entrapped air in modern slides. Shreve (1968b) and Legros (2002) both agreed that partial fluidization of debris by air may contribute to mobility even if it is not the primary mechanism. Nevertheless, Howard (1973), Hsu (1975), and Legros (2002) are critical of the claim that air fluidization alone can explain long-runout events. In terrestrial cases, air will escape too quickly (Legros, 2002), and it cannot account for potential long-runout events on the Moon (Howard, 1973) or Mars (McEwen, 1989).

5.3.2 Air Lubrication:

Shreve (1966) argued that the long-runout of the rockfall/landslide that covered the Sherman Glacier in 1964 was the result of air trapped between the debris and the underlying topography. The Sherman landslide in Alaska was an enormous failure triggered by an earthquake. According to Shreve (1966) it trapped and compressed air which reduced friction between the sliding mass and the ground. This allowed the debris to maintain a high velocity for an extended distance as it moved like a flexible sheet across the flat-lying topography. He argued that the effects of water could not have played a role in the lubrication of the debris because of the freezing temperatures (Shreve, 1966). For different reasons he argued that water could not have lubricated the Blackhawk and Silver Reef landslides either (Shreve, 1968a). However, Howard (1973), Hsu (1975), and Legros (2002) are all critical of this view. They argue that: 1) due to the relationship between fluidization and permeability (Wilson, 1984) entrapped air will rise as bubbles through the debris (Legros 2002), 2) these events were flows and not slides (Hsu, 1975), and 3) this mechanism does not explain potential extraterrestrial long-runout events (Howard, 1973).

5.3.3 Dust Fluidization:

Howard (1973) speculated that avalanches on the Moon flowed in the absence of fluids or gasses. Hsu (1975) further developed this hypothesis by postulating that fine-grained debris between colliding blocks could fluidize the larger blocks. He corroborated this with eyewitness accounts of the landslide at Elm, as well as the matrix of rock flour discovered between blocks at the Films event. Finally, he mentioned the clouds of dust that were visible at the landing of the Apollo crafts (Hsu, 1975), displaying the fluidization of particles in the absence of fluids or gasses. Against this view, Legros (2002) argued that particles in a vacuum travel in ballistic trajectories, so the clouds of dust visible at the landing of the Apollo crafts were probably the result of the gas emitted by the jets during the descent. Furthermore, he argued that the long-runout events found on the Moon are likely the result of impacts rather than dust fluidization (Legros 2002). These arguments, however, do not contradict the dust fluidization theory itself, but only the lunar evidence for it.

5.3.4 Water Fluidization:

Water has long been considered a fluidizing mechanism. Heim believed that the Elm sturzstrom was lubricated by wet mud (according to Hsu, 1975). Johnson (1978) proposed that water fluidized the base of the Blackhawk landslide. Later Voight and Sousa (1994) considered the possibility of "a two-layer composite debris flow, involving partly unsaturated relatively strong debris riding piggy-back on mobile, water-saturated pumiceous slurry". More recently, Legros (2002) has argued fluidization by water as the primary mechanism for long-runout landslides, where high pore water pressures result in decreased friction between grains. This creates a slurry at the base of the landslide along which the overlying material can slide. Water, he argued, is a better candidate for generating and maintaining the necessary pore pressures than air. He gives three reasons: 1) it is denser, which reduces granular shear stress, 2) it requires

minimal volume contraction to reach lithostatic pressures as it is incompressible, and 3) it is significantly more viscous than air reducing the rate of escape of fluidized water by a factor of 100 over that of air. Furthermore, given this model, the runout distance should be dependent upon the saturated volume, which would help to explain the longer runout of large volume landslides (Legros, 2002). This mechanism might even be able to account for Martian landslides (Lucchitta, 1987), although some disagree (McEwen, 1989).

5.3.5 Pore Fluid Vaporization:

Goguel (1978) proposed that for some long-runout events frictional heat vaporizes water along the slide plane, elevating pore water pressures, and thereby lowering friction along the slide plane. Such a mechanism is highly scale dependent. Small landslides would not generate the heat necessary to vaporize water. Only larger events, such as the rockslides at Vajont and possibly Goldau, would have the forces and distances required. He also argued that a significant proportion of the resulting vapor must be confined to the gliding plane and is therefore dependent upon the rockmass permeability being less than 1E-4 darcy (Goguel, 1978). Legros (2002) endorsed this theory as a possible mechanism in certain cases.

5.3.6 Undrained Loading:

Hutchinson et al. (1971) proposed a mechanism whereby rapid loading of the head of a landslide elevates pore pressures and reduces friction between the sliding mass and the underlying topography. The speed of the loading allows too little time for the pore water to escape. The rear portion of the mass movement then drives the frontal portion forward. This can cause movement along very shallow slopes or rapid velocities on steeper slopes (Hutchinson et al., 1971). This mechanism has received wide acceptance, appearing in accounts of recent events such as with the Oso landslide in 2014 (Stark et al., 2017). This mechanism was proposed by Hutchinson et al. (1971) to explain long-runout mudslides, which they characterize as “relatively

slow moving, lobate or elongate masses of softened, argillaceous debris which advance chiefly by sliding on discrete boundary shear surfaces". The proposed mechanism also applies to other forms of mass movements, of which they give four examples: the translational stages of a landslide in Panama, an earthflow in south Wales, submarine failures, and failures in man-made fills (Hutchinson et al., 1971).

5.3.7 Artesian Pressure Theory:

Chandler (1972) proposed a mechanism to explain the existence of highly mobile mudslides in environments where the steep slopes needed for undrained loading were not available. The mudslides he considers have a pronounced shear surface at the base along which they primarily move. He proposed that artesian water pressures along this surface can cause movements in clay with slope angles as low as 3°-4°. This mechanism requires elevated artesian pore water pressures to explain the movement at these slow slope angles, and four possible explanations for these artesian pore water pressures are offered (Chandler, 1972). Vallejo (1980) counters that conditions that generate artesian pressures are rare, especially over the large areas that are characteristic of mudflows.

5.3.8 Vallejo's Flow Process:

Vallejo (1980) proposed to explain long-runout mudflows, providing an alternative to the undrained loading and artesian pressure mechanisms by interpreting some of these events as propagating primarily by flowing rather than sliding. He argued that hardened clay clods or rocks suspended in mud act like a high concentration of grains in a fluid. In such cases "the force on the grains in the direction of movement consists largely of a component of the effective weight of the grains themselves" (Vallejo, 1980). He then provided four mudflow cases in which the actual mobilization angles closely approximate the predicted minimum angles of mobilization using this model (Vallejo, 1980).

5.3.9 Grain Crushing:

The grain crushing mechanism (alternatively called sliding-surface liquefaction) is a recent hypothesis explaining long-runout landslides and rapid failure velocities. Movement of the landslide causes the crushing of grains in the shear zone. To occur this mechanism requires: 1) relatively coarse-grained material along the shear zone, 2) sufficient overburden pressures to crush the grains, and 3) sufficient brittleness of the grains. Grain crushing then causes the volume of material in the shear zone to diminish along with a corresponding decrease in permeability. Consequently, the pore water pressures along the shear zone increase, causing a decrease in effective stress and corresponding decrease in frictional resistance that facilitates long-runout or rapid failure (Sassa, 2000). This mechanism has been cited in relation to rainfall triggered events (Sassa, 2005; Wang et al., 2002), as well as events triggered by earthquakes (Wang et al., 2000; Gerolymos, 2008).

5.3.10 Other Mechanisms:

A number of other mechanisms have been proposed to explain long-runout events. Melosh (1979) speculated that acoustic fluidization can explain the long-runout of many rock avalanches such the Blackhawk landslide. Davies (1982) proposed two hypotheses in which the long-runout of rock avalanches is explained by 1) fluid-like spreading of debris under gravity, or 2) fluidization of debris due to high basal shear rates. Straub (1997) proposed that the long-runout can be explained by granular flow. Campbell (1989) similarly suggested that long-runout landslides can be accounted for purely by particle flow. Erismann (1979) discussed the possibility of lubrication of gliding surfaces by melted rock in large landslides such as Kofels and Films. Voight et al., (1983) proposed that hot volcanic fluids were responsible for the mobility of the Mount St Helens rockslide-debris avalanche. Finally, other mechanisms have

been proposed, as described in Legros (2002), but these have not been widely discussed and therefore will not be summarized here.

5.4 Post-Failure Parameters:

Considerable effort has also been put into analyzing the characteristics of long-runout landslides that can only be known after the failure has occurred. For this reason, the characteristics are useful in understanding the natures of different types of landslides, although they may not be suitable for prediction. This includes the mechanisms of failure and propagation, as well as how they are deposited. It is also possible to obtain information about how post-failure parameters affect landslide morphology. Finally, in some cases, these post-failure characteristics may be estimated before failure, allowing them to be used for prediction of landslide mobility (Scheidegger, 1973). A summary of a number of potentially relevant post-failure parameters is provided below.

5.4.1 Volume:

The correlation between landslide volume and mobility has been accepted since Heim proposed it in 1932 (as noted by Scheidegger, 1973). Results from a number of studies show this correlation to be strong. Scheidegger (1973) found that the log of the volume plotted against the log of H/L for 33 catastrophic landslides could be fit linearly with a correlation coefficient, r, of -.82. Corominas (1996) found a similar result for 204 landslides of different types including rockfalls, translational slides, debris flows, earthflows, and mudslides. Similarly, Hsu (1975) plotted the excess travel distance, L_e, against the log of the volume and found that larger volume landslides have larger values of L_e while small volume landslides fail to have any excess travel distance. However, some studies have reported much weaker correlations. Nicoletti et al. (1991) also produced a similar linear regression as Scheidegger (1973) when plotting 40 rock avalanches, but with a much lower correlation coefficient (r = -.37). A study of over 1100 man-

altered slopes in China showed a similarly small correlation coefficient (Finlay, 1999). Finally, Skermer (1985) proposed that landslide volume may not contribute to greater mobility at all. Instead, the fall height is what controls the H/L value and any correlation to volume is the result of larger volume landslides having greater fall heights (Skermer, 1985).

Davies (1982) postulated that the apparent connection between the long-runout of large volume landslides and the volume is entirely due to spreading. If so, then H_{CM} / L_{CM} should show no correlation with landslide volume. However, Legros (2002) gave H_{CM} / L_{CM} values for a number of large landslides and concluded that this is not the case.

Scheidegger (1973) reported that landslide volumes less than 1 x 10^6 m^3 tend to have constant effective coefficients of friction. Hsu (1975) similarly claimed that landslides with volumes less than 5 x 10^5 m^3 tend to have equivalent coefficients of friction of about .6. Corominas (1996) challenged these claims, however, contending that many landslides with volumes less than 5 x 10^5 m^3 have effective coefficients of friction below .6 and that all sizes of landslides show decreases in H/L with increasing volume. His data also suggested that many small landslides have significant relative excess travel distance, L_r (Corominas, 1996).

5.4.2 Area:

Legros (2002) contended that one advantage of using areas is that they can be easily and accurately estimated. In contrast, volumes are much more difficult to estimate for landslides that have already occurred, and in practice, volumes are often determined by multiplying the area by an assumed thickness. Studies that have compared the area of a landslide to its volume have found that the two parameters are closely correlated, and the area is proportional to the volume raised to the 2/3, (i.e. $A \sim V^{2/3}$) (Legros 2002; Dade et al., 1998). Similarly, the same relation closely describes the correlation between area and potential energy for rockfalls and debris

avalanches (Dade et al., 1998). Finally, evidence has been presented that shows that the area of a landslide has only a weak connection to its height (Legros, 2002).

5.4.3 Height:

Heim speculated that the total travel distance, L, of a landslide is dependent primarily on the height of fall, topographic regularity, and size of the landslide (according to Hsu, 1975). This has been supported by several studies (Corominas, 1996; Finlay, 1999; and Legros, 2002). Skermer (1985) proposed that that H/L is controlled by height and topography alone and that any correlation to the landslide volume is a function of larger landslides generally having greater fall heights. Against this, some findings suggest that the effective coefficient of friction (i.e. H/L) is largely independent of the height (Davies, 1982; Corominas, 1996; Legros 2002). Despite this, Corominas (1996) argues that the height of fall does control the total runout, L, as well as the excess travel distance, L_e.

5.4.4 Velocity:

Landslide velocities can be divided into seven categories: extremely slow, very slow, slow, moderate, rapid, very rapid, and extremely rapid (Cruden and Varnes, 1996). The velocities corresponding to these categories are depicted in Figure 5-1. General estimates of failure velocities for various failure modes have been provided in Table 5-1 (Hungr et al., 2005). Hungr et al. (2014) explained differences in velocities in translational rockslides, rotational rockslides, rotational slides in soil, and planar slides in soil and debris. Translational rockslides are often extremely rapid as they are not self-stabilizing. In contrast, rotational rockslides are often self-stabilizing as the gravitational driving forces are reduced as the failure advances. As a result, these events frequently attain only slow to moderate failure velocities. In cases where weak rock is overlain by a cap of strong and brittle rock, however, failure can generate rock avalanches that move at extremely rapid velocities. Rotational failures in soil occur most

frequently in fine-grained soils and often range between slow and rapid velocities. Failures in sensitive or collapsible soils, however, can reach extremely rapid failure velocities.

Translational slides in fine-grained soils are rarer than rotational and compound soil failures, but show similar velocities to rotational soil slides, ranging from slow and rapid. Coarse-grained soil and debris slides are prone to disaggregate and become flows that can move at extremely rapid velocities (Hungr, et al., 2014).

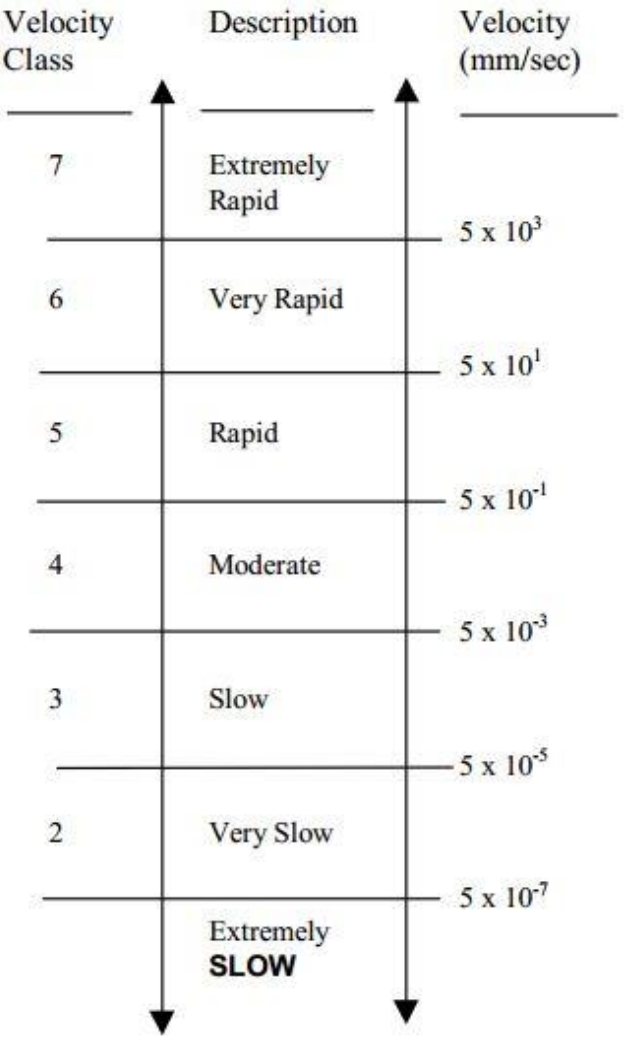

Figure 5-1: Failure Velocity Classification adopted from Cruden and Varnes (1996).

Table 5-1: Common failure velocities by failure mode. Table from Hungr et al. (2005).

TYPE	VELOCITY CLASS*							COMMENT
	ES	VS	S	M	R	VR	ER	
SLIDES IN ROCK								
Translational (or Wedge) Rock Slide							■	May be slow in very weak rocks
Rotational Rock Slide(Slump)	■	■	■	■	■			Very weak rock mass
Compound Rock Slide	■	■	■	■	■	■	■	Various types of mechanisms
Rock Collapse							■	Strong rock, joints, rock bridges
FALLS AND TOPPLES								
Rock (Debris) Fall							■	Fragmental fall, small scale
Rock Block Topple							■	Single or multiple blocks
Rock Flexural Topple	■	■	■	■	■			Very weak rock mass
SLIDES IN SOIL								
Clay Slump (Rotational)	■	■	■	■	■			Non- sensitive
Clay Slide (Compound)	■	■	■	■	■			Non- sensitive
Sand (Gravel, Talus, Debris) Slide					■	■	■	Usually shallow
FLOW-LIKE LANDSIDES								
Dry Sand (Silt, Gravel, Talus Debris) Flow	■	■	■	■	■			No cohesion
Sand (Silt, Debris, Peat) Flow Slide							■	Liquefaction involved
Sensitive Clay Flow Slide							■	Quick clay
Debris Avalanche							■	Non-channelized
Debris (Mud) Flow						■	■	Channelized
Debris Flood						■	■	High water content
Earth Flow	■	■	■	■	■			Plastic clay
Rock Avalanche							■	Begins in bedrock
Rock Slide-Debris Avalanche							■	Entrains debris

Even though it is an important parameter, few landslides have reliable estimates for velocity (Legros, 2002). This makes comparisons between landslide velocity and mobility difficult. There is some evidence that for landslides that exhibit fluid-like behavior, the velocity does not greatly affect the landslide shape (Legros, 2002). Corominas (1996) also pointed out that earthflows, mudflows, and some translational slides are slow-moving but have H/L values that are as low as those for fast moving landslides such as rock avalanches. Additionally, Sheller (1970) proposed an increase in velocity with landslide volume (according to Schreidegger, 1973). However, Schreidegger (1973) argued that the Elm rock avalanche and Vajont rockslide contradict any correlation between velocity and volume for these fast-moving landslide types.

5.4.5 Movement Type:

Corominas (1996) analyzed 204 landslides of different types including rockfalls, translational slides, debris flows, earthflows, and mudslides. Removing all landslides with obstructions he found that rockfalls and rock avalanches with volumes less than 1 x 10^7 m^3 were the least mobile in terms of H/L. Translational landslides, debris flows, and debris avalanches were more mobile. Rockfalls and rock avalanches with volumes greater than 1 x 10^7 m^3 were also more mobile than those with smaller volumes. Finally, earthflows, mudflows, and mudslides displayed the smallest values of H/L. However, of all landslides with volumes less than 1 x 10^5 m^3, earthflows and translational slides exhibited the greatest mobility (Corominas, 1996).

5.4.6 Scale Effects:

Goguel (1978) proposed that the scale of a landslide could significantly alter its behavior. One such example is suggested to explain the long-runout of the Goldau rockslide. In that case, the initial sliding of the failing block was large enough to generate the heat needed to vaporize water along the failure plane. Smaller landslides could not propagate by such a mechanism because they would not be able to create the frictional energy needed to vaporize water. Other theories of long-runout such as the air fluidization of Kent (1966) and the air lubrication of Shreve (1966) are also only possible at certain scales. More recently, scale effects have been endorsed to explain the proposed relationship between increasing volume and decreasing H/L (Corominas, 1996).

CHAPTER 6

CONDITIONS OF STUDY AREA SELECTION

Selection of study areas is dependent upon the locations that have landslide data available and which of these meet the conditions used to limit variability among unknown parameters. Due to this, the study areas could not be selected randomly. Therefore, it cannot be guaranteed that the eight study areas are representative of landslides in the Western United States. Despite this, the parameters used for the analysis of mobility should not be greatly dependent upon the study area conditions and thus the study areas are probably as representative of landslides in the Western United States as can be obtained. The five conditions for study area selection are discussed below.

6.1 Condition 1: Western U.S.

All study areas were located within the western half of the continental U.S. These limits were chosen primarily because of the need for a detailed and comprehensive understanding of landslide mobility in this region. Additionally, some variation in climactic and geologic characteristics have been constrained by excluding other regions from the study. Eventually, a detailed and comprehensive account of landslide mobility across the entire U.S. and even the world is desirable, however, that is beyond the scope of the current research.

6.2 Condition 2: At Least 30 Events

All study areas contain at least 30 landslide events. There is no standard value for the minimum number of landslides needed for statistically relevant conclusions: the more landslides, the more likely that significant relationships can be shown. The number 30 was chosen as a minimum value because of the difficulty in finding groups of easily identifiable landslides with very large numbers of events that met the remaining three conditions. An additional component

to this condition was that all 30 landslides were required to be primarily translational, rotational or both. No debris flows, rockfall, or other mass wasting events were considered.

6.3 Condition 3: Similar Climate, Geology, and Vegetation

Study areas were selected so as to limit the variability in unknown parameters. Specifically, variability was minimized with respect to unknown material and hydrological properties of the sliding mass immediately before failure. Variability in known parameters can be statistically analyzed, however, it is impossible to analyze the statistical relevance of any unknown parameters. To address this, differences in climate, geology, topography, and vegetation across the study area were checked. These four categories of variability were used as indicators of the overall variability in unknown parameters. For example, the greater the variability in climate between landslides on one side of a study area and the other, the greater the differences in unknown parameters between those two landslides. The variability in these four known categories were rated as low, medium, or high and assumed to directly indicate similar variability in unknown parameters. If there was one high or two medium ratings for a prospective study area, then it was rejected.

6.4 Condition 4: Easily Locatable

All landslides in the study area were required to be easily locatable. This could either be because the landslides have already been mapped, or else because they are identifiable on satellite imagery or aerial photographs, or both. This condition was included because of the difficulty in adding new data for landslides that have not been accurately mapped. If a landslide can be located, then topographic, geologic, vegetative, and possibly hydrological data can be gathered through literature research or examination of imagery of the area. If this is not the case, then no new information would have been procurable and the site would have been poorly suited for this study.

6.5 Condition 5: Sufficient Variation in H/L

There must be sufficient range in the mobility within the set of landslides at an area. As H/L is the most commonly used measure of landslide mobility, it is important that any data collected contain a sufficient range of H/L values such that correlations can be made between this measure of mobility and other parameters. Other landslide mobility measures are considered and used for this research, so variability in L as well as H are also required. To meet this condition there must be at least a 50% variation in the H, L and H/L values within the study area.

CHAPTER 7

GEOLOGIC BACKGROUND OF STUDY AREAS

A tabulation of all of the landslides used for this study is included in the Appendix, Table B-2. A descriptive summary of each geographic area containing the landslides in given below.

7.1 California, Ferndale:

The California Ferndale study area sits between Ferndale on the northeast, Petrolia on the southeast and the Pacific Ocean on the west. The area is characterized by a warm-summer Mediterranean climate, Csb, under the Köppen-Geiger climate classification (Kottek, 2006). In the north, the primary geological units containing recent landslide activity are the "marine and nonmarine overlap deposits" (Qwt) composed of weakly lithified sandstones and mudstones, and the older landslide deposits (Qls) composed of unsorted clay to boulder sized debris. Landslides also appear in the units designated as melange (co1) composed of "highly folded argillite," and the sedimentary rocks of False Cape terrace (fc) composed primarily of sandstone and dolomitic limestone (McLaughlin et al., 2000). The primary geological units containing recent landslide activity in the southern portion are the Franciscan Formation (fss) composed of the brittle and fractured graywacke sandstone with minor shale, and the marine sediments (Tp) composed of mudstone. Landslides also appear in (fssh) composed primarily of sheared micaceous shale, and (fsr) composed primarily of sheared micaceous shale (Dibblee, 2008). Landslides in the area were classified as deep-seated translational/rotational slides, earthflows, debris slides, and debris flows. These were further distinguished by activity as active, dormant, or uncertain (Spittler, 1984). Only active deep-seated translational/rotational slides were used for the current research.

7.2 California, Riverton:

The California Riverton study area sits along US-50 W between Riverton and Kyburz California. The area is characterized by a warm-summer Mediterranean climate, Csb, under the Köppen-Geiger climate classification (Kottek, 2006). Subsurface geology in the area is dominated by the Sierra Nevada Batholith (Kgr), a Cretaceous-aged granite, and a highly deformed, prebatholithic mixture of quartz-mica schist and gneiss (pKm). The Mehrten Formation (Tm), and andesitic mudflow, is also located in the area. Surficial geology contains landslide deposits, colluvium, and material containing both landslide deposits and colluvium (Wagner, 1997). Landslides in the area were classified as deep-seated translational/rotational slides, earthflows, debris slides, and debris flows. These were further distinguished by degree of confidence in mapping extent with confident, approximate, and uncertain boundaries being marked. Landslide stability was classified into groups A, B, C, D, and E. Landslides of group A moved during the winter of 1996-1997. Landslides of group B did not fail during the winter of 1996-1997 but displayed distinct surface features of landslide motion. Groups C, D and E represent possibly unstable slopes, dormant landslides, and locations where landsliding might have occurred, respectively (Wagner, 1997). Landslides from groups C, D and E were not included in the current research because of uncertainties in their boundaries. Only deep-seated translational/rotational slides with confident boundaries from groups A and B were used for this study.

7.3 Colorado Springs:

The Colorado Springs study area extends across the southwestern to northwestern portions of Colorado Springs. The area is characterized by a cold semi-arid climate, BSk, under the Köppen-Geiger climate classification (Kottek, 2006). According to Carroll et al. (2000) and Thorson et al. (2002), most recent landslide activity in the area is located within older landslide

material (Qls). These older landslides generally formed through failures in the Pierre Shale, and currently consists of clay, silt, sand, and rock fragments. Other old landslide deposits with recent landslides originated through failures in the upper member of the Laramie Formation, which is characterized as a sandy shale with some shaly sandstone. A few landslides have also been found that are located directly in the Pierre Shale (Kp), in a pediment gravel (Qg2), in older fan deposits (Qfro), or in the Pikes Peak Granite (Ypp) (Carroll et al., 2000; Thorson et al., 2002). Landslide locations and dimensions used for this project were taken from recent landslides (Qlsr) in Carroll et al. (2000) and Thorson et al. (2002).

7.4 Oregon:

The Oregon study area is centered around Scottsburg Oregon, extending about 30km north and 20 km south of the Umpqua River. The area is characterized by a warm-summer Mediterranean climate, Csb, under the Köppen-Geiger climate classification (Kottek, 2006). The primary geological unit containing recent landslide activity is the Tyee Formation (Tl) composed by alternating beds of arkosic, micaceous sandstone and siltstone (Baldwin, 1956). A basalt dike (Tte) also underlies landslides located in the lower portion of the study area. Finally, a few landslides are located within old landslide deposits (Qal) (Baldwin, 1961). Burns (2017) supplied the shapefiles for all landslides. Landslide types in the area included translational landslides, rotational landslides, rockfalls, debris flows, and earthflows. Landslides were further divided into prehistoric and historic landslides (Burns, 2017). Only historic translational, historic rotational or historic complex slides involving significant translational or rotational components were used.

7.5 Utah North:

The Utah North study area is located about 20 km east of Mt. Pleasant Utah. It sits between North Hughes Canyon in the northwest, Bob Wright Canyon on the northeast, Gentry

Ridge on the southeast, and Horse Canyon on the southwest. The area is characterized by a subarctic climate, Dfc, under the Köppen-Geiger climate classification (Kottek, 2006). The primary geological units underlying recent landslide activity are the Blackhawk Formation (Kbh), the Star Point Sandstone (Ksp), the upper part of the Blue Gate Member (Kmub), and the North Horn Formation (TKn). According to Witkind et al. (1991), the Blackhawk Formation (Kbh) is composed of sandstone, shaly siltstone, and shale. The Star Point Sandstone (Ksp) is also composed of sandstone, shaly siltstone, and shale. The upper part of the Blue Gate Member (Kmub) is primarily composed of shale and shaly siltstone. Finally, the North Horn Formation (Tkn) is primarily composed of mudstone, claystone, sandstone and conglomerate. Additionally, a few landslides have been found over the Price River Formation (Kpr) and the Castlegate Sandstone (Kc) both of which are primarily composed of sandstone and conglomerate with minor shale (Witkind et al., 1991). Landslide shapefiles were taken from the inventory found at https://gis.utah.gov/data/geoscience/landslides/#LandslideInventoryPolygons (Landslides and Debris Flows). The inventory contains records of falls, flows, rotational slides, and translational slides and were mapped with high, moderate, and low confidence levels. Mostly translational slides mapped with high confidence were used. Only a few translational slides were used that were mapped with moderate confidence. No low confidence landslides were used. No rotational slides, falls, or flows were used.

7.6 Utah South:

The Utah South study area is located southeast of Manti, Utah. The north is bounded by Six Mile Canyon and the North Fork of Six Mile Canyon. The study area extends as far west as Ferron Mountain and as far south as White Mountain. The area is characterized by either a subarctic climate, Dfc, or a warm-summer humid continental climate, Dfb, under the Köppen-Geiger climate classification (Kottek, 2006). The primary geological units underlying recent

landslide activity are Quaternary mass wasting deposits (Qmw), the Flagstaff Limestone (Tf), the North Horn Formation (TKn), and the Price River Formation (Kpr). According to Witkind (1987), the Flagstaff Limestone is composed of locally dolomitic limestone. The North Horn Formation (Tkn) is primarily composed of mudstone, claystone, sandstone, and conglomerate. Finally, the Price River Formation (Kpr) is primarily composed of conglomerate, sandstone, and minor shale. Additionally, a few landslides have been found over the Blackhawk Formation (Kbh) that is composed of sandstone, shaly siltstone, and shale, and the Castlegate Sandstone (Kc) that is composed of sandstone, conglomerate, and minor shale (Witkind, 1987). Landslide shapefiles were taken from the inventory found at https://gis.utah.gov (Landslides and Debris Flows). The inventory contains records of falls, flows, rotational slides, and translational slides and were mapped with high, moderate, and low confidence levels. Mostly translational slides mapped with high confidence were used. Only a few translational slides were used that were mapped with moderate confidence. No low confidence landslides were used. No rotational slides, falls, or flows were used.

7.7 Washington, Grays Bay:

The Washington Grays Bay study area is located west of Naselle, east of Skamokawa, north of Grays Bay and its northern-most boundary is about 15 km south of Lebam. The area is characterized by a warm-summer Mediterranean climate, Csb, under the Köppen-Geiger climate classification (Kottek, 2006). The primary geological units underlying recent landslide activity are the lower member of the Astoria Formation (Tas), the Lincoln Creek Formation (Tlc), and Unit B (Tb). According to Wolfe et al. (1968) the lower member of the Astoria Formation (Tas), also called the Naselle unit (Tan) by Wells (1989), is composed of siltstone to very fine-grained sandstone. The Lincoln Creek Formation (Tlc) is composed of siltstone with minor sandstone. Finally, Unit B (Tb) is also composed of siltstone with minor sandstone

(Wolfe et al., 1968). Landslides were originally mapped by Cashman et al., (2006). Only landslides characterized as “active deep-seated landslides” were used for this project.

7.8 Washington, Puget Sound:

The Washington Puget Sound study area is located along the edge of the Puget Sound, extending from Everett in the north to about 8 km south of Mukilteo. The area is characterized by a warm-summer Mediterranean climate, Csb, under the Köppen-Geiger climate classification (Kottek, 2006). The primary geological sources for recent landslide activity are old landslide deposits (Qls), advance outwash deposits (Qva), translational bed deposits (Qtb), and the Whidbey Formation (Qw). According to Minard (1982) and Minard (1985), the advance outwash deposits (Qva) are composed primarily of clean unconsolidated sands with some gravel and cobbles. The translational bed deposits (Qtb) are composed primarily of clay, silt, and very fine to fine-grained sands. Finally, the Whidbey Formation (Qw) is composed of material varying from coarse sands to silty sands (Minard, 1982; Minard, 1985). All landslides used for the present research moved in the winter of 1996 to 1997 (Baum et al., 2000). Two winter storms triggered the events, and both storms occurred over the course of several days. The first was solely a rainstorm while the second was a warm rain that resulted in the melting of 1-2ft of snow (Baum et al., 2000). Landslides were originally mapped by Baum et al. (2000). Only landslides characterized as “earth slides” were used for this project. No historical landslides were used.

CHAPTER 8

METHODS USED FOR DATA COLLECTION

Satellite imagery, aerial photography, geologic maps, topographic maps, and other maps specific to a given study area were loaded into ArcGIS or Google Earth Pro. From there shapefiles were created for each landslide unless already provided. To ensure that sampling was as random as possible, all translational or rotational landslides not exclusively in rock were chosen. Any sampling biases contained in the original mapping of the landslides cannot be accounted for.

Once assembled, the length, height, area, and location information could be measured and recorded for each landslide. Next, additional parameters were selected for collection. Many parameters that might be useful for prediction of landslide mobility were not accessible given the wide range of study areas and lack of opportunity for site investigation. Similarly, parameters were excluded if they would be useful in predicting mobility, but remote collection of such data would involve excessive subjective judgment on the part of the data collector. Finally, parameters were excluded if common sense and general scientific knowledge suggest that they are probably not useful for prediction, such as average barometric pressure or soil color. Eight parameters were retained for further study: proximity to surface water bodies, topographic morphology, geology, type of vegetation, previous movement, depth to bedrock, initial slope angle, and topographic obstacles. For all landslides, any parameters that could not be confidently assessed were marked as such or left blank.

8.1 Proximity to Surface Water Bodies:

The proximity of the landslide to surface water bodies was used as a proxy for the height of the groundwater table. Landslides that occur near lakes or streams will presumably have

higher water tables. This parameter was measured in two ways. First, distances were measured from the centroid of the landslide to the nearest surface water body along the horizontal. Second, distanced were measured from the closest point on the perimeter of the landslide to the closest surface water body. Surface water bodies were identified using topographic maps or other maps as well as aerial photography and satellite imagery. Only the closest identified water body was recorded.

8.2 Topographic Morphology:

The topographic morphology was also used as a proxy for groundwater levels, as hollows and concavities were assumed to have shallower groundwater tables. Morphological categories include gentle angle slope, convex slope, concave slope, near topographic high, and near topographic low. Landslides were classified as near topographic high if its centroid was within the top 20% of the local relief, and near topographic low if its centroid was within the bottom 20% of local relief. Landslides were classified as gentle angle, convex, or concave if its centroid was in the center 60% of the local relief.

Further classification into concave, convex, and gentle were based upon the slope grade, the relative scale of the landform to the landslide, and the curvature of the topographic contours. If a landslide on a slope of greater than 10° and was in a well-defined hollow or it was in a concavity where there was a change in the strike of the slope by 30° within 20 meters occurring on both sides of the concavity, the topography was classified as concave. If a landslide was on a slope of greater than 10° and a concave are was within the boundaries of the landslide, then if the width of the landslide was less than 4 times that of the concavity at the elevation of the centroid of the landslide, then the topography was classified as concave. If a landslide was on a slope of greater than 10° and it was on a convexity where there was a change in the strike of the slope by 30° within 20 meters occurring on both sides of convexity, then the topography was classified as

convex. If a landslide was on a slope of greater than 10° and a convex area was within the boundaries of the landslide, then if the width of the landslide was less than that of the convexity at the elevation of the centroid of the landslide, the topography was classified as convex. If the slope was less than 10° or the conditions for concavity or convexity were not met, the topography was classified as gentle (see Figures 8-1 and 8-2).

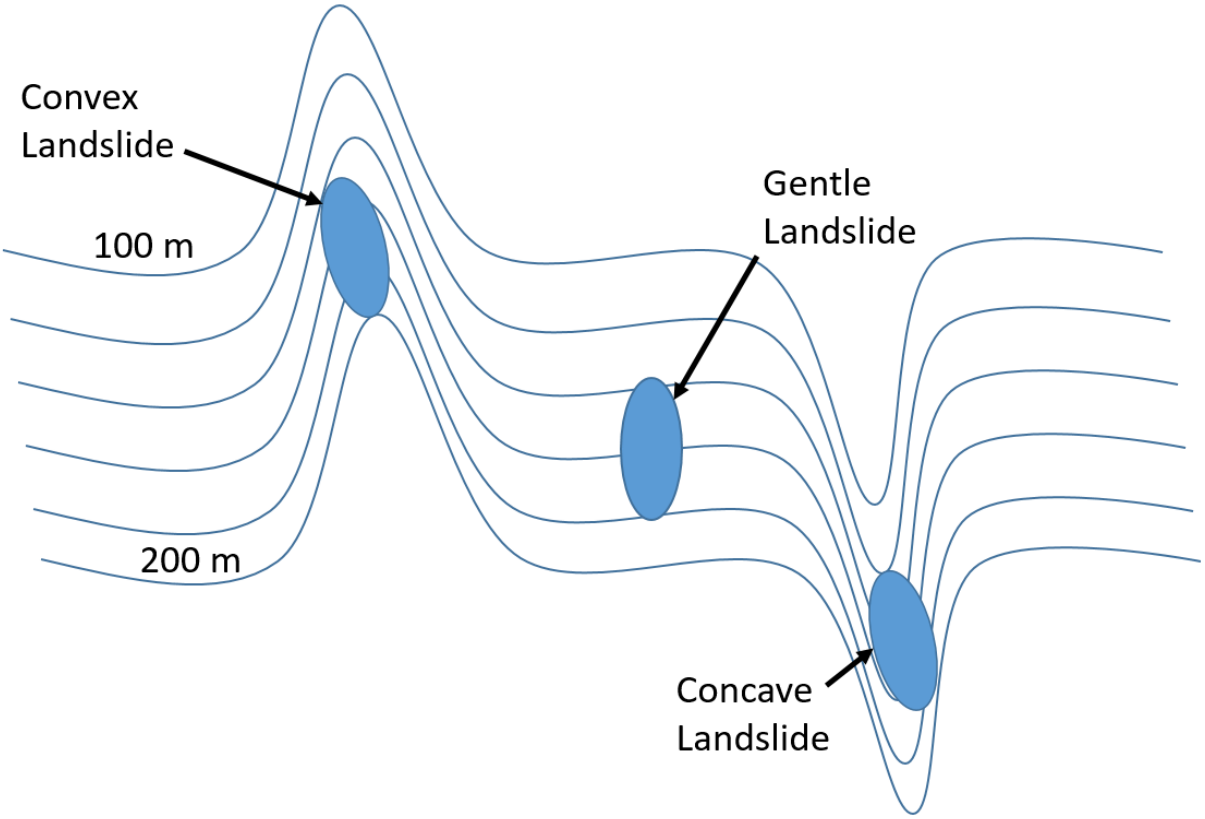

Figure 8-1: Diagram depicting examples of concave, gentle, and convex landslides.

Finally, some locations met the conditions for both concave and convex classifications. For these, if the centroid of the landslide was closer to the center of the gorge at the centroid's elevation than it was to the convex feature at the same elevation, then it was classified as concave. Otherwise, it was classified as convex.

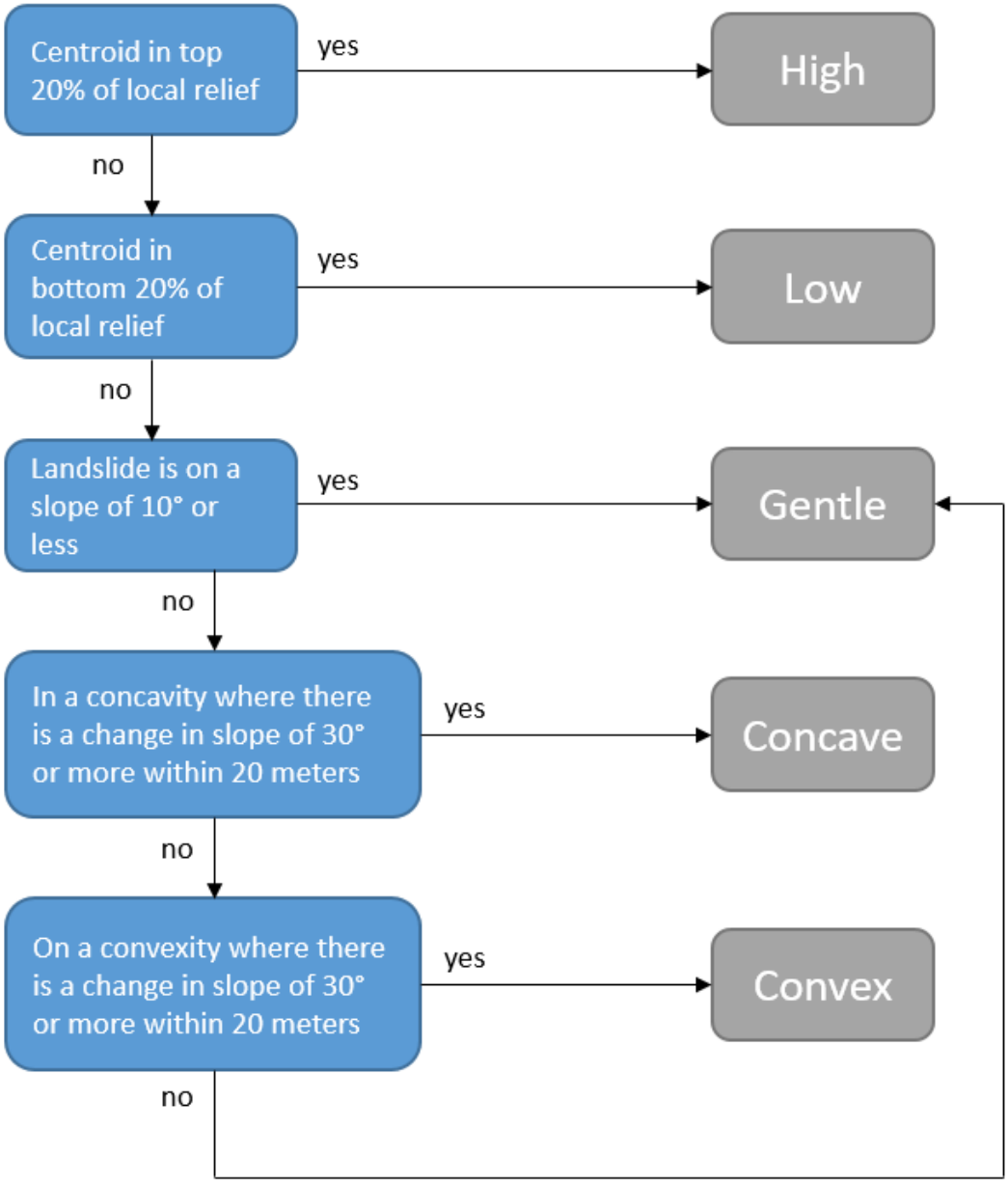

Figure 8-2: Flowchart for determining the topographic morphology classification of a landslide.

8.3 Geology:

Ideally, the geology along the failure surface of the landslide would have been recorded in published literature. Due to the absence of site investigation or field samples, the geology along the failure surface could not be acquired directly for this study, but the underlying bedrock was obtained from published geologic maps. If a landslide was found covering two units, the

upper unit was used under the assumption that the majority of the source material originated in that unit. However, in cases where the geologic unit was thin enough that the failure surface was expected to penetrate down through it, then the unit directly below it was used.

To facilitate the comparison of geology across all eight study areas, the type of geology was classified into one of five groups: clay, granular, sandstone/siltstone, shale, and hard rock. The classification of clay was assigned to landslides in loose soil that contained a significant proportion of clay. These also included a mixture of silt and sand, and a number included larger grain sizes up to boulders. The classification of granular was assigned to landslides in loose soil with no mention of clay. These were dominated by sand, silt, and gravel. The classification of sandstone or siltstone was assigned to landslides whose subsurface geology was classified as sandstone or siltstone. The classification of shale was assigned to landslides whose subsurface geology was classified as shale, sandstone with interbedded shale, mudstone, mudflow deposits, argillite, and claystone. Finally, classification of hard rock was assigned to landslides whose subsurface geology was classified as basalt, limestone, or granite.

8.4 Type of Vegetation:

The type of vegetation was identified by visual inspection of satellite imagery or aerial photography. Five categories of vegetation were used: barren (little to no vegetation), grass covered, shrub covered, light forest, and heavy forest. There was difficulty in identifying the type of vegetation that existed before failure for many of the slides in Oregon, and these were marked with the most likely vegetation type, based on surrounding terrain, and the qualifier "Ukn" for unknown.

8.5 Previous Movement:

The proximity of previous landslide movement was divided into two categories: previous movement and no previous movement. The previous movement classification was given if all or

part of the landslide was located within the extent of previous landslide material. Additionally, the area of recent landslides must have been within an order of magnitude of the current landslide area to count. This was done because historical landslides that are greatly larger or smaller may not have altered the material adjacent to the failure surface of the recent landslide and are therefore unlikely to affect mobility. Previous movements that were either too small or too large were recorded as having no previous movement. When the sizes of previous movements are unclear due to erosion or the joining of multiple adjacent failures, then it was assumed that they were within the order of magnitude. Additionally, landslides that merely deposit on top of previous landslide material were categorized as having no previous movement. These categories were determined using landslide inventories as well as surficial geology maps.

8.6 Depth to Bedrock:

The depth to bedrock was estimated from surficial geology maps of the study areas. This category could only be reliably recorded for a couple of study areas. In these locations, the depth to bedrock was broken down into three levels: shallow, medium, and deep. All landslides where the depth to bedrock was estimated as being less than 2 meters were considered shallow. All landslides where the depth to bedrock was estimated as being greater than 2 meters and less than 10 meters was considered medium. All landslides where the depth to bedrock was estimated as being greater than 10 meters were considered deep.

8.7 Initial Slope Angle:

Calculations of the initial slope angle were made using digital elevation models and topographic maps. Where possible, pre-failure topography was used, and where it was not possible, the initial slope angle was inferred from surrounding topography. If the estimated initial slope angle was less than 10° it was rounded to the nearest 1° from horizontal. When the

estimated initial slope angle was greater than 10° it was rounded to the nearest 5° from the horizontal.

8.8 Topographic Obstacles:

Topographic obstacles were classified into three levels and were modeled after the classification of topographic obstacles outlined by Corominas (1996). The levels included open slope, confined, and opposing wall. An opposing wall classification was assigned when the sliding mass contacts a topographic obstacle that lies within 30° of perpendicular to the original travel direction of the sliding mass. A confined classification was given when more than 20% of the length of travel was within a channel or gorge, and the landslide did not contact an opposing wall. A classification of open slope was given when the landslide was not otherwise classified as confined or opposing wall. Identification of the obstacle type was performed using digital elevation models or topographic maps that predated the failure, or else it was inferred from existing topography.

8.9 Other Data:

For all landslides the height, H, and length, L, of the landslide were also recorded from digital elevation models or topographic maps. Additionally, the total area of the landslide including both the scarp and deposit, was also collected. Finally, the Köppen-Geiger climate classification was recorded for each study area to assess the degree of climatological variability between regions.

CHAPTER 9

METHODS USED FOR DATA ANALYSIS

Most of the analysis was performed using a subset of the assembled data. Except where explicitly stated, all landslides that contacted an opposing wall were excluded. This was done because the mobility of landslides that contact an opposing wall may be limited by the presence of this topographic feature to varying degrees, inviting scatter into the dataset as observed by Corominas (1996).

9.1 Testing Significance of Continuous Variables:

The parameters recorded during data collection divide into continuous variables and categorical variables. Four continuous variables were chosen for analysis: the initial slope angle (ISA), the area (A), the distance from the nearest water source to the centroid of the landslide (WPC), and WPC/A. ISA and WPC were chosen because of their potential for predicting mobility. Area was chosen because, like volume, it has previously been correlated to landslide mobility measures such as H/L (Legros, 2002). Finally, WPC has been normalized by the area of the landslide to form an additional continuous parameter (WPC/A). This variable was chosen because the depth of the water table needed to produce a mobile failure may differ depending on the size of the landslide. A larger landslide will tend to have a deeper failure plane with the potential for a greater area of intersection with the water table. Therefore, WPC/A is a parameter created to represent the depth to the water table relative to the size of the landslide.

Next, six mobility measures were selected for the continuous variable analysis: H/L, L, L_e, L_r, L_e/L and L/A. L was chosen because of how frequently it is used in the literature, despite not being commonly identified as a mobility index. L/A was chosen because it is an index that normalizes length by the size of a landslide which is a representation of mobility not covered by

the other measures. The last four measures of mobility, H/L, L_e, L_r, and L_e/L, were chosen because they are typically used in the literature and are calculable using the data already collected for this research.

To compare the six mobility measures against the four continuous parameters, plots were made, least-squares regressions fitted, and R^2 values calculated. This was done for each of the study areas individually and also for the cumulative dataset. Several assumptions of linear and power regressions were not met for the individual study areas and the cumulative dataset. As a result, these equations were not intended to be used predictively. Instead they serve two purposes. First, they provide a general understanding of the relative importance of the continuous parameters in predicting mobility. Second, they are used to evaluate the six mobility measures and identify the most appropriate mobility measures for continued use in the remainder of the data analysis.

9.2 Testing Significance of Categorical Variables:

Next, the categorical variables were analyzed for each of the individual study areas and also for the cumulative dataset. Six categorical variables were chosen: depth to bedrock, geology, topographic morphology, previous movement, topographic obstacles, and type of vegetation. These were compared against the two mobility measures that were retained following the analysis of continuous variables, H/L and L.

To evaluate the significance of the various categorical parameters on mobility, ANOVAs and Kruskal-Wallis tests were completed on the categorical variables. The ANOVA compares the means of each subgroup for a parameter using the null hypothesis that the means are the same. The test statistically identifies whether populations are distinctly different. The Kruskal-Wallis is a similar test for non-parametric datasets, but uses medians instead of means. Because it is a more robust test, the ANOVA was used whenever possible and the Kruskal-Wallis was

used only if the conditions for the ANOVA were not met. There are also conditions that must be met for the Kruskal-Wallis test to be used, but all data met these less rigorous conditions. There are three assumptions for an ANOVA:

1. Samples are independent
2. The values for all subgroups are normally distributed
3. The variances for all subgroups are the same

As the data for every landslide was taken independently of every other landslide, assumption 1 is met for all data. To test assumption 2, the Lilliefors test was run using Matlab. To test assumption 3 a test of equal variance (vartest2) was made using Matlab. For both tests an alpha value of .05 was used, meaning that if the null hypothesis was true there was only a 5% probability that it was rejected due to chance. As neither H/L nor L was normally distributed, transformations were explored. No simple transformation could be found for H/L, however L was found to be log normal. Once this was completed ANOVAs and Kruskal-Wallis tests were made, and alpha values of .1, .05, and .01 were all used to give a more robust picture of the degree of significance for each parameter in predicting H/L and $\log_{10}(L)$. P-values were then tabulated for the ANOVA and Kruskal-Wallis tests.

For the response variable H/L, a selection of L vs H plots were created for parameters with mean values that differed at the greatest level of significance. Once plotted, regressions were made for each subgroup for a given categorical parameter. For linear fits passing through the origin, H/L is represented by the slope of the line. For non-linear fits, H/L is dependent upon the value of L of the individual landslide, and is equal to the slope of the line drawn from the origin to the point corresponding to L on the fitted curve. For this research, L vs H plots were given power fits rather than linear fits, for two reasons. First, R^2 values for power fits were

slightly higher on average than those of linear fits. Second, there is good reason to believe that even for smaller landslides, H/L values are dependent upon volume of the landslide (Corominas, 1996) and presumably landslides with larger H and L values are on average larger events. Because of this, curvilinear behavior is expected for L vs H plots rather than a linear behavior, which disincentivizes the use of linear fits.

For the response variable L, no plots similar to the L vs H plots could be made because L does not break down naturally into constituent variables. For this reason, the relationship between L and the subgroups of the categorical parameters was represented using box and whisker plots. The plots were made for combinations of study areas and parameters which showed significant difference in the means of the subgroups. For both response variables, L was used instead of the $\log_{10}(L)$ because L has a more direct relationship to H, and also any significant difference in the means of $\text{Log}_{10}(L)$ will almost certainly be visible in the distributions of L.

9.3 Testing Significance of All Variables by Multiple Regression:

Continuous and categorical variables were analyzed using multiple regression for both H/L and $\log_{10}(L)$. Multiple regressions were run for each of the eight study areas, as well as a cumulative dataset using the Matlab function stepwiselm. This function begins with only a constant term and then adds the best of the available terms to the model if the F-test for the term's addition has a p-value .05 or less. (A p-value in a regression tests the null hypothesis that the coefficient of a term is zero.) Then when no terms can be added to the model it removes the worst term if the p-value for its removal F-test is .1 or larger. These steps are repeated until terms can neither be added or removed. P-values for addition and removal of terms in predicting $\text{Log}_{10}(L)$ were adjusted to .1 and .15 respectively for two study areas in order to ensure that at least one predictor variable was used in the regression.

To include categorical variables in the multiple regression, the categorical variables were converted to dummy variables. Optimal dummy variables were identified using the Matlab function multcompare.

Several assumptions of the multiple regressions were not met for the individual study areas and the cumulative dataset. As a result, these equations are not intended to be used predictively, except where they have been verified independently by data not used in the creation of the equations. Otherwise their function is to provide a general understanding of the relative importance of continuous and categorical parameters in predicting mobility.

CHAPTER 10

DATA ANALYSIS RESULTS

A summary of basic statistics for each study area is compiled in the Appendix, Table B-1, along with all data, Table B-2.

10.1 Results for Significance of Continuous Variables:

Four continuous variables were considered in relation to mobility: ISA, A, WPC, and WPC/A.

10.1.1 Predictor Variable ISA:

The R^2 values for the capacity of ISA to predict the six mobility measures (H/L, L, L_e, L_r, L_e/L, and L/A) are recorded in Table 10-1. For the ISA regressions, a linear model was found to be the most appropriate, and so all R^2 values correspond to linear fits of the data.

Table 10-1: R^2 values for linear regressions of mobility vs ISA. Each column represents a different mobility measure compared to ISA.

Study Areas	N*	H/L	L	L_e	L_r	L_e/L	L/A
Cal. Ferndale	37/37	0.105	5.82E-4	.0154	0.127	0.105	0.00292
Cal. Riverton	26/26	**0.708**	0.231	0.476	**0.675**	**0.708**	0.00922
Colorado Springs	42/42	**0.626**	0.117	0.210	**0.523**	**0.626**	0.0473
Oregon	61/60	**0.767**	0.0116	0.0919	**0.623**	**0.704**	0.0279
Utah North	24/24	**0.557**	0.00665	0.123	0.425	**0.557**	0.0717
Utah South	44/41	0.479	0.00856	0.0715	0.441	0.397	0.0855
Wash. Grays Bay	18/16	0.157	0.0669	0.157	0.189	0.444	0.0274
Wash. P.S.	30/19	0.262	0.0121	0.114	0.189	0.284	0.00324
Cumulative Dataset	282/ 264	**0.619**	0.00298	0.0374	0.417	**0.595**	0.0412

*N specifies the number of landslides: without walls / without walls or negative L_e values. R^2 values greater than .5 in bold.

Table 10-1 shows that the initial slope angle, ISA, is strongly correlated with H/L, L_e/L and to a lesser extent L_r. It exhibits little to no correlation with L, L_e, or L/A.

The correlation of H/L with ISA for the cumulative dataset was found to have an R^2 value of .619. The weakest correlations between H/L with ISA were found in Cal. Ferndale, and in the two Washington study areas, Wash. Grays Bay and Wash. P.S., all of which had R^2 values between .105 and .262.

The correlations between L_e/L and ISA are similar to those of H/L. Specifically, the correlations for Cal. Ferndale, Cal. Riverton, Colorado Springs, and Utah North are all identical for H/L or L_e/L. The cause of this appears to be an artifact of the mathematics. The two measures, H/L and L_e/L rely on similar in input variables in similar ratios. Because of this, when R^2 values are calculated for a linear fit they are identical (even though they differ for power and exponential fits). The reason that the other four study areas do not have identical values for their R^2 values is that they possess landslides with negative L_e values, and landslides with negative L_e values were dropped from all comparisons involving L_e, L_r and L_e/L. For consistency this was done for all four predictor variables (ISA, A, WPC and WPC/A) because some fits cannot be made with negative values, including power and exponential fits.

The correlations between L_r and ISA are also very similar to those of H/L and L_e/L. The weakest correlations for both L_r and H/L are associated with Cal. Ferndale, Wash. Grays Bay, and Wash. P.S.

10.1.2 Predictor Variable Area:

The R^2 values for the capacity of area to predict the six mobility measures (H/L, L, L_e, L_r, L_e/L, and L/A) are recorded in Table 10-2. For the area comparisons, power fits were found to be the best and so all R^2 values correspond to power fits of the data.

Table 10-2: R^2 values for power regressions of mobility vs area. Each column represents a different mobility measure compared to A.

Study Areas	N*	H/L	L	L_e	L_r	L_e/L	L/A
Cal. Ferndale	37/37	8.47E-6	**0.673**	**0.546**	0.00133	4.02E-3	**0.637**
Cal. Riverton	26/26	0.0396	**0.766**	0.338	0.0501	0.0515	**0.765**
Colorado Springs	42/42	0.216	**0.748**	**0.678**	0.317	0.130	**0.748**
Oregon	61/60	0.0166	**0.854**	**0.634**	0.0375	0.0067	**0.863**
Utah North	24/24	0.0163	**0.524**	**0.547**	0.0224	0.0307	**0.628**
Utah South	44/41	0.332	**0.732**	**0.662**	0.297	0.325	**0.813**
Wash. Grays Bay	18/16	0.493	**0.901**	**0.709**	0.186	0.123	**0.858**
Wash. P.S.	30/19	0.116	**0.615**	0.0975	0.0117	0.0125	**0.859**
Cumulative Dataset	282/ 264	0.0694	**0.807**	**0.546**	0.0454	0.0511	**0.799**

*N specifies the number of landslides: without walls / without walls or negative L_e values. R^2 values greater than .5 in bold.

There is a general consensus that as volume increases, so does H/L. While volumes were not estimated for this project, areas were gathered for all landslides, and it is suggested that areas and volumes are closely correlated (Legros, 2002). Nonetheless, little evidence for a strong correlation between area and H/L was found. For locations with the highest correlations, the study area in Colorado Springs exhibited a correlation with R^2 of .216, Utah South showed a correlation with R^2 of .332, and Wash. Grays Bay showed the strongest correlation with R^2 of .493. All three correlations exhibit the anticipated relationship, with H/L values decreasing as area increases. Nevertheless, no other study areas or collections of study areas showed significant correlations. Similarly, L_r and L_e/L also both correlate very poorly with area. The few study areas that do show R^2 values above .1 are the same as for H/L.

L/A shows very strong correlations with area. Despite this, the predictor variable A is a component of the response variable L/A, which suggests that any positive correlations are biased and may not have as much meaning as other measures. For this reason, L/A will not be further considered with respect to the predictor variable A.

Disregarding L/A, Length, L, has the strongest correlations with A, with R^2 for the cumulative dataset of .807 and the lowest R^2 for any study area being .524 for Utah North. The second best correlations are between L_e and A with R^2 for the cumulative dataset of .546. The poorest correlation for L_e was the from Wash. P.S. with an R^2 of .0975. This study area is relatively small, however, with only 19 landslides not excluded because of walls or negative L_e values. All other study areas have R^2 values for L_e at or above .338.

10.1.3 Predictor Variable WPC:

The R^2 values for the capacity of WPC to predict the six mobility measures (H/L, L, L_e, L_r, L_e/L, and L/A) are recorded in Table 10-3. For the WPC comparisons, power fits were found to be the best and so all R^2 values correspond to power fits of the data.

Table 10-3: R^2 values for power regressions of mobility vs WPC. Each column represents a different mobility measure compared to WPC.

Study Areas	n*	H/L	L	L_e	L_r	L_e/L	L/A
Cal. Ferndale	37/37	3.95E-4	0.374	0.323	0.00160	0.00777	0.0187
Cal. Riverton	26/26	0.00169	0.00563	0.00270	0.00688	0.0141	0.0137
Colorado Springs	42/42	0.0971	7.96E-4	0.00665	0.0521	0.0476	0.137
Oregon	61/60	0.0520	0.00915	0.0178	0.0760	0.0530	0.0358
Utah North	24/24	0.0149	0.0286	0.0286	0.0239	0.00518	0.0101
Utah South	44/41	0.0609	0.0293	0.00814	0.0169	0.00748	0.0118
Wash. Grays Bay	18/16	0.122	0.0374	0.00415	0.00474	0.00342	0.0907
Wash. P.S.	30/19	0.0857	0.0314	8.95E-5	0.0136	0.00626	0.0848
Cumulative Dataset	282/ 264	0.0161	0.130	0.0477	0.00740	1.07E-4	0.0340

*N specifies the number of landslides: without walls / without walls or negative L_e values. R^2 values greater than .5 in bold.

None of the six mobility measures is strongly correlated to WPC for any study areas except Cal. Ferndale. For Cal. Ferndale, both L and L_e are correlated to WPC with R^2 values of .374 and .323 respectively. Apart from this, L is the best-predicted mobility measure with an R^2

for the cumulative dataset at .13. The second best-predicted mobility measure is L_e with a very low R^2 of .0477.

10.1.4 Predictor Variable WPC/A:

The R^2 values for the capacity of WPC/A to predict the six mobility measures (H/L, L, L_e, L_r, L_e/L, and L/A) are recorded in Table 10-4. For the WPC/A comparisons, power fits were found to be the best and so all R^2 values correspond to power fits of the data.

Table 10-4: R^2 values for power regressions of mobility vs WPC/A. Each column represents a different mobility measure compared to WPC/A.

Study Areas	n*	H/L	L	L_e	L_r	L_e/L	L/A
Cal. Ferndale	37/37	4.76E-4	0.0520	0.0357	3.82E-06	4.56-E4	0.434
Cal. Riverton	26/26	0.0313	**0.518**	0.178	0.0163	0.0122	**0.552**
Colorado Springs	42/42	0.374	0.486	**0.500**	0.386	0.296	0.143
Oregon	61/60	0.0638	**0.501**	0.474	0.0417	0.0472	**0.645**
Utah North	24/24	0.0454	0.0252	0.0276	0.0135	0.0195	0.395
Utah South	44/41	0.371	0.210	0.250	0.275	0.233	**0.602**
Wash. Grays Bay	18/16	0.336	**0.525**	0.452	0.168	0.112	**0.539**
Wash. P.S.	30/19	0.261	0.453	0.0821	0.0291	0.0230	**0.558**
Cumulative Dataset	282/ 264	0.116	0.448	0.336	0.0677	0.0508	**0.600**

*N specifies the number of landslides: without walls / without walls or negative L_e values. R^2 values greater than .5 in bold.

The strongest correlations for WPC/A are found with L, L_e, and L/A. Once again L/A is dismissed as A is a significant component of both the predictor and response variables. If a meaningful correlation existed (beyond the strong correlation of A with itself), it should be found in the comparison of L with WPC in Table 10-3.

The best correlations for WPC/A were with L followed closely by L_e. The correlation of L with WPC/A for the cumulative dataset was found to have an R^2 value of .448 and the correlation of L_e with WPC/A for the cumulative dataset was found to have an R^2 value of .336. Likewise, the weakest correlations for individual study areas also match well between L and L_e.

The weakest correlations with L occur in Cal. Ferndale and Utah North whereas the weakest correlations with L_e occur in Cal. Ferndale, Utah North, and Wash. P.S., all of which have R^2 values below .1. Generally, however, both L and L_e correlated moderately well with WPC/A.

Finally, a number of study areas also display moderate correlations with H/L, L_r and L_e/L. These include Colorado Springs, Utah South, Wash. Grays Bay, and Wash P.S. Of these, Colorado Springs displays the greatest consistency between correlations with H/L, L_r and L_e/L, all of which have R^2 values within .1 of each other. The correlations with H/L, L_r, and L_e/L vary the most in Wash. P.S. with R^2 values of .261, .0291, and .023 respectively.

10.1.5 Assessment of the Six Mobility Measures:

Before further statistical analysis is completed, including evaluation of categorical parameters, the number of mobility measures should be reduced using information from the continuous variable analysis. In order to assess the merits of the six mobility indices (H/L, L, L_e, L_r, L_e/L, and L/A) each index are considered with respect to three criteria. First, mobility measures should not be overly similar. Two measures may both be good representations of the mobility of a landslide but if they are too similar then little new information is gained from using both as opposed to just one. Therefore, to minimize redundancy mobility measures should be significantly different. Second, mobility measures should correlate strongly with important, easily obtained parameters. Mobility measures that correlate poorly with easily obtained parameters are not as useful as measures that correlate well. Third, it is practically preferable if the measures of mobility are easy to use in future studies and have already been commonly used in past studies. If a new or infrequently used mobility index is found to be superior to a commonly used index, then it may be justifiable to use the new index, but otherwise a standard index is preferable. Once the six mobility measures have been assessed a subset can be selected

for use in the remainder of this study and suggested for use in future studies in landslide mobility.

First, there are two major indicators of similarities between mobility measures: their structure and their results. To assess the similarity of the six mobility measures in terms of their structure, it should be noted that they can be divided into three groups by dimensional analysis. The first group includes, H/L, L_r, and L_e/L. All of these are dimensionless mobility measures. The second group contains L and L_e which both have units of length. Finally, the third group contains only L/A which has units of 1/length. Furthermore, both H/L and L_e/L have identical denominators, and have even been shown to produce the same R^2 values for linear fits when plotted against a predictive variable. Therefore, the structural similarities of the six mobility measures places them into three groups, dimensionless measures: H/L, L_r, and L_e/L; measures with units of length: L and L_e; and measures with units of 1/length: L/A.

To assess the similarity of the six mobility measures in terms of their results, it should be noted that for all four of the predictor variables considered (ISA, A, WPC, and WPC/A), the strength of correlations can be divided two groups. The first group is composed of the three dimensionless mobility measures: H/L, L_r, and L_e/L. These three indexes had strong correlations with ISA and little to no correlations with A, WPC, or WPC/A. The second group is composed of the dimensional mobility measures L, L_e and L/A. All three of these displayed strong correlations with A, and to a lesser extent WPC/A, but little to no correlation to ISA. Additionally, while no groups showed a strong correlation with WPC, the three strongest correlations all belonged to L, L_e, and L/A. Given both the similarities in dimensional analysis and results it seems prudent to choose two or three mobility measures by selecting one from

among the three dimensionless mobility measures, H/L, L_r, and L_e/L, and then either one or two from the dimensional mobility measures L, L_e, and L/A.

The mobility measures that display the best correlations to the continuous data are H/L, L_e/L, L, and L/A. The dimensionless mobility measures (H/L, L_r, and L_e/L), have the strongest correlations for ISA. Of these, H/L and L_e/L have the exact same linear fit R^2 values in all cases where negative L_e landslides were not dropped from the fits, with H/L correlations being slightly stronger when using the cumulative dataset. Additionally, both H/L and L_e/L have stronger correlations than L_r for the cumulative dataset, and in the most individual study areas. L_r only has stronger correlations than H/L in Cal. Ferndale and Wash. Grays Bay, and it only has stronger correlations than L_e/L in Cal. Ferndale and Utah South. Furthermore, in none of these cases where L_r displays a stronger correlation than H/L or L_e/L, is the difference in R^2 values larger than .05. This is not the case for all R^2 values where H/L or L_e/L have stronger correlations that L_r. Specifically, the R^2 values for the cumulative datasets for both H/L and L_e/L show differences greater than .15. Overall, L_r generally displays weaker correlations than H/L and L_e/L for ISA which is the only predictor variable where any of these dimensionless mobility measures has consistently strong correlations. Therefore, L_r displays poorer correlations than H/L and L_e/L, and so by the criteria of strong correlations to easily obtained parameters, H/L and L_e/L are preferable to L_r.

For the dimensional mobility measures (L, L_e, and L/A), L and L/A have the strongest correlations for A and WPC/A. For the predictor variable A, both response variables L and L/A have R^2 values that are more than .25 greater than the R^2 value for L_e for the cumulative dataset. Additionally, for the individual study areas, L_e only has a slightly stronger correlation than L in Utah North, and displays weaker correlations for all individual study areas for L/A. For the

predictor variable WPC/A, both response variables L and L/A have R^2 values that are more than .1 greater than the R^2 value for L_e for the cumulative dataset. Additionally, for the majority of study areas, L and L/A have stronger correlations than L_e. Finally, for the predictor variable WPC, the R^2 of L is 2.7 times greater than the R^2 value for L_e, although the R^2 values for L_e are nearly the same as that of L/A. Overall, L_e generally displays weaker correlations than L and L/A for A and WPC/A, which are the predictor variables where the dimensional mobility measures display consistently strong correlations. Therefore, L_e displays poorer correlations than L and L/A and so by the criteria of strong correlations with common parameters, L and L/A are preferable to L_e.

Of the four remaining mobility measures (H/L, L_e/L, L, and L/A), H/L and L are the most practical mobility measures based on the ease of future usability and consistency in past use. Of the two remaining dimensionless mobility measures (H/L and L_e/L), H/L has a slight advantage over L_e/L in terms of future usability because of the inability to include data with negative L_e values for power and exponential fits. Also, for the two remaining dimensionless mobility measures (H/L and L_e/L), H/L has an advantage over L_e/L in terms of the frequency of past use as H/L is one of the most common mobility measures and L_e/L is one of the most obscure. Therefore, H/L does better on the criteria of practical past and future use than L_e/L.

Of the two remaining dimensional mobility measures (L and L/A), L has an advantage over L/A in terms of past usage, as L is one of the most commonly reported parameters for landslides and L/A is not commonly used. Also, the issue of future usability is the greatest concern for L/A. Shapes increase in area at a faster rate than they do across any single dimension, which means that large landslides will almost always have low values for L/A while small landslides have high values for L/A. This means that L and L/A are both measures of

landslide size and L is a more intuitive and practical index for assessing this aspect of mobility. L/A can be modified to be less dependent on size, but only by greatly complicating the calculations needed to interpret L/A (see Appendix A). Therefore, L does better on the criteria of practical past and future use than L/A.

As a result of the analysis using these three criteria, H/L and L are suggested for use as mobility measures in future studies and are used for the remainder of the current data analysis. L_e, L_r, L_e/L and L/A are not suggested for use in future studies and are not used for the remainder of the current data analysis.

10.2 Results for Significance of Categorical Variables:

Six categorical variables were considered in relation to mobility. These were depth to bedrock, geology, topographic morphology, previous movement, topographic obstacles, and type of vegetation.

10.2.1 Mobility Measure H/L:

As all categories failed at least one of the assumptions for the ANOVA, only Kruskal-Wallis tests were performed. Kruskal-Wallis tests were made for all parameters at each study area as well as for the cumulative dataset. The p-values for each tests are recorded in Table 10-5.

Of the six categorical parameters tested, all except the type of vegetation were found to have p-values less than .1 for at least one study area. Of the two study areas where enough depth to bedrock data was available for testing, only Utah South showed significant results with a p-value of .0254. However, for the Utah South study area, depth to bedrock is closely correlated to previous movement, with deep bedrock strongly associated with locations where previous movement has occurred. Additionally, the p-value of the previous movement category for Utah

South is .00340, considerably smaller than the depth to bedrock p-value. Therefore, depth to bedrock will not be analyzed further.

Table 10-5: P-values for the capacity of each categorical parameter (columns) to predict H/L for each study area and the cumulative dataset (rows).

Study Areas	Depth to Bedrock	Geology	Topographic Morphology	Previous Movement	Topographic Obstacles	Type of Vegetation
Cal. Ferndale	x	0.582	**0.057**	.124	**0.0378**	0.143
Cal. Riverton	x	0.295	0.253	**0.0402**	0.167	0.167
Colorado Springs	0.288	0.281	**0.0303**	0.136	0.491	0.466
Oregon	x	0.220	**0.0105**	0.186	**0.0109**	0.941
Utah North	x	**0.0902**	**0.0227**	x	0.194	0.314
Utah South	**0.0254**	**0.0194**	0.544	**0.00340**	0.196	0.183
Wash. Grays Bay	x	x	0.116	x	0.186	x
Wash. P. S.	x	0.181	**1.59E-04**	x	x	0.446
Cumulative Dataset	x	**2.73E-08**	**9.22E-06**	**0.0058**	0.331	0.325

Cells colored by p-value significance. Green: p > .1, Yellow: .1 > p > .05, Orange: .05 > p > .01, Red: .01 > p. "x" marks cells where data was insufficient in quantity or quality.

For geology, only Utah North and Utah South showed significant results at the $\alpha = .1$ level of significance. However, the geological formations of each individual study area are unique, and these constitute the categories used for the parameter of geology for the individual study areas. This was done to show as much detail as possible for the influence of geologies on mobility, however, because of this, the parameter of geology cannot be directly compared between study areas. Additionally, in order to make geologies comparable for the cumulative

dataset, all geologies were placed into five generalized categories (clay, granular, sandstone/siltstone, shale, and hard rock), and so the main results for the two Utah study areas cannot be compared to the cumulative dataset either.

The p-value for the cumulative dataset for geology is the most significant for any category, at 2.73E-8. Therefore, L vs H was plotted by geology in order to depict the different trends in H/L of the various underlying materials. Power fits were made and R^2 values were recorded. The plot depicting the three best represented geologies is shown in Figure 10-1, and equations with corresponding R^2 values for all geologies are recorded in Table 10-6.

Table 10-6: L vs H power regression equations and R^2 values (columns) for the cumulative dataset by geology (rows).

Geology	N*	Equation	R^2
Clay	23	$y = 2.1056\ x^{.6696}$	.487
Granular	69	$y = 1.8629\ x^{0.664}$	.593
Sandstone / Siltstone	31	$y = 1.2804\ x^{.7089}$	.586
Shale	109	$y = .2923\ x^{0.9881}$	.789
Hard Rock	51	$y = .1676\ x^{1.124}$	.847

*N specifies the number of landslides used in each geology category.

While recorded in the table, clay was otherwise excluded in the analysis because of its relatively small sample size as well as the fact that most clay landslides originated in Wash. P. S. The classification of sandstone/siltstone was excluded for similar reasons. This leaves the granular, shale, and hard rock classifications. Of these, the largest H/L values (highest exponent in the equation) are found in terrain where the dominant geology is hard rock.

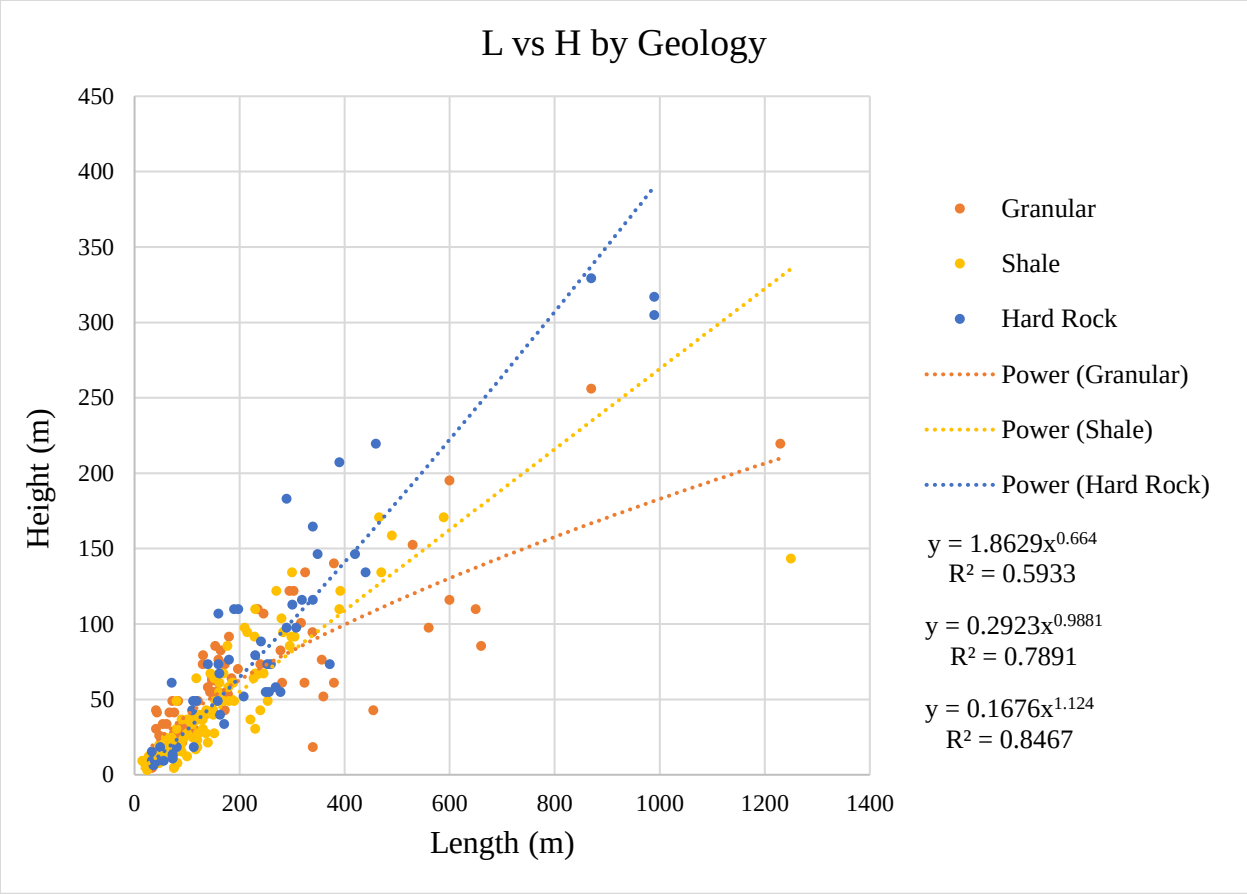

Figure 10-1: L vs H plot by geology. Regression equations are presented in the same order as the sidebar legend.

While power fits have been chosen for L vs H plots in this research, the power fits for the most mobile geology (hard rock), and the second most mobile geology (shale), can both be closely approximated as linear fits for landslides of this size. Doing this allows for the H/L values to be compared, suggesting that landslides in granular and shale-dominated geologies will on average have H/L values of at least 1.4 times the H/L values for hard rock geologies for landslides greater than 300m in length. Despite this, more data is needed to establish this relationship as a pairwise comparison of hard rock against shale does not indicate a statistically significant difference at $\alpha = .05$, although it is statistically different from granular soils. Some support is gained when the geology of Utah South is reclassified as the generalized geology (i.e.

clay, granular, sandstone/siltstone, shale, and hard rock), as it produces a similar result as the cumulative dataset. However, no other study areas have enough geological variation when classified as generalized geologies to be useful for comparison.

For topographic morphology, four of the eight study areas show a significant correlation at $\alpha = .05$ and five of the eight at $\alpha = .1$. Additionally, the p-value for the cumulative dataset is also very significant at 9.22E-6. The L vs H plot for the cumulative dataset reveals that only topographic lows are statistically different from other morphologies as seen in Figure 10-2. This was confirmed by a pairwise comparison of all morphologies which shows that topographic lows have significantly smaller values of H/L than any other morphology.

However, the cumulative dataset results for topographic lows were controlled by two study areas, Colorado Springs and Oregon. Both of these study areas showed significant correlations between topographic morphology and H/L with $p < .05$. Additionally, no study areas significantly rejected this trend. Despite this, the fact that these results rely upon only two study areas does diminish confidence that a regional trend has been discovered.

Another trend for topographic morphology is the relationship between concave, gentle, and convex morphologies, as seen in Table 10-7, which displays the mean values for each of these morphologies by study area. This trend was not well depicted in the plot of the cumulative dataset (Figure 10-2), or the pairwise comparison of the cumulative dataset. However, a close inspection of the individual study areas reveals that, as expected, gentle landslides generally have higher values of H/L than concave landslides. This trend is displayed by five study areas. A pairwise comparison of these study areas revealed only one study area (Wash. P.S.), where concave and gentle landslides displayed significant differences in medians at $\alpha = .05$. However,

of the three study areas with conflicting results, one has only a single concave landslide and the other has only three gentle landslides.

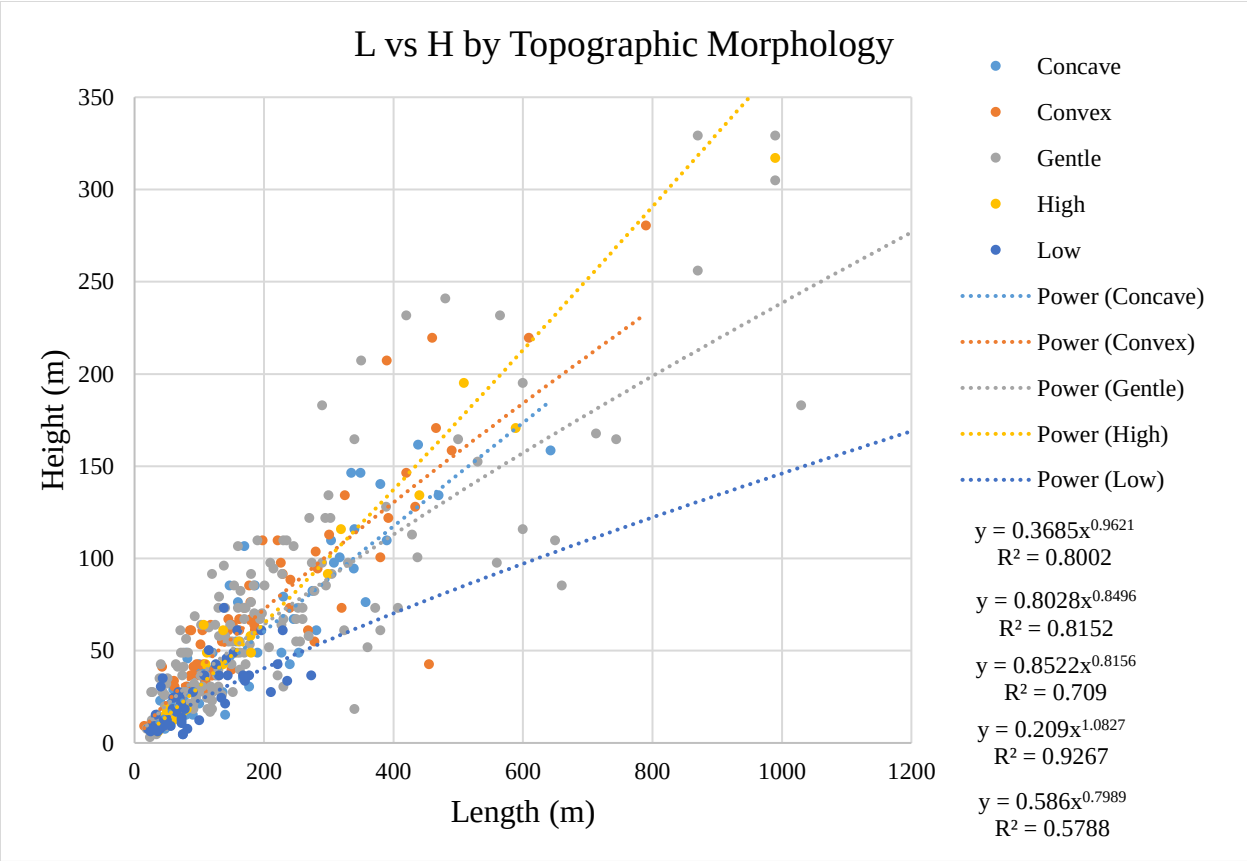

Figure 10-2: L vs H plot by topographic morphology (cumulative dataset). Regression equations are presented in the same order as the sidebar legend.

Similarly, seven of eight study areas show that convex landslides have higher median values for H/L than gentle landslides and all eight study areas show that convex landslides have higher median H/L values than concave landslides. Additionally, the one study area (Wash. P.S.) that shows convex landslides with lower H/L values than gentle landslides bases this result on only three convex landslides.

Table 10-7: Median concave, gentle, and convex landslide H/L values by study area.

Study Area	N	Concave	Gentle	Convex
Cal. Ferndale	4 / 7 / 18	.237	.288	.368
Cal. Riverton	5 / 18 / 3	.369	.408	.542
Colorado Springs	1 / 27 / 4	.277	.227	.390
Oregon	6 / 19 / 7	.282	.249	.375
Utah North	4 / 6 / 8	.210	.286	.305
Utah South	5 / 32 / 5	.281	.380	.430
Wash. Grays Bay	7 / 3 / 7	.277	.248	.346
Wash. P. S.	7 / 20 / 3	.374	.631	.550

*N specifies the number of landslides by morphology (concave / gentle / convex). Cells colored by median value, green < yellow < orange. Median values calculated for less than three landslides are colored grey.

The parameter of previous movement displayed significant results at $\alpha = .05$ for two study areas, Cal. Riverton and Utah South. Both the L vs H plots for Cal. Riverton and Utah South display the same trend: landslides located in areas with previous movement are more mobile on average than those located in areas without previous movement. A comparison of means and medians for all eight study areas reveals that only the data from Cal. Ferndale contradict this trend. This higher mobility for landslides on previously moved material is further confirmed by the cumulative dataset as seen in Figure 10-3. Comparing the slopes of the cumulative dataset regressions it can be seen that H/L values for landslides with previous movement are, on average, 0.7 times as large as those without, corresponding to 40% longer runout for a given height.

For topographic obstacles, Cal. Ferndale and Oregon showed significant results at $\alpha = .05$. Both indicated that confined landslides have lower H/L values (more mobile) than open landslides. Similarly, while not reaching the threshold of significance at $\alpha = .1$, all other study areas show the same trend for both medians and means, except for the two Utah study areas as shown in Table 10-8. Surprisingly, the cumulative dataset is not significant at $\alpha = .1$, and it shows almost no trend in its mean or median values (Table 10-8).

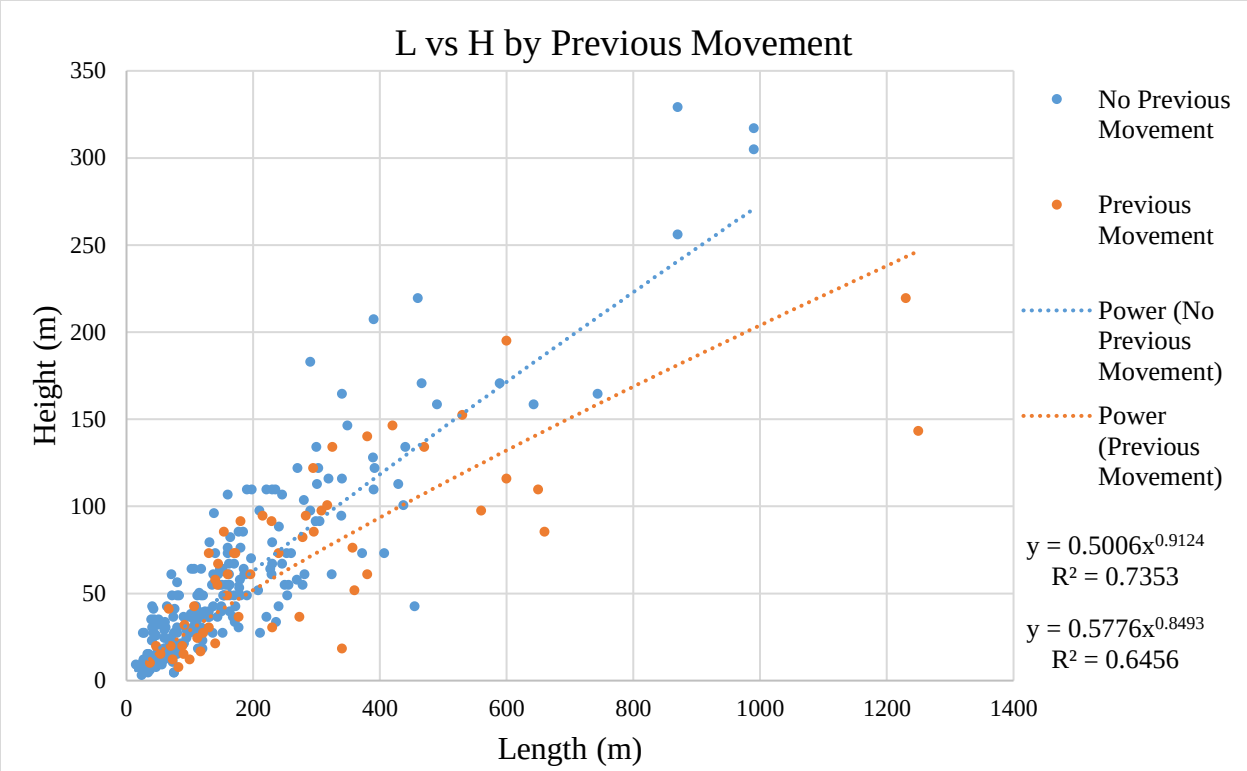

Figure 10-3: L vs H plot by previous movement (cumulative dataset). Regression equations are presented in the same order as the sidebar legend.

Table 10-8: Median and mean H/L for topographic obstacles by study area.

Study Area	N*	Confined H/L (Median)	Open H/L (Median)	Ratio O:C (Median)	Confined H/L (Mean)	Open H/L (Mean)	Ratio O:C (Mean)
Cal. Ferndale	**4 / 33**	**.295**	**.324**	**1.10**	**.275**	**.338**	**1.23**
Cal. Riverton	13 / 13	.363	.425	1.17	.389	.453	1.16
Colorado Springs	5 / 37	.190	.230	1.26	.196	.260	1.33
Oregon	**16 / 45**	**.234**	**.263**	**1.12**	**.260**	**.300**	**1.15**
Utah North	6 / 18	.305	.279	.917	.301	.275	.914
Utah South	12 / 32	.449	.334	.744	.426	.346	.813
Wash. Grays Bay	4 / 14	.248	.288	1.16	.296	.340	1.13
Wash. P. S.	1 / 29	.374	.614	1.64	.374	.615	1.65
Cumulative Dataset	61 / 221	.317	.318	1.00	.324	.357	1.10

*N specifies the number of landslides by topographic obstacle (confined / open). Cells colored by median or mean value, green < orange. Median or mean values calculated with less than three landslides are colored grey. Study areas with $p < .05$ in bold.

10.2.2 Mobility Measure L:

ANOVA and Kruskal-Wallis tests were made for all parameters at each study area and the cumulative dataset using L as the mobility measure. The p-values for each test are recorded in Table 10-9.

Table 10-9: P-values for the capacity of each categorical parameter (columns) to predict L for each study area and the cumulative dataset (rows).

Study Areas	Depth to Bedrock	Geology	Topographic Morphology	Previous Movement	Topographic Obstacles	Type of Vegetation
Cal. Ferndale	x	6.49E-06	0.838*	.861	0.457	0.632
Cal. Riverton	x	0.673	0.524	1.67E-04	0.533	0.794
Colorado Springs	5.38E-05	0.228	.0573*	8.65 E-04*	0.622	0.333
Oregon	x	0.0704	6.53E-05	0.683	0.128	0.185
Utah North	x	0.276	0.00180	x	0.712*	0.0166
Utah South	0.8667	0.247	0.0915	0.338	0.381	0.357
Wash. Grays Bay	x	x	0.167	x	0.105	x
Wash. P. S.	x	0.0541	0.645	x	x	0.698
Cumulative Dataset	x	8.33E-9*	.132	2.30E-05	9.44E-04	0.341

Cells colored by p-value significance. Green: p > .1, Yellow: .1 > p > .05, Orange: .05 > p > .01, Red: .01 > p. "x" marks cells where data was insufficient in quantity or quality. * marks places where a Kruskal-Wallis test was used instead of an ANOVA.

Of the six categorical parameters tested, all except the topographic obstacles were found to have p-values less than .1 for at least one study area. Despite this, topographic obstacles for

the cumulative dataset were found to have a p-value of 9.44E-4. Therefore, the results for all six parameters are considered.

Of the two study areas where enough depth to bedrock data was available for testing, only Colorado Springs showed significant results with a p-value of 5.38E-5. This contrasts with the H/L significance tests which found only Utah South, not Colorado Springs, to be significant for prediction. These conflicting results require additional investigation; but the current study does not have sufficient depth to bedrock data to make any meaningful conclusions, and therefore it will not be analyzed further.

For geology, only Cal. Ferndale showed significant results at $\alpha = .01$, although both Oregon and Wash. P.S. showed significant results at $\alpha = .1$. Once again, because geology is not comparable between study areas or to the cumulative dataset, these results will not be considered beyond noting that geology does seem to be a uniquely significant predictor for landslides in Cal. Ferndale, and possibly also around the Oregon and Wash. P.S. study areas.

In contrast, the cumulative dataset shows geology to be the most significant parameter for predicting L, with a p-value of 8.33E-9. The differences between geologies can be further analyzed using the box and whisker plot in Figure 10-4. The smallest L-values are represented by landslides dominated by clay. This is confirmed by a pairwise comparison of clay against all other geologies which shows a statistical difference in L-values at $\alpha = .05$. Once again, however, the small sample size and fact that most of these landslides were found in the same study area undercuts the importance of this result.

Of the three best represented geologies, the granular and hard rock materials both have similar L-values. Those landslides located in regions dominated by shales, however, have smaller L-values than either granular or hard rock geologies. A pairwise comparison of shales to

all other geology types shows that shales have significantly different mean L-values at α = .05. This result is confirmed by the Utah South study area, which has roughly even proportions of granular, hard rock, and shale geologies. Utah South is, however, the only study area which has enough variation in general geological categories to be useful for comparison. Without other individual study areas to compare against, it is hard to be sure that this trend is regional. Nevertheless, the evidence from Utah South and the cumulative dataset suggest that shales form landslides with smaller L-values than landslides formed in granular or hard rock geologies.

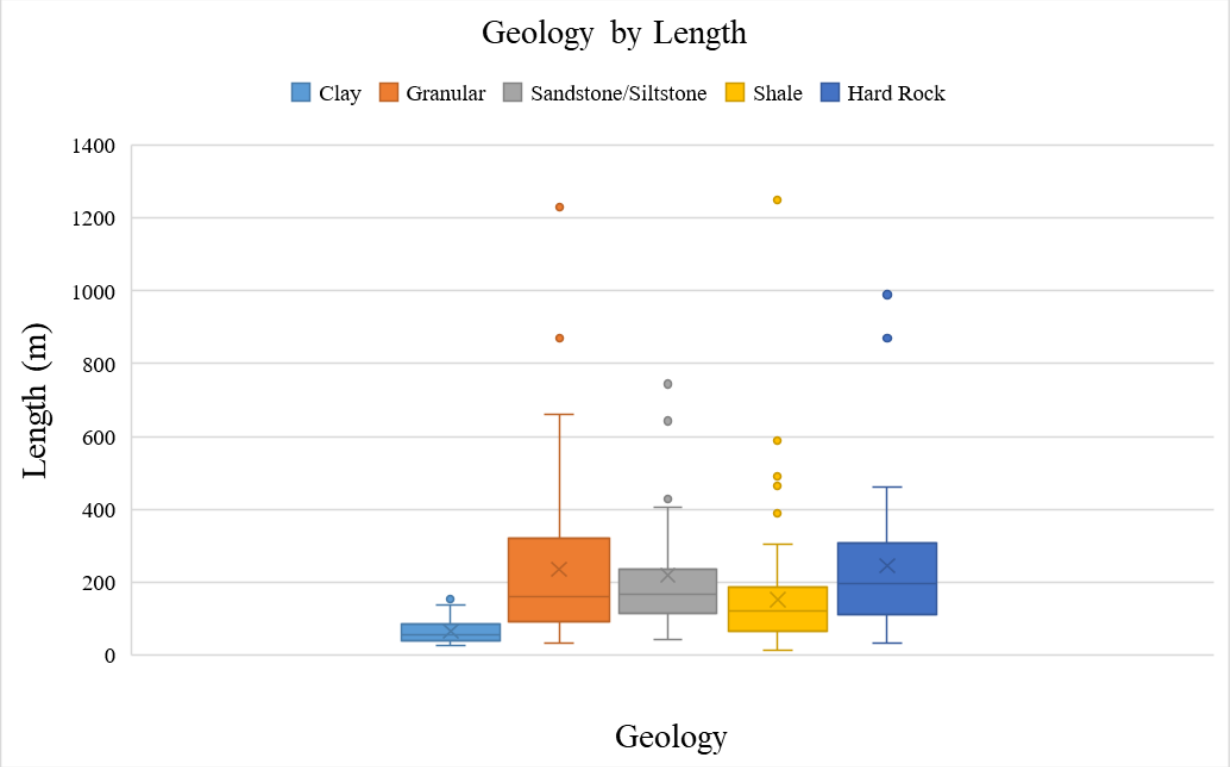

Figure 10-4: Box and whisker plot of landslides by geology (cumulative dataset).

The parameter with the strongest correlations to L for the individual study areas was topographic morphology, with two of the eight study areas displaying significant correlations at α = .01 and four displaying significant correlations at α = .1. Despite the number of study areas with significant p-values, the cumulative dataset shows almost no correlation with a p-value of

.132. To understand why local but no general trends emerge for topographic morphology, a closer look at the individual study area data is needed (see the discussion in Chapter 11). The box and whisker plots for the three study areas with the smallest p-values (Colorado Springs, Oregon, and Utah South) are provided in Figures 10-5 to 10-7. The box and whisker plot for Utah North was not included because of its close similarity to that for Utah South.

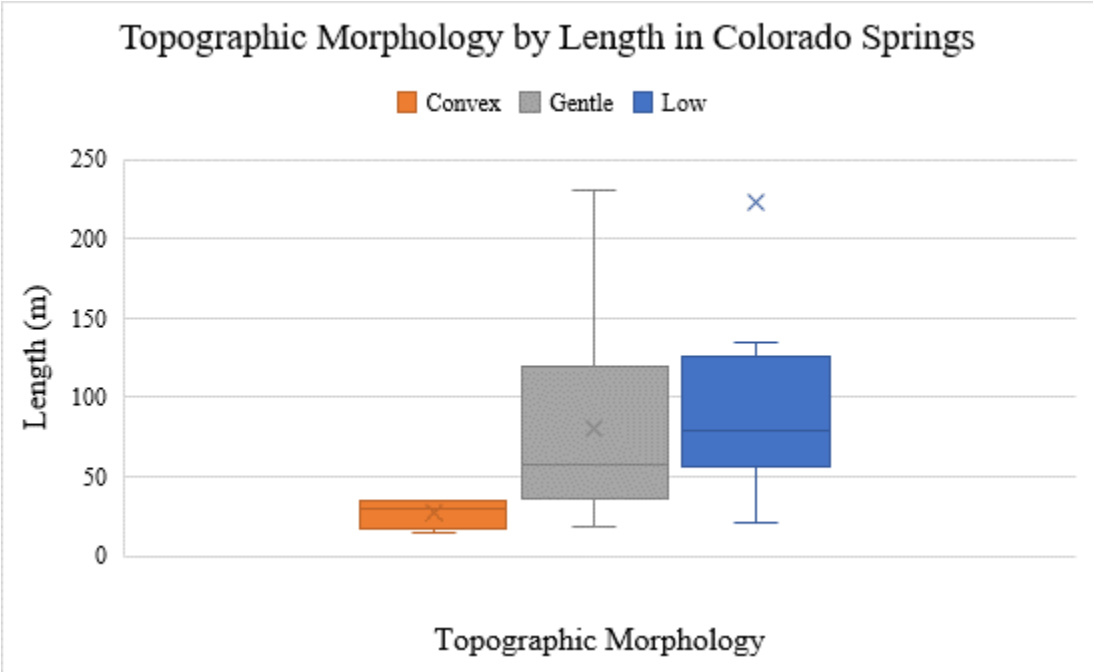

Figure 10-5: Box and whisker plot of Colorado Springs landslides by topographic morphology.

The parameter of previous movement displayed significant results at $\alpha = .01$, for two study areas, Cal. Riverton and Colorado Springs. For both Cal. Riverton and Colorado Springs, landslides originating over previously moved material have considerably greater mobility than those with no prior movement. A closer look reveals that all individual study areas have longer median and mean L-values for previously moved material, as shown in Table 10-10.

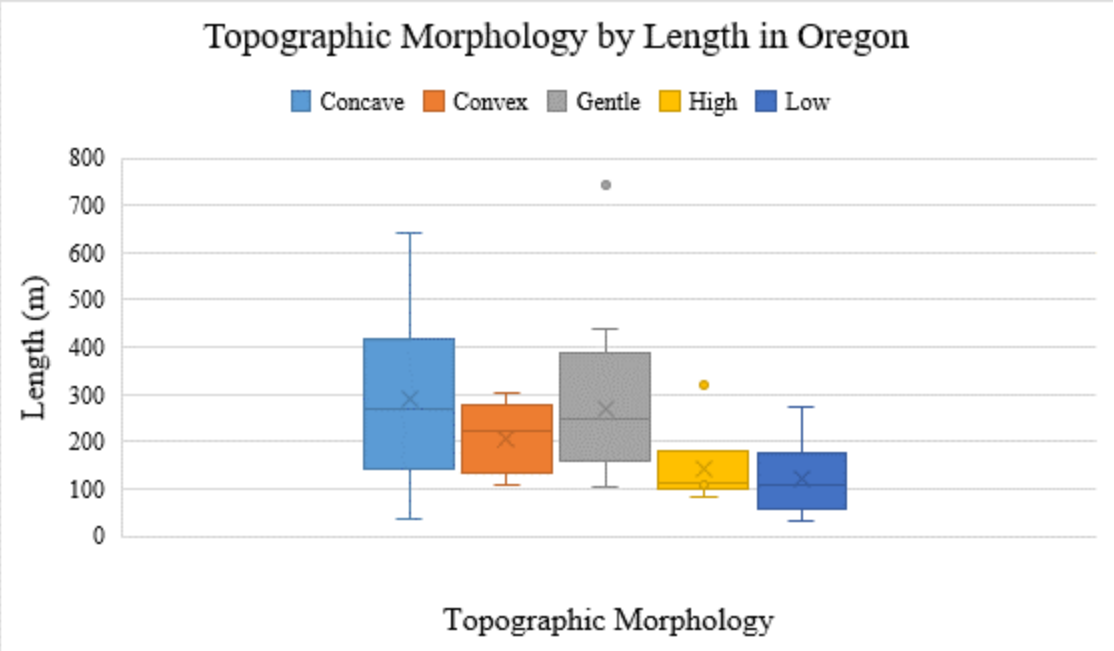

Figure 10-6: Box and whisker plot of Oregon landslides by topographic morphology.

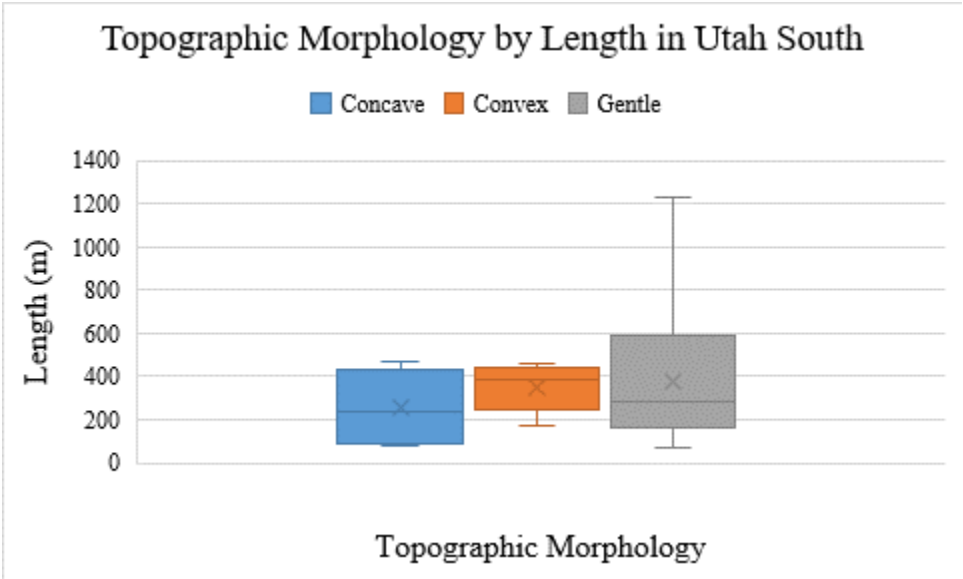

Figure 10-7: Box and whisker plot of Utah South landslides by topographic morphology.

Finally, the cumulative dataset also indicates a significant correlation between L and previous movement with a p-value of 2.30E-05, and displays the same trend as Cal. Riverton and Colorado Springs as seen in Figure 10-8. It shows the mean length for landslides occurring on previously moved material to be about 1.5 times longer than other landslides (Table 10-10).

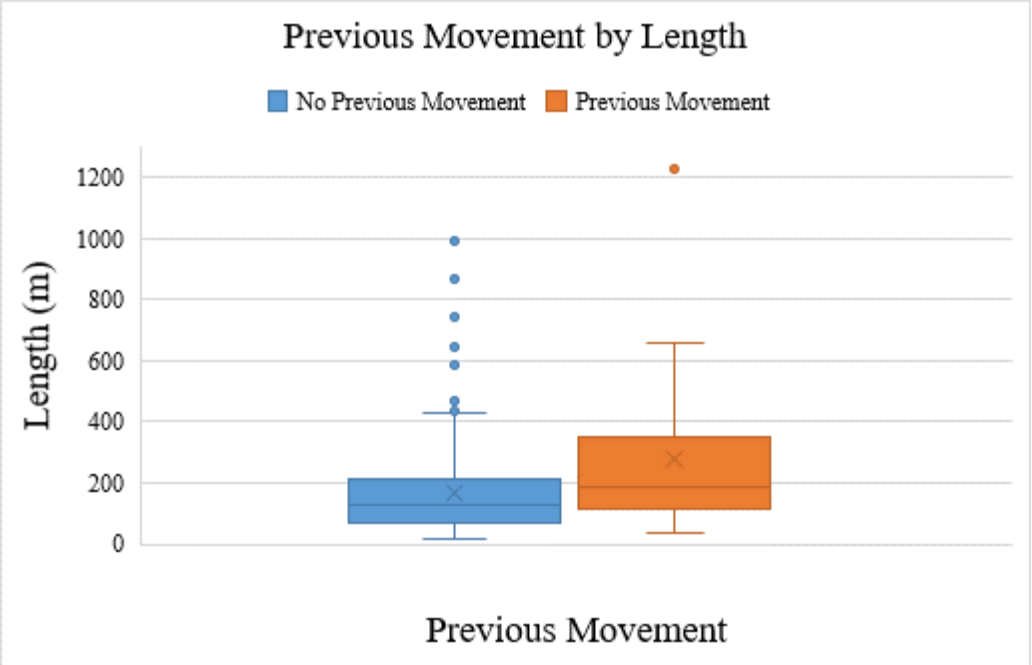

Figure 10-8: Box and whisker plot of landslides in cumulative dataset by previous movement.

Table 10-10: Ratios of previously moved landslides to not previously moved landslides by median and mean L-values.

Study Area	N (Number of Previously Moved / Number of Not Previously Moved)	Median Previous Movement L / Median No Previous Movement L	Mean Previous Movement L / Mean No Previous Movement L
Cal. Ferndale	6 / 31	1.36	1.01
Cal. Riverton	9 / 17	1.88	1.68
Colorado Springs	13 / 29	2.08	3.24
Oregon	6 / 55	1.14	1.01
Utah North	1 / 23	1.40	1.41
Utah South	18 / 26	1.40	1.18
Wash. Grays Bay	1 / 17	2.27	1.98
Wash. P.S.	2 / 28	1.51	1.19
Cumulative Dataset	56 / 226	1.49	1.64

As already noted, topographic obstacles is the only parameter where no study areas were found with significant results at $\alpha = .1$. Despite this, the p-value for the cumulative dataset is 9.44E-04. The effect of topographic obstacles can be further analyzed using the box plot in

Figure 10-9. According to this, on average, landslides that occur in confined topography travel about 1.3 times farther than landslides that occur in open topography.

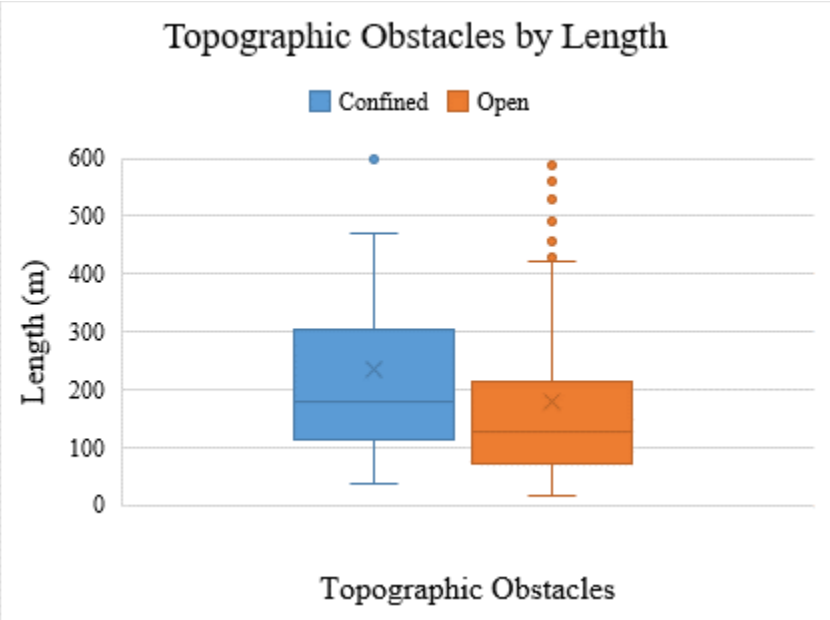

Figure 10-9: Box and whisker plot of confined and open landslides. (Cumulative Dataset)

This result is confirmed by the individual study areas which show, in Table 10-11, that both medians and means of confined landslides were larger for five study areas. Two study areas displayed larger median values for confined landslides but smaller mean values. Both of these study areas, however, had relatively small proportions of confined landslides with both Cal. Ferndale and Colorado Springs at around 10% confined events. For both cases, the means for open topography landslides are highly dependent upon a few extremely large events. Finally, only Cal. Riverton showed both larger mean and median values for open topographies. It is unknown why this is the case, however, as the dataset is so small, this result is based on only a few landslides.

Table 10-11: Median and mean landslide L-values (meters) for topographic obstacles.

Study Area	N	Confined L (Median)	Open L (Median)	Ratio C:O (Median)	Confined L (Mean)	Open L (Mean)	Ratio C:O (Mean)
Cal. Ferndale	4 / 33	190	177	1.08	186	213	.872
Cal. Riverton	13 / 13	148	190	.779	181	228	.793
Colorado Springs	5 / 37	51	50	1.02	58.6	103	.567
Oregon	16 / 45	245	137	1.79	274	168	1.63
Utah North	6 / 18	115	85	1.35	112	97.3	1.15
Utah South	12 / 32	320	275	1.16	387	374	1.03
Wash. Grays Bay	4 / 14	310	151	2.05	284	164	1.74
Wash. P. S.	1 / 29	102	54	1.88	102	66.2	1.54
Cumulative Dataset	**61 / 221**	**180**	**128**	**1.41**	**235**	**178**	**1.32**

*N specifies the number of landslides by topographic obstacle (confined / open). Cells colored by median or mean value, green > orange. Median or mean values calculated with less than three landslides are colored grey. Datasets with $p < .05$ in bold.

Finally, type of vegetation only shows significant results in Utah North. The cumulative dataset also does not show a significant response to the type of vegetation. For these reasons, vegetation will not receive any additional analysis beyond the note that it may be useful for prediction in the area around the Utah North study area.

10.3 Results for All Parameters using Multiple Regressions:

Multiple regressions were created using both the continuous and categorical variables.

10.3.1 Mobility Measure H/L:

Multiple regressions to predict H/L were created for all study areas and the cumulative dataset. Clay and Sandstone/Siltstone geologies were excluded from the cumulative dataset regression due to local biases, however all other categorical variables were included. Regression equations, descriptions of variables, R^2, and p-values are recorded in Tables 10-12. All regressions were found to have significant correlation to H/L at $\alpha = .05$, and the p-value for the cumulative dataset was found to be 3.74E-62.

The ISA appears in the regressions for all eight study areas as well as the cumulative dataset, and is the most significant parameter. This agrees well with the findings in the initial analysis (see Table 10-1). For example, Cal. Ferndale displays the weakest correlation between ISA and H/L and has the largest multiple regression p-value. Conversely, Oregon has the strongest correlation between ISA and H/L and has the smallest multiple regression p-value.

Previous movement and topographic obstacles appear the second most with three of the eight study areas using these each. Surprisingly, geology, which was more significant than previous movement or topographic obstacles (see Table 10-5), was never used. Therefore, the continuous data analysis matches well with the multiple regressions for H/L, but the categorical data analysis does not.

The prediction of long-runout (in the form of H/L) using all parameters in the Western United States is most completely conveyed in the multiple regression of the cumulative dataset. In order to visualize these results the values predicted for H/L by the regression equation were plotted against the actual H/L values for those landslides (Figure 10-10).

To validate the multiple regression equation with data not used in its creation, the landslides classified as striking an opposing wall were added to the plot. The wall landslide data was found to have an R^2 of .4585 verses an R^2 of .6383 for the non-wall data. The lower R^2 for the validation data is somewhat expected as Corominas (1996) found that wall landslides contain more scatter of H/L than non-wall landslides. However, it may also indicate that the multiple regression did not predict the H/L values for the validation (wall) data as well as the creation (non-wall) data. The other test for prediction was the relative positions of the regression fits. The fits for both the validation and creation data were constrained to pass through the origin, however, no other constraints were placed on the validation data fit. (Note that the creation data

lies right along the 1:1 predicted vs actual line.) As seen in Figure 10-10, the linear fit for the validation data nearly overlaps that of the creation data.

Table 10-12: Presents equations and variables of multiple regressions (columns) in predicting H/L.

Study Area	Equation	x1	x2	x3	R^2	p-value
Cal. Ferndale	$.238 + .00442(x1) + .0657(x2)$	ISA	TO	-	0.192	**1.25E-02**
Cal. Riverton	$.156 + .0135(x1) - .0897(x2) - .0475(x3)$	ISA	TO	PM	0.697	**1.96E-09**
Colorado Springs	$.00295 + .0171(x1) - .0091(x1)(x3) + .0788(x2) + .0883(x3)$	ISA	M (convex)	PM	0.809	**3.76E-13**
Oregon	$-.00512 + .0164(x1)$	ISA	-	-	0.768	**1.01E-27**
Utah North	$.0721 + .0106(x1) + .000114(x2)$	ISA	WPC	-	0.635	**3.70E-08**
Utah South	$.0889 + .012(x1)$	ISA	-	-	0.534	**1.13E-09**
Wash. Grays Bay	$.0734 + .146(x1)$	ISA	-	-	0.378	**2.33E-04**
Wash. P.S.	$.375 + .00823(x1) - .219(x2) - .158(X3)$	ISA	M (concave)	PM	0.567	**1.05E-06**
Cumulative Dataset	$.1012 + .010621(x1) + .0045771(x1)(x2) - .066766(x2)$	ISA	TO	-	0.638	**4.27E-61**

Note: all variables are listed from most to least significant (x1=most significant, x3=least significant). TO: topographic obstacles, PM: previous movement, M: topographic morphology. P-values less than .05 in bold.

This suggests two things. First, it is improbable that the fits align so closely by chance, suggesting that the multiple regression does a good job in predicting H/L for data from the current study areas. Second, it suggests that there is little difference in the average H/L values due to contact with an opposing wall.

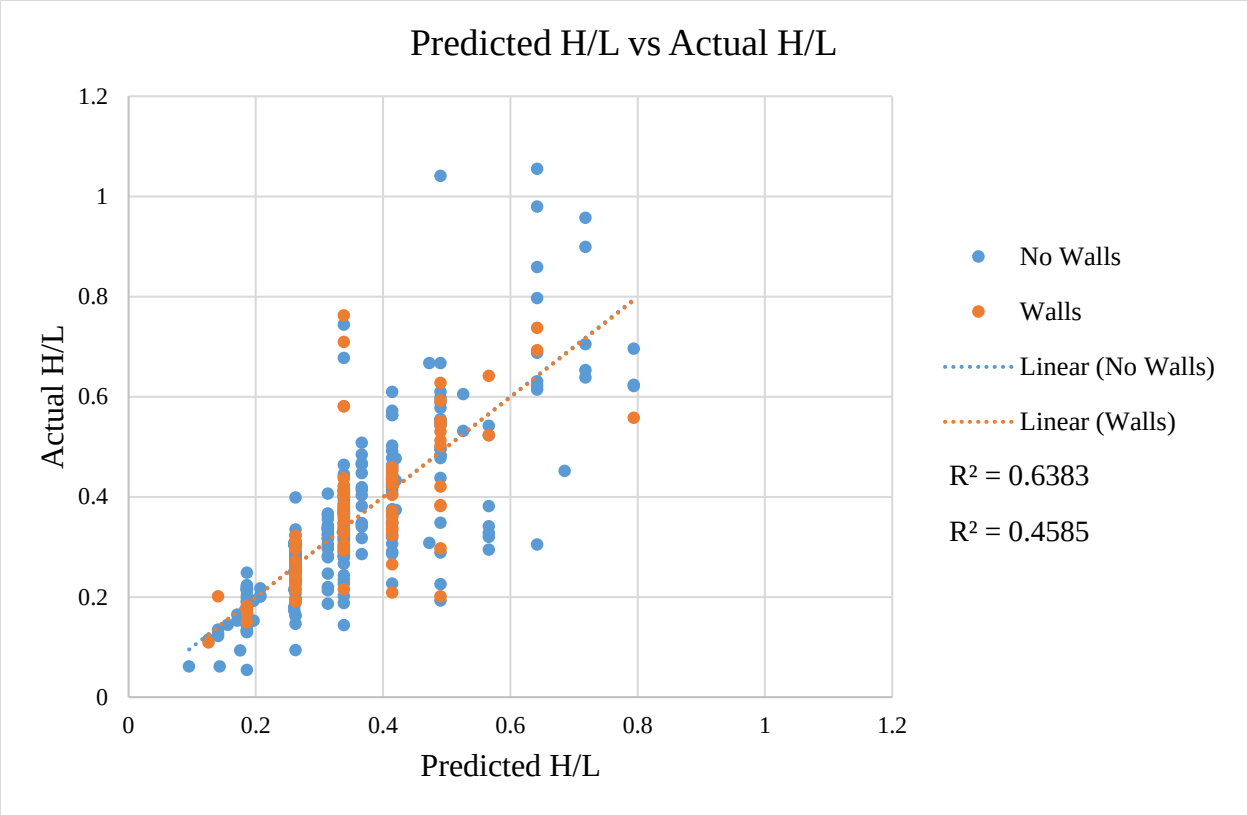

Figure 10-10: Plot of the predicted values for H/L against the actual values of H/L both with and without opposing wall classified landslides. R^2 values are presented in the same order as the sidebar legend.

10.3.2 Mobility Measure L:

For L as a mobility index, the regressions for six of eight study areas were found to have a significant correlation at $\alpha = .05$ (see Table 10-13). The p-values for L prediction for almost all study areas, as well as the cumulative dataset, were found to be less significant than those of H/L. Additionally, all study areas except for Cal. Ferndale also had lower R^2 values for the L prediction equations. Therefore, the L prediction equation is both more poorly correlated and less significant than the equation predicting H/L.

Also, unlike the regressions for H/L the regressions for L are found to closely match the categorical variable analysis. For example, the most commonly appearing parameter for $\log_{10}(L)$ is some aspect of the local geology, appearing four times in the eight regression equations and

once for the regression of the cumulative dataset. This corresponds very closely to the analysis of the categorical variables in Table 10-9, which lists significant p-values for local geology for the same study areas where geology was used in the regression. Additionally, the second most commonly appearing parameter is previous movement which appears only twice among the individual study areas and again for the cumulative dataset. This also corresponds closely to the categorical variable analysis in Table 10-9. Therefore, while the significant categorical variables for H/L were not well represented in the regressions, the significant categorical variables for L were well represented.

Table 10-13: Presents equations and variables of multiple regressions (columns) in predicting $\log_{10}(L)$ for each study areas and the cumulative dataset (rows).

Study Area	Equation	x1	x2	R^2	p-value
Cal. Ferndale	$2.08 + .419(x1) + .17(x2)$	G(*)	G(**)	0.536	**2.11E-06**
Cal. Riverton	$2.18 + .225(x1)$	PM	-	0.27	**6.55E-03**
Colorado Springs	$2.02 + .375(x1) - .0236(x2)$	PM	ISA	0.43	**1.73E-05**
Oregon	$2.27 - .517(x1) + .305(x1)(x2) + .0785(x2)$	M(low)	G(sandstone /siltstone)	0.387	**3.49E-06**
Utah North	$1.87 + .178(x1)$	M(gentle or convex)	-	0.248	**1.32E-02**
Utah South	$2.25 + .000444(x1) + .199(x2)$	WPC	G(Qmw)	0.184	**1.56E-02**
Wash. Grays Bay	$1.75 + .218(x1)$	TO	-	0.216	5.22E-02***
Wash. P.S.	$2.14 + .296(x1)$	G(gravelly sand)	-	0.102	8.51E-02***
Cumulative Dataset	$2.09 + .251(x1) + .000407(x2) - .155(x3)$	x1: PM	x2: WPC	x3: TO	0.17	**3.41E-11**

Note: all variables are listed from most to least significant (x1=most significant, x3=least significant). G: geology, PM: previous movement, M: topographic morphology, *: sandstone with interbedded shale, **: weakly lithified siltstone, sandstone, and mudstone, ***: p-value threshold for variable inclusion was increased to .1. P-values less than .05 in bold.

CHAPTER 11

DISCUSSION OF RESULTS AND SYNTHESIS WITH PREVIOUS RESEARCH

Several important observations warrant more detailed discussion:

- ISA strongly predicts H/L,
- A does not predict H/L well,
- A and WPC/A both predict L,
- There is sometimes a disconnect between the results of individual study areas and the cumulative dataset,
- Geology, topographic morphology, previous movement, and topographic obstacles may predict H/L,
- Geology, previous movement, and topographic obstacles may predict L,
- The results of the multiple regressions for H/L strongly agree with the continuous variable analysis, but seem to disagree with the categorical variable analysis, whereas the results for L generally agree with both the continuous and categorical variable analyses, and
- Some multiple regressions have low R^2 or p-values while others are more promising.

11.1 Capacity of ISA to Predict H/L:

Significant correlations of ISA to H/L were found both in the continuous variable analysis and the multiple regression analysis. Similarly, in previous studies, strong correlations between ISA and H/L have been noticed for flows, (Iverson et al., 2015) and possibly rock avalanches (Keefer, 1984). Despite this, these previous studies have supported the intuitive conclusion that steeper ISAs lead to smaller H/L values. In contrast, the current study found that steeper ISAs lead to larger H/L values. There are three explanations for this.

First, the current study is composed of relatively small translational and rotational landslides. Less than 6% of the slides considered in this study possess areas in excess of $1x10^5$ m^2, so many of the landslide lengths are relatively small compared to the slope lengths on which they initiated. Because of the relatively small sizes of these landslides, they are less likely to cross a significant break in the slope, and without a change in the slope grade, it is geometrically impossible for the H/L value to deviate significantly from the ISA.

Second, as a mobility measure, H/L does not take the average displacement of particles into account. This means that a very large landslide might move only a few inches, but could still be "long-runout" according to the mobility measure H/L, if the length from the head to toe of the landslide was large in comparison to the height. The deeper failure surfaces associated with many translational and rotational landslides means that when they reach a break in slope, the break itself is likely to stabilize the landslide toe, decreasing the chance of continued movement. This prevents translational and rotational landslides from diverging greatly from ISA. In contrast, the flows of Iverson et al. (2015) and rock avalanches of Keefer (1984) are more likely to travel above the ground surface and have large average particle displacements. These parameters increase the chance that flows and rock avalanches reach and traverse a break in the slope, leading to smaller H/L values.

Third, translational and rotational landslides are likely to break apart and adopt a different movement type if they move too far and their average particle displacement becomes too great. Therefore, the larger the particle displacements in a landslide (which are needed to increase the chance of reaching a break in the slope), the less likely an event is classified as primarily translational or rotational.

11.2 Capacity of Area to Predict H/L:

There is a general consensus that as volume increases, so does H/L. While volumes were not estimated for this project, areas were calculated for all landslides, and it has been shown that areas and volumes are closely correlated (Legros, 2002). Nonetheless, little evidence for a strong correlation between area and H/L was found. A number of authors have expressed concern that the relationship between volume and H/L fails to hold true for smaller landslides (Scheidegger, 1973; Hsu, 1975), which might explain the general lack of correlation found in the current study, which is dominated by smaller landslides. Corominas (1996), however, disagrees, claiming that even small landslides can display decreasing H/L values with increasing landslide volume. The current research suggests that the relationship between area (or volume) and H/L may hold for small landslides at some locations, however, the dominant predictor of H/L for small landslides is ISA.

11.3 Capacity of Area and WPC/Area to Predict L:

Area is not generally a strong predictor of mobility although it can be used in special circumstances (Scheidegger, 1973). However, a strong connection between A and L was found in the current study, which is intuitive: while transitional and rotational landslides exhibit a range of different shapes, in general the length of the landslide increases with increasing area. Therefore, if A can be reliably estimated prior to failure, then its length can probably also be reliably estimated, so correlation between A and L is not required in order to estimate L.

The relationship between L and WPC/A is probably not useful for prediction either. WPC/A is still requires an estimate of A. Moreover, the correlation between A and L is stronger than WPC/A and L. Thus, if A is already known, there is no reason to use it to calculate the inferior predictor WPC/A.

11.4 Differences between Results of Individual Study Areas and the Cumulative Dataset:

For both the continuous and categorical data analyses the results of individual study areas differed from each other and from the cumulative dataset. Several important differences were considered in detail, and a summary of possible explanations for other cases was tabulated (see Table 11-1).

11.4.1 Topographic Obstacles and H/L:

Surprisingly, while two study areas show a significant correlation between confined landslides and low H/L values, and most other study areas support this trend, the cumulative dataset does not indicate a significant correlation (Table 10-8). This is a statistical problem caused by combining datasets from diverse study areas into a cumulative dataset. The values of H/L vary widely between the eight study areas, and therefore relatively mobile landslides in one study area are relatively immobile landslides in another. For example, in Cal. Riverton where the topography is steep, the mean H/L for confined landslides is .389, but in Colorado Springs where the topography is smooth, the mean H/L for open landslides is .260 (Table 10-8). This problem compounds when the numbers of confined landslides in high H/L study areas are relatively large compared to the number of open landslides, and vice versa. Cal. Riverton has 13 confined landslides and 13 open landslides. In contrast, Colorado Springs has only five confined landslides and 37 open landslides. This heavily weights the results towards the relatively immobile confined landslides and also relatively mobile open landslides. Adding in the opposing trend of the two Utah study areas, and the cumulative dataset supports a conclusion that is contrary to almost every study area that composes it. The same statistical problem explains the failure of the cumulative dataset to statistically demonstrate the relative mobility (for H/L) of concave landslides as compared to convex landslides, a trend supported by all eight study areas (Table 10-7).

11.4.2 Topographic Morphology and H/L:

All eight study areas indicate that landslides in concave topography have lower H/L values than landslides in convex topography, but it is less clear that they have lower H/L values than landslides in gentle topography. Only five study areas display this relation. Of the three that display the opposite trend, two have relatively low numbers of concave or gentle landslides, but the third does not. Additionally, the most significant evidence that concave landslides have lower H/L values than gentle landslides comes from Wash. P.S. However, an examination of the Wash. P.S. study area reveals that almost all concave slopes are found in shallow inland gorges, while almost all gentle morphologies are located on the steep cliffs bounding the Puget Sound. Furthermore, the connection between ISA and H/L suggests that because the inland gorges are shallow they will tend to produce landslides with lower H/L values, and because the cliffs are steep, they will tend to produce landslides with higher H/L values. Therefore, the strong results of the Wash. P.S. study area may be explained as a local correlation between topographic morphology and ISA. This somewhat undercuts the evidence that concave landslides have lower H/L values than gentle landslides. Overall, the claim that concave landslide are more mobile than gentle landslides is intuitive, and the evidence does seem to favor this conclusion; however, the evidence is less compelling than for the relationship between concave and convex landslides.

11.4.3 Topographic Morphology and L:

Colorado Springs, Oregon, Utah North, and Utah South all display significant correlations between topographic morphology and L. Despite this, the specific relationships displayed by these study areas differ and the cumulative dataset showed no general correlation between topographic morphology and L. In this case, topographic morphology and L are probably complexly related to other parameters causing only local trends but no universal trends.

For instance, concave morphologies have proportionately larger L-values in comparison to other morphologies in Oregon than they do in the two Utah study areas. This could be due to a difference in climate. The wetter climate in Oregon may lead to larger slope failures, especially in concavities where the water table is closer to the surface, and the dense vegetation prevents small, shallow slope failures (Montgomery et al., 2000). In contrast, the arid climate and sparse vegetation in Utah may produce more frequent but shallower slope failures, removing material and leaving less to fail in large events, especially around concavities where erosion is high. This, however, is only one possible explanation. There are numerous unknown parameters such as the rockmass quality of the bedrock, the porosity of the soil, the precise clay content of the soil, and the permeability of the bedrock. Any of these factors or others could be contributing to the differences between Oregon and Utah.

11.4.4 Other Differences:

Some additional differences between individual study areas and the cumulative dataset have been tabulated and possible explanations for these anomalies are provided (see Table 11-1).

Table 11-1: Additional differences between study areas and cumulative dataset with possible explanations.

Difference	Possible explanations for differences.
Weak correlation between H/L and ISA in Cal. Ferndale, Wash. Grays Bay, and Wash. P.S.	All are coastal study areas. The most anomalous landslides runout into the sea, so establishing accurate H/L values is therefore difficult.
Strong correlation between L and WPC in Cal. Ferndale.	Locally, largest failures are on the tops of hills and far away from streams, with small failures located near rivers or along coast.
No correlation between L and WPC/A in Cal. Ferndale.	Mathematical consequence of strong correlations with both WPC and A, so the effects are cancelled.
No correlation between L and WPC/A in Utah North.	Correlations between WPC/A and L are controlled by the correlation between A and L. Utah North has the weakest correlation between A and L.
Colorado Springs correlates strongly with L for depth to bedrock but not H/L. Utah South displays opposite trend.	No real disagreement. There is a weak correlation between Colorado Springs and H/L, it is just not statistically significant. The same is true for Utah South and L.

Table 11-1: Continued.

Concave landslides have larger H/L than gentle landslides in Oregon.	Unknown – may be related to wet climate and heavy vegetation, or gentle slopes may be more susceptible to failure along regional bedding planes.
Larger H/L for slides in previously moved material in Cal. Ferndale.	Much previously moved material lies on steep cliffs or hills. Cause: erosion of coastline and many self-stabilizing failures periodically reinitiated in hills.
Opposite relation between confined and open landslides for H/L in both Utah study areas.	Large landslides located in less steep topography, and confined landslides primarily in steep topography.
Larger mean and median values for L in open topographies in Cal. Riverton.	Most regions of confined topography are narrow so larger landslides do not fit.

11.5 Categorical Variables that Predict H/L:

The current research suggests that geology, topographic morphology, topographic obstacles, and previous movement may be used to predict H/L and this is consistent with some previous work on landslide mobility. For geology, many of the individual study areas do not possess enough geological variability within them to produce significant correlations to H/L. This partially undermines the conclusion that general geological categories can be a useful predictor for H/L. Despite this, the general geological categories are well represented in the cumulative dataset and suggest that landslides in granular soils (and possibly shale) possess smaller H/L values than landslides in regions underlain by hard rock. This could be caused by the contraction and resulting increase in pore water pressure of granular soils with large void ratios (Iverson et al., 2016) or the potential for grain crushing in predominantly granular material (Sassa, 2000). Alternatively, if this trend applies to shales, then the higher proportions of fines available in weathered shales may facilitate mobile failures (Wang and Sassa, 2003). These correlations are promising, and a more thorough investigation into the relationships between general geological categories and mobility would be valuable.

Topographic Morphology may be used to predict H/L for topographic lows. Multiple mechanisms of long-runout require shallow water tables and deep bedrock characteristic of topographic lows in order to explain mobile translational landslides in soil (Hutchinson et al., 1971); (Chandler, 1972); (Sassa, 2000). The geology of many topographic lows may also relate to other antecedent conditions for highly mobile failures, such as an accumulation of fine grain sizes (Wang and Sassa, 2003). However, as the majority of the topographic lows were located in just two study areas, this conclusion, while plausible, is not adequately supported by the findings of the current study.

Despite this, the current study does provide strong evidence that concave topographies produce smaller H/L values than convex topographies. The relatively shallow water tables expected in concave topographies and deep water tables expected in convex topographies makes this conclusion intuitive. Water could fluidize the bottom of a translational landslide without saturating the entire mass (Legros, 2002). This would allow the landslide to travel farther and reach a break in the slope resulting in a lowered H/L value.

A similar argument applies to confined topographies, or hollows, which are locations where surface water collects, and groundwater is routed (McKenna, 2011). Additionally, confined topographies may keep material from spreading laterally which retards movement for some kinds of landslides (Corominas, 1996), although some researchers contradict this idea, claiming that spreading of landslides does not reduce travel distance (Johnson et al., 2016). Finally, the geology along the interior of hollows may be significant for landslide mobility. Previous research suggests that hollows cutting into bedrock are more likely to result in rapid landslides (May, 2004), and rapid landslides are more likely to traverse a break in slope.

Finally, previous movement can be used to predict H/L, which is unsurprising in light of previous work on landslide mobility. For example, Skempton (1964) argued that failure surfaces that have already moved will have less resistance to future failures. The current study did not distinguish between recently reactivated failure surfaces and landslides that are merely occurring over materials deposited by previous mass wasting events. Therefore, some landslides classified as occurring on previously moved material may have propagated along reactivated failure planes. Other related principles are also likely at work, however. Specifically, the loosely packed grain structures associated with mass wasting deposits will tend to consolidate when sheared, causing an increase in pore-water pressures and decrease in grain friction (Iverson et al., 2000; Iverson et al., 2016). Previous movement may therefore provide a useful proxy in locating soils at risk for mobile failures due to large initial soil porosities. These deposits may also be at elevated risks for proposed mechanisms of long-runout landslides such as grain crushing (Sassa, 2000).

11.6 Categorical Variables that Predict L:

The current research suggests that geology, previous movement, and topographic morphology can all be used to predict L. The correlation between geology and L suggests that landslides located in regions dominated by shales have smaller L-values than either granular or hard rock regions, but why this is the case is unclear. Three explanations are considered. First, shale layers may fail more readily than other rock types and therefore they disintegrate through numerous smaller events. Second, topography dominated by shale may be smoother or have less relief than those dominated by other rock types, and therefore there is less potential energy released during a failure resulting in a smaller L. Third, the added cohesion of clay minerals reduces the deformation during failure and resists elongation of the failing mass. Regardless, this conclusion is not in conflict with the possibility of shales having smaller values of H/L. The two mobility measures are distinct and so shales can be both mobile on one measure (i.e. H/L)

and not mobile on another (i.e. L). However, the absence of more than one study area with both significant quantities of shales and other geologies makes it difficult to verify these conclusions.

Previous movement can also be used to predict L, with the mean length for landslides occurring on previously moved material being 1.5 times longer than other landslides. The cause of this is likely very similar to the cause of low H/L values for landslides in previously moved material.

Finally, the current research suggests that landslides that occur in confined topography are likely to travel farther than landslides that occur in open topography. The cause of this is also likely similar to the cause of low H/L values for these landslides.

11.7 Continuous, Categorical, and Multiple Regression Analysis:

The results of the multiple regressions for H/L strongly agree with the continuous variable analysis, but seem to disagree with the categorical variable analysis. In contrast, the multiple regressions for L generally agree with both the continuous and categorical analyses. There are two reasons for this. First, ISA is significant in predicting H/L, which may reduce the relative significance of categorical variables for the multiple regressions. No similarly dominant continuous variable was used in the multiple regression analysis of L. Second, in order to use categorical parameters in the multiple regressions, the subgroups of each category needed to be replaced with semi-quantitative dummy variables, where the number of dummy variables is one less than the number of subgroups. The effect of this was to divide the informational content of a single parameter into several parameters, making the resultant parameters less significant. This is why parameters such as topographic obstacles and previous movement, which each had only two subgroups, were used more frequently than more significant parameters such as geology or topographic morphology in the H/L regressions.

11.8 Quality of Multiple Regressions:

The R^2 and p-values for multiple regressions predicting L were generally low, and therefore the equations are probably not useful for prediction. In contrast, the multiple regressions predicting H/L possessed higher R^2 and lower p-values. However, when tested for normality of residuals and homoscedasticity, all of the regressions predicting H/L failed to pass at least one of the tests. Nevertheless, while the R^2 value for the cumulative dataset multiple regression predicting H/L was lower when tested against wall data, this was not unexpected, and the R^2 was still good. Therefore, cumulative dataset multiple regression predicting H/L seems to approximate H/L reasonably well.

CHAPTER 12

CONCLUSIONS

The current research has involved the collection and analysis of 282 non-wall landslides from eight study areas and the cumulative dataset that resulted from their compilation. From this research, a number of key conclusions can be identified. Some of these observations (noted below) are based on the cumulative dataset and should be considered tentative because there may be other contributing factors encompassed by the geographic and geologic breadth of the cumulative group. The current research suggests that:

- H/L and L are both excellent mobility measures, with minimal similarity, strong correlations, and high utility.
- Initial Slope Angle (ISA) strongly predicts H/L for small landslides where the material does not traverse across a break in slope.
- Area does not predict H/L well for small landslides.
- Landslides in concave topography are likely to have smaller H/L values than landslides in convex topography.
- H/L values for landslides with previous movement are 0.7 times as large on average as other landslides (Based on the cumulative dataset).
- Landslides in confined topography are likely to have smaller H/L values than landslides in open topography.
- Landslides occurring on previously moved material are generally about 1.5 times longer on average than other landslides (Based on the cumulative dataset).
- Landslides occurring in confined topography generally travel about 1.3 times farther on average than landslides that occur in open topography (Based on the cumulative dataset).

- H/L was found to be approximated reasonably well by the following equation:

$$.1012 + .010621(\text{ISA}) + .0045771(\text{ISA})(\text{TO}) - .066766(\text{TO})$$

  (This equation should only be used for translational or rotational landslides in the Western United States with an expected area smaller than 1×10^5 m^2.)

- L was not well approximated by a multiple regression equation.

While the initial results appear promising, incorporation of additional study areas could add new insights and increase the statistical significance of general conclusions about mobility in the Western United States. One suggestion for future research would be the assessment and possible incorporation of $L/(A^{1/2})$ as a mobility measure quantifying the elongation of landslides. This new measure could replace L/A as a dimensionless variable, and may avoid some of the limitations associated with L/A.

REFERENCES

Baldwin, E. M. (1956). *Geologic map of the lower Siuslaw River area, Oregon* [Map]. Washington, D.C.: The Survey.

Baldwin, E. M. (1961). *Geologic map of the lower Umpqua River area, Oregon* [Map]. Washington, D.C.: The Survey.

Baum, R. L., Harp, E. L., & Hultman, W. A. (2000). *Map Showing Recent and Histrorical Landslide Activity on Coastal Bluffs of Puget Sound between Shilshole Bay and Everett, Washington* [Map]. U.S. Geological Survey.

Brunsden, D. (1984). Chapter 9: Mudslides. In *Slope Instability* (pp. 363-418). Wiltshire, UK: Page Brothers (Norwich) Ltd.

Burns, W.J., Herinckx, H.H., and Lindsey, K.O. (2017). Landslide inventory of portions of northwest Douglas County, Oregon: Department of Geology and Mineral Industries, Open-File Report O-17-04, Esri geodatabase, 4 map pl., scale 1:20,000.

Campbell, C. (1989). Self-Lubrication for Long Runout Landslides [Abstract]. *The Journal of Geology, 97*(6), 653-665. Retrieved from http://www.jstor.org/stable/30062196

Carroll, C. J., & Crawford, T. A. (2000). *Geologic map of the Colorado Springs quadrangle, El Paso County, Colorado* [Map]. Denver, CO: Colorado Geological Survey.

Cashman, C. J., & Brueengo, M. J. (2006). LHZ -- Final Map -- Landforms and Hazard Ratings -- Grays Bay Watershed [Map]. In *Grays Bay Landslide Hazard Zonation Project, Wahkiakum and Pacific County, Washington*. Washington: Washington State Department of Natural Resources.

Chandler, R. J. (1972). Periglacial mudslides in Vestspitsbergen and their bearing on the origin of fossil solifluction shears in low angled clay slopes. *Quarterly Journal of Engineering Geology and Hydrogeology*, *5*(3), 223-241. doi:10.1144/gsl.qjeg.1972.005.03.02

Committee on Ground Failure Hazards. Reducing Losses From Landsliding in the United States (Commission on Engineering and Technical Systems, National Research Council). (1985). Washington, D.C.: National Academy Press. doi: 10.17226/19286

Corominas, J. (1996). The angle of reach as a mobility index for small and large landslides. *Canadian Geotechnical Journal*, *33*(2), 260-271. doi:10.1139/t96-005

Cruden, D. M. (1991). A simple definition of a landslide. *Bulletin of the International Association of Engineering Geology*, *43*(1), 27-29. doi:10.1007/bf02590167

Cruden, D. M., & Varnes, D. J. (1996). Landslide types and processes. In *Landslides Investigation and Mitigation* (pp. 36-75). Washington, D.C.: National Academy Press.

Dade, W. B., & Huppert, H. E. (1998). Long-runout rockfalls. *Geology, 26*(9), 803. doi:10.1130/0091-7613(1998)026<0803:lrr>2.3.co;2

Dai, F., & Lee, C. (2002). Landslide characteristics and slope instability modeling using GIS, Lantau Island, Hong Kong. *Geomorphology*, *42*(3-4), 213-228. doi:10.1016/s0169-555x(01)00087-3

Davies, T. R. (1982). Spreading of rock avalanche debris by mechanical fluidization. *Rock Mechanics, 15*(1), 9-24. doi:10.1007/bf01239474

Dibblee, T. W., Jr. (2008). Geologic Map of the Cape Mendocino & Scotia 15 Minute Quadrangles, Humboldt County California [Map]. Santa Barbra, California: Santa Barbra Museum of Natural History.

Erismann, T. (1979). Mechanisms of large landslides. *Rock Mechanics, 12*, 15-46. doi:https://doi.org/10.1007/BF01241087

Finlay, P., Mostyn, G., & Fell, R. (1999). Landslide risk assessment: Prediction of travel distance. *Canadian Geotechnical Journal, 36*, 556-562. doi:10.1139/cgj-36-3-556

Gerolymos, N., "Analysis of Two Case Histories of Violent Landslides Triggered by Earthquakes" (2008). International Conference on Case Histories in Geotechnical Engineering. 7. http://scholarsmine.mst.edu/icchge/6icchge/session13/7

Goguel, J. (1978). Scale-Dependent Rockslide Mechanisms, with Emphasis on the Role of Pore Fluid Vaporization. In *Rockslides and Avalanches, 1 Natural Phenomena* (Vol. 14A, pp. 693-705). Amsterdam, The Netherlands: Elsevier Scientific Publishing Company.

Guo, C., Zhang, Y., Montgomery, D. R., Du, Y., Zhang, G., & Wang, S. (2016). How unusual is the long-runout of the earthquake-triggered giant Luanshibao landslide, Tibetan Plateau, China? *Geomorphology*, *259*, 145-154. doi:10.1016/j.geomorph.2016.02.013

Howard, K. A. (1973). Avalanche Mode of Motion: Implications from Lunar Examples. *Science*, *180*(4090), 1052-1055. doi:10.1126/science.180.4090.1052

Hungr, O., Corominas, J., & Eberhardt, E. (2005). Estimating landslide motion mechanism, travel distance and velocity. In *Landslide Risk Management* (pp. 99-128). London, England: Taylor & Francis.

Hungr, O., Leroueil, S., & Picarelli, L. (2014). The Varnes classification of landslide types, an update. *Landslides, 11*(2), 167-194. doi:10.1007/s10346-013-0436-y

Hutchinson, J. N., & Bhandari, R. K. (1971). Undrained Loading, A Fundamental Mechanism of Mudflows and other Mass Movements. *Géotechnique, 21*(4), 353-358. doi:10.1680/geot.1971.21.4.353

Hutchinson, J. N., Prior, D. B., & Stephens, N. (1974). Potentially dangerous surges in an Antrim mudslide. *Quarterly Journal of Engineering Geology and Hydrogeology, 7*(4), 363-376. doi:10.1144/gsl.qjeg.1974.007.04.08

Hsu, K. J. (1975). Catastrophic Debris Streams (Sturzstroms) Generated by Rockfalls. *Geological Society of America Bulletin, 86*(1), 129-140. doi:10.1130/0016-7606(1975)86<129:CDSSGB>2.0.CO;2

Iverson, R., George, D., Allstadt, K., Reid, M., Collins, B., Vallance, J., . . . Bower, J. (2015). Landslide mobility and hazards: implications of the 2014 Oso disaster. *Earth and Planetary Science Letters, 412*, 197-208. doi:10.1016/j.epsl.2014.12.020

Iverson, R. M., & George, D. L. (2016). Modelling landslide liquefaction, mobility bifurcation and the dynamics of the 2014 Oso disaster. *Géotechnique, 66*(3), 175-187. doi:10.1680/jgeot.15.lm.004

Iverson, R. M., Reid, M. E., Iverson, N. R., LaHussen, R. G., Logan, M., Mann, J. E., & Brien, D. L. (2000). Acute Sensitivity of Landslide Rates to Initial Soil Porosity. *Science, 290*(5491), 513-516. doi:10.1126/science.290.5491.513

Iverson, R. M., Reid, M. E., & Lahusen, R. G. (1997). Debris-Flow Mobilization From Landslides. *Annual Review of Earth and Planetary Sciences, 25*(1), 85-138. doi:10.1146/annurev.earth.25.1.8

Jeong, S., Lee, K., Kim, J., & Kim, Y. (2017). Analysis of Rainfall-Induced Landslide on Unsaturated Soil Slopes. *Sustainability, 9*(12), 1280. doi:10.3390/su9071280

Johnson, B. (1978). Blackhawk Landslide, California, U.S.A. In *Rockslides and Avalanches, 1 Natural Phenomena* (Vol. 14 A, pp. 481-504). Amsterdam, The Netherlands: Elsevier Scientific Publishing Company.

Johnson, B. C., Campbell, C. S., & Melosh, H. J. (2016). The reduction of friction in long runout landslides as an emergent phenomenon. *Journal of Geophysical Research: Earth Surface, 121*(5), 881-889. doi:10.1002/2015jf003751

Keefer, D. K. (1984). Rock Avalanches Caused by Earthquakes: Source Characteristics. *Science, 223*(4642), 1288-1290. doi:10.1126/science.223.4642.1288

Kent, P. E. (1966). The Transport Mechanism in Catastrophic Rock Falls. *The Journal of Geology, 74*(1), 79-83. doi:10.1086/627142

Kottek, M., Grieser, J., Beck, C., Rudolf, B., and Rubel, F. (2006). World Map of the Köppen-Geiger climate classification updated. *Meteorol. Z.*, 15, 259-263. DOI: 10.1127/0941-2948/2006/0130.

Landslides 101. (n.d.). Retrieved June 1, 2018, from https://landslides.usgs.gov/learn/ls101.php

Landslides and Debris Flows. (n.d.). Retrieved June 1, 2018, from https://gis.utah.gov/data/geoscience/landslides/#LandslideInventoryPolygons

Legros, F. (2002). The mobility of long-runout landslides. *Engineering Geology, 63*(3-4), 301-331. doi:10.1016/s0013-7952(01)00090-4

Lucchitta, B. K. (1987). Valles Marineris, Mars: Wet debris flows and ground ice. *Icarus, 72*(2), 411-429. doi:10.1016/0019-1035(87)90183-7

May, C. L., & Gresswell, R. E. (2004). Spatial and temporal patterns of debris-flow deposition in the Oregon Coast Range, USA. *Geomorphology, 57*(3-4), 135-149. doi:10.1016/s0169-555x(03)00086-2

McEwen, A. S. (1989). Mobility of large rock avalanches: Evidence from Valles Marineris, Mars. *Geology, 17*(12), 1111. doi:10.1130/0091-7613(1989)017<1111:molrae>2.3.co;2

McKenna, J. P., Santi, P. M., Amblard, X., & Negri, J. (2011). Effects of soil-engineering properties on the failure mode of shallow landslides. *Landslides, 9*(2), 215-228. doi:10.1007/s10346-011-0295-3

McLaughlin, R. J., Ellen, S. D., Irwin, W. P., Clarke, S. H., Jr., Jayko, A. S., Blake, M. C., . . . Carver, G. A. (2000). Geology of the Cape Mendocino, Eureka, Garberville, and southwestern part of the Hayfork 30 x 60 minute quadrangles and adjacent offshore area, northern California. Sheet 1: Eureka and Southwestern Hayfork quadrangles [Map]. Reston, VA: U.S. Geological Survey.

McSaveney, M. (1978). Sherman Glacier Rock Avalanche, Alaska, U.S.A. In *Rockslides and Avalanches, 1 Natural Phenomena* (Vol. 14 A, pp. 197-258). Amsterdam, The Netherlands: Elsevier Scientific Publishing Company.

Melosh, H. J. (1979). Acoustic fluidization: A new geologic process? *Journal of Geophysical Research: Solid Earth, 84*(B13), 7513-7520. doi:10.1029/jb084ib13p07513

Minard, J. P. (1982). *Distribution and description of geologic units in the Mukilteo quadrangle, Washington* [Map]. Reston, VA: U.S. Geological Survey.

Minard, J. P. (1985). *Geologic map of the Everett 7.5 minute quadrangle, Snohomish County, Washington* [Map]. Reston, VA: U.S. Geological Survey.

Nicoletti, P., & Sorriso-Valvo, M. (1991). Geomorphic controls of the shape and mobility of rock avalanches. *Geological Society of America Bulletin, 103*, 1365-1373. doi:https://doi.org/10.1130/0016-7606(1991)1032.3.CO;2

Qi, S., Xu, Q., Zhang, B., Zhou, Y., Lan, H., & Li, L. (2011). Source characteristics of long runout rock avalanches triggered by the 2008 Wenchuan earthquake, China. *Journal of Asian Earth Sciences, 40*(4), 896-906. doi:10.1016/j.jseaes.2010.05.010

Rogers, W. P. (2003). Critical landslides of Colorado [Map]. Colorado: Colorado Geological Society.

Sassa, K., Fukuoka, H., Ochiai, H., Wang, F., & Wang, G. (2005). Aerial Prediction of Earthquake and Rain Induced Rapid and Long-Traveling Flow Phenomena (APERITIF) (M101). *Landslides*, 99-108. doi:10.1007/3-540-28680-2_11

Sassa, K. (2000). Mechanism of flows in granular soils. Proc., Int. Conf. of Geotechnical and Geological Engineering, GEOENG2000, Vol. 1, Technomic Publishing, Lancaster, PA, 1671–1702.

Scheller, E. (1970). *Geophysikalische Untersuchungen zum Problem des Taminser Bergsturzes*. Zürich: Juris Dr. & Verl.

Schuster, R. L., & Turner, A. K. (1996). *Landslides: investigation and mitigation*. Washington D.C.: National Academy Press.

Shreve, R. L. (1966). Sherman Landslide, Alaska. *Science*, *154*(3757), 1639-1643. doi:10.1126/science.154.3757.1639

Shreve, R. L. (1968a). *The Blackhawk landslide*. Boulder (Colo.): *Geological Society of America*. doi:https://doi.org/10.1130/SPE108-p1

Shreve, R. L. (1968b). Leakage and Fluidization in Air-Layer Lubricated Avalanches. *Geological Society of America Bulletin, 79*(5), 653. doi:10.1130/0016-7606(1968)79[653:lafial]2.0.co;2

Skempton, A. W. (1964). Long-Term Stability of Clay Slopes. *Géotechnique, 14*(2), 77-102. doi:10.1680/geot.1964.14.2.77

Skermer, N. A. (1985). Discussion of paper "Nature and mechanics of Mount St Helens rockslide-avalanche of 18 May 1980". *Géotechnique, 35*: 357-362.

Spittler, T. E. (1984). Geology and Geomorphic Features Related to Landsliding Capetown 7.5' Quadrangle, Humboldt County, California [Map]. California: California Department of Conservation.

Stark, T. D., Baghdady, A. K., Hungr, O., & Aaron, J. (2017). Case Study: Oso, Washington, Landslide of March 22, 2014—Material Properties and Failure Mechanism. *Journal of Geotechnical and Geoenvironmental Engineering, 143*(5), 05017001. doi:10.1061/(asce)gt.1943-5606.0001615

Straub, S. (1997). Predictability of long runout landslide motion: Implications from granular flow mechanics. *Geologische Rundschau, 86*(2), 415-425. doi:10.1007/s005310050150

Thorson, J. P., Carroll, J. C., & Morgan, M. L. (2002). *Geologic Map of the Pikeview 7.5 Minute Quadrangle, El Paso County, Colorado* [Map]. Denver, Colorado: Colorado Geological Survey.

Tian, Y., Xu, C., Chen, J., Zhou, Q., & Shen, L. (2017). Geometrical characteristics of earthquake-induced landslides and correlations with control factors: a case study of the 2013 Minxian, Gansu, China, Mw 5.9 event. *Landslides, 14*(6), 1915-1927. doi:10.1007/s10346-017-0835-6

Vallejo, L. (1980). Mechanics of mudflow mobilization in low-angled clay slopes. *Engineering Geology, 16*(1-2), 63-70. doi:10.1016/0013-7952(80)90007-1

Voight, B., Janda, R. J., Glicken, H., & Douglass, P. M. (1983). Nature and mechanics of the Mount St Helens rockslide-avalanche of 18 May 1980 [Abstract]. *Géotechnique, 33*(3), 243-273. doi:10.1680/geot.1983.33.3.243

Voight, B., & Sousa, J. (1994). Lessons from Ontake-san: A comparative analysis of debris avalanche dynamics. *Engineering Geology, 38*(3-4), 261-297. doi:10.1016/0013-7952(94)90042-6

Wagner, D.L., and Spittler, T.E. (1997). Landsliding along the Highway 50 Corridor: Geology and slope stability of the American Canyon between Riverton and Strawberry, California: California Division of Mines and Geology, Open-File Report 97-22, scale 1:12,000.

Wang, F., Sassa, K., & Fukuoka, H. (2000). Geotechnical Simulation Test for the Nikawa Landslide Induced by January 17, 1995 Hyogoken-Nambu Earthquake. *Soils And Foundations*, *40*(1), 35-46. doi:10.3208/sandf.40.35

Wang, G., & Sassa, K. (2003). Pore-pressure generation and movement of rainfall-induced landslides: Effects of grain size and fine-particle content. *Engineering Geology*, *69*(1-2), 109-125. doi:10.1016/s0013-7952(02)00268-5

Wang, F., Sassa, K., & Wang, G. (2002). Mechanism of a long-runout landslide triggered by the August 1998 heavy rainfall in Fukushima Prefecture, Japan. *Engineering Geology*, *63*(1-2), 169-185. doi:10.1016/s0013-7952(01)00080-1

Wells, R. E. (1989). *Geologic map of the Cape Disappointment--Naselle River area, Pacific and Wahkiakum counties, Washington* [Map]. Reston, VA: U.S. Geological Survey.

White, J., Morgan, M. & Berry, K. (2015). The West Salt Creek Landslide: A Catastrophic Rockslide and Rock/Debris Avalanche in Mesa County, Colorado [Bulletin]. Golden, CO: Colorado Geological Survey.

Wilson, C. (1984). The role of fluidization in the emplacement of pyroclastic flows, 2: Experimental results and their interpretation. *Journal of Volcanology and Geothermal Research*, *20*(1-2), 55-84. doi:10.1016/0377-0273(84)90066-0

Witkind, I. J., & Weiss, M. P. (1991). *Geologic map of the Nephi 30' X 60' quadrangle, Carbon, Emery, Juab, Sanpete, Utah, and Wasatch Counties, Utah* [Map]. U.S. Geological Survey.

Witkind, I. J., Weiss, M. P., & Brown, T. L. (1987). *Geologic map of the Manti 30' x 60' quadrangle, Carbon, Emery, Juab, Sanpete, and Sevier Counties, Utah* [Map]. U.S. Geological Survey.

Wolfe, E. W., & McKee, E. H. (1968). *Geology of the Grays River quadrangle, Wahkiakum and Pacific Counties, Washington* [Map]. Olympia: Washington Dept. of Natural Resources, Division of Mines and Geology.

Zhang, D., & Wang, G. (2007). Study of the 1920 Haiyuan earthquake-induced landslides in loess (China). *Engineering Geology*, *94*(1-2), 76-88. doi:10.1016/j.enggeo.2007.07.007

APPENDIX A

For similar shapes, A increases at a faster rate than L making it merely a measure of landslide size. To make it independent of size it must be transformed. For the cumulative dataset landslides were ranked using the transformation: ln(L+5meters)/ln(A). The upper and lower quartiles, designated high and low L/A respectively, were then plotted separately on a log-log plot of L vs A as seen in Figure A-1. Comparisons of the high and low L/A groups were then made for a range of parameters including: topographic obstacles (Table A-1), previous movement (Table A-2), type of vegetation (Table A-3), topographic morphology (Table A-4), generalized geology (Table A-5), ISA (Table A-6), movement type (Table A-7), and study area (Table A-8).

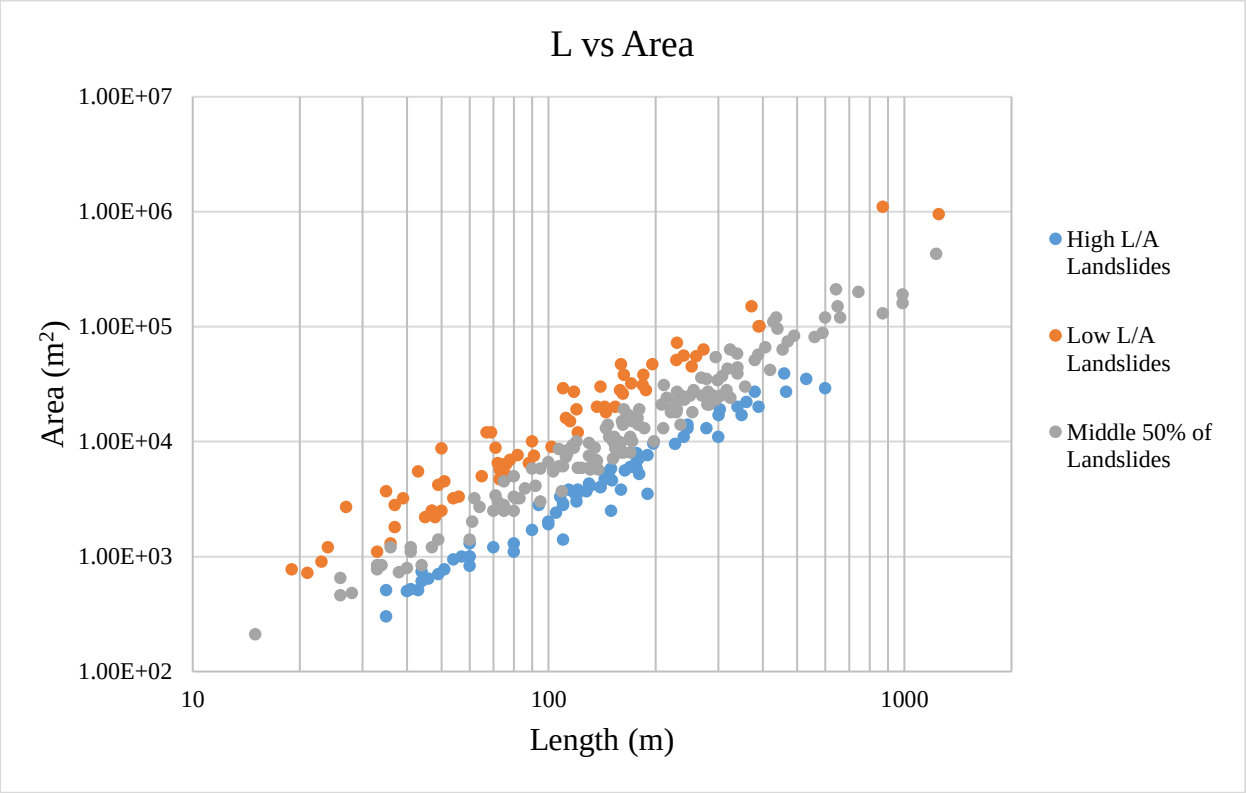

Figure A-1: Log-log plot of L vs A for the cumulative dataset. This figure displays the division of low and high L/A landslides.

The percentages for all categories of low L/ A landslides, high L/A landslides, and the cumulative dataset and are recorded in Tables 1-8 below.

Table A-1: Counts and percentages for all low L/A, high L/A, and all landslides by topographic obstacles.

Topographic Obstacles	Count (Low L/A)	Percent (Low L/A)	Count (High L/A)	Percent (High L/A)	Count (All L/A)	Percent (All L/A)
Confined	7	10%	22	31%	61	22%
Open	64	90%	49	69%	221	78%

Table A-2: Counts and percentages for all low L/A, high L/A, and all landslides by previous movement.

Previous Movement	Count (Low L/A)	Percent (Low L/A)	Count (High L/A)	Percent (High L/A)	Count (All L/A)	Percent (All L/A)
Yes	17	24%	11	15%	56	20%
No	54	76%	60	85%	226	80%

Table A-3: Counts and percentages for all low L/A, high L/A, and all landslides by type of vegetation.

Type of Vegetation	Count (Low L/A)	Percent (Low L/A)	Count (High L/A)	Percent (High L/A)	Count (All L/A)	Percent (All L/A)
Barren	6	8%	5	7%	19	7%
Grass	18	25%	9	13%	52	18%
Shrub	13	18%	17	24%	54	19%
Light Forest	8	11%	24	34%	57	20%
Heavy Forest	26	37%	16	23%	100	35%

Table A-4: Counts and percentages for all low L/A, high L/A, and all landslides by topographic morphology.

Topographic Morphology	Count (Low L/A)	Percent (Low L/A)	Count (High L/A)	Percent (High L/A)	Count (All L/A)	Percent (All L/A)
Concave	6	8%	13	18%	39	14%
Convex	9	13%	16	23%	51	18%
Gentle	34	48%	35	49%	136	48%
High	4	6%	1	1%	21	7%
Low	18	25%	6	8%	35	12%

Table A-5: Counts and percentages for all low L/A, high L/A, and all landslides by geology.

Geology	Count (Low L/A)	Percent (Low L/A)	Count (High L/A)	Percent (High L/A)	Count (All L/A)	Percent (All L/A)
Clay	5	7%	6	8%	22	8%
Granular	9	13%	21	30%	69	24%
Hard Rock	12	17%	9	13%	51	18%
Sandstone/Siltstone	11	15%	5	7%	31	11%
Shale	34	48%	30	42%	109	39%

Table A-6: Counts and percentages for all low L/A, high L/A, and all landslides by initial slope angle.

ISA	Count (Low L/A)	Percent (Low L/A)	Count (High L/A)	Percent (High L/A)	Count (All L/A)	Percent (All L/A)
<10	5	7%	2	3%	14	5%
10	10	14%	2	3%	30	11%
15	20	28%	18	25%	59	21%
20	20	28%	17	24%	77	27%
25	6	8%	15	21%	49	17%
30	5	7%	8	11%	24	9%
35	2	3%	3	4%	9	3%
40	1	1%	2	3%	11	4%
45	2	3%	2	3%	5	2%
50			2	3%	3	1%
55			0		1	0%

Table A-7: Counts and percentages for all low L/A, high L/A, and all landslides by movement type.

Movement Type	Count (Low L/A)	Percent (Low L/A)	Count (High L/A)	Percent (High L/A)	Count (All L/A)	Percent (All L/A)
Rotational	13	18%	4	6%	28	10%
Trans. or Rot.	33	46%	22	31%	119	42%
Trans. and Rot.	1	1%	2	3%	5	2%
Translational	24	34%	43	61%	130	46%

Table A-8: Counts and percentages for all low L/A, high L/A, and all landslides by study area.

Study Area	Count (Low L/A)	Percent (Low L/A)	Count (High L/A)	Percent (High L/A)	Count (All L/A)	Percent (All L/A)
Cal. Ferndale	7	10%	4	6%	37	13%
Cal. Riverton	1	1%	16	23%	26	9%
Colorado Springs	23	32%	3	4%	42	15%
Oregon	21	30%	6	8%	61	22%
Utah North	2	3%	20	28%	24	9%
Utah South	8	11%	12	17%	44	16%
Wash. Grays Bay	3	4%	0	0%	18	6%
Wash. P.S.	6	8%	10	14%	30	11%

APPENDIX B

Table B-1: Summary statistics for each study area.

Study Area	N*	Mean H/L**	Median H/L**	Mean L (m)**	Median L (m)**	Mean Area (m^2)**	Köppen-Geiger climate classification
Cal. Ferndale	44/37	.331	.320	210	177	2.14E4	Csb
Cal. Riverton	40/26	.421	.403	205	168	1.31E4	Csb
Colorado Springs	43/42	.252	.231	98.1	50.5	2.78E4	BSk
Oregon	84/61	.289	.258	196	163	3.09E4	Csb
Utah North	37/24	.282	.296	101	100	2.68E3	Dfc
Utah South	51/44	.368	.363	378	295	7.96E4	Dfc and Dfb
Wash. Grays Bay	31/18	.326	.278	190	159	2.09E4	Csb
Wash. P.S.	40/30	.607	.593	67.4	57.0	3.34E3	Csb

*N specifies the number of landslides: with walls / without walls. ** Does not include walls.

Table B-2: Summary of the Entire Dataset for the Current Study.

Study Area	ID	Lat	Long	H (m)	L (m)	H/L	Area	Movement Type	WPC	Topographic Morphology	Geology	Geo2	Type of Vegetation	Previous Movement	Depth to Bedrock (m)	ISA	Topographic Obstacles
CF		40.49213	-124.372	67	246	0.2726	1.30E+04	Tran or Rot	635	concave	sandstone with interbedded shale	Shale	s	n	N/A	15	open
CF		40.49124	-124.373	91	305	0.2998	2.50E+04	Tran or Rot	621	gentle	sandstone with interbedded shale	Shale	lf	n	N/A	20	open
CF		40.48569	-124.302	146	335	0.4367	1.70E+04	Tran or Rot	284	concave	sandstone with interbedded shale	Shale	lf	n	N/A	20	wall
CF		40.49017	-124.296	171	589	0.2898	8.80E+04	Tran or Rot	621	high	sandstone with interbedded shale	Shale	g	n	N/A	25	open
CF		40.48961	-124.295	49	180	0.2709	1.90E+04	Tran or Rot	650	high	sandstone with interbedded shale	Shale	g	n	N/A	15	open
CF		40.47225	-124.269	171	466	0.3663	2.70E+04	Tran or Rot	481	convex	sandstone with interbedded shale	Shale	s	n	N/A	20	open
CF		40.46701	-124.27	85	147	0.5806	1.80E+04	Tran or Rot	63	concave	sandstone with interbedded shale	Shale	g	n	N/A	20	wall
CF		40.45513	-124.292	85	177	0.4822	7.90E+03	Tran or Rot	141	convex	mudstone	Shale	lf	n	N/A	30	open
CF		40.38582	-124.33	195	509	0.3832	7.70E+04	Tran or Rot	245	high	sandstone with interbedded shale	Shale	lf	n	N/A	20	wall
CF		40.38127	-124.338	85	186	0.4588	1.50E+04	Tran or Rot	920	concave	sandstone with interbedded shale	Shale	s	n	N/A	25	wall
CF		40.38255	-124.345	91	299	0.3058	3.40E+04	Tran or Rot	897	high	sandstone with interbedded shale	Shale	g	n	N/A	25	open
CF		40.37731	-124.352	40	124	0.3195	5.90E+03	Tran or Rot	510	convex	shale	Shale	s	n	N/A	25	open
CF		40.40245	-124.337	162	438	0.3688	5.30E+04	Tran or Rot	844	concave	sandstone with interbedded shale	Shale	s	n	N/A	20	wall
CF		40.44117	-124.372	37	105	0.3483	6.10E+03	Tran or Rot	54	concave	shale	Shale	g	n	N/A	25	wall
CF		40.46239	-124.37	94	215	0.4395	2.40E+04	Tran or Rot	253	gentle	mudstone	Shale	lf	y	N/A	20	open
CF		40.46405	-124.357	37	130	0.2814	9.70E+03	Tran or Rot	110	convex	mudstone	Shale	lf	n	N/A	20	open
CF		40.45866	-124.344	24	95	0.2567	5.80E+03	Tran or Rot	147	gentle	shale	Shale	hf	n	N/A	15	open
CF		40.46111	-124.329	91	229	0.3993	1.80E+04	Tran or Rot	239	convex	sandstone with interbedded shale	Shale	g	y	N/A	20	open
CF		40.46088	-124.327	94	283	0.3339	2.10E+04	Tran or Rot	310	convex	sandstone with interbedded shale	Shale	g	y	N/A	20	open
CF		40.4622	-124.327	158	490	0.3235	8.30E+04	Tran or Rot	300	convex	sandstone with interbedded shale	Shale	g	n	N/A	15	open
CF		40.46123	-124.324	104	280	0.3701	2.10E+04	Tran or Rot	470	convex	sandstone with interbedded shale	Shale	s	n	N/A	20	open
CF		40.51667	-124.381	61	145	0.4204	1.30E+04	Tran or Rot	157	convex	sandstone/limestone	Sand/Siltstone	s	n	N/A	25	open

Table B-2: Continued.

CF		40.51965	-124.378	43	107	0.3988	6.10E+03	Tran or Rot	122	convex	diamicton	Clay	g	y	N/A	15	open
CF		40.5234	-124.377	24	71	0.3434	8.80E+03	Tran or Rot	93	convex	folded argillite	Shale	g	n	N/A	20	open
CF		40.52479	-124.375	18	72	0.254	6.50E+03	Tran or Rot	121	gentle	diamicton	Clay	lf	n	N/A	15	open
CF		40.53728	-124.367	61	186	0.3277	1.30E+04	Tran or Rot	211	convex	weakly lithified, siltstone, sandslone and mudstone	Shale	s	n	N/A	35	open
CF		40.53906	-124.366	64	152	0.4211	7.10E+03	Tran or Rot	124	convex	weakly lithified, siltstone, sandslone and mudstone	Shale	s	n	N/A	20	open
CF		40.54802	-124.359	49	227	0.2148	2.30E+04	Tran or Rot	12	concave	weakly lithified, siltstone, sandslone and mudstone	Shale	lf	n	N/A	20	wall
CF		40.54749	-124.357	49	254	0.192	1.80E+04	Tran or Rot	112	concave	weakly lithified, siltstone, sandslone and mudstone	Shale	lf	n	N/A	9	confined
CF		40.54977	-124.361	27	136	0.2017	6.90E+03	Tran or Rot	43	concave	weakly lithified, siltstone, sandslone and mudstone	Shale	lf	n	N/A	20	open
CF		40.55141	-124.361	37	90	0.4064	5.80E+03	Tran or Rot	100	convex	weakly lithified, siltstone, sandslone and mudstone	Shale	lf	n	N/A	25	open
CF		40.55362	-124.36	67	145	0.4625	1.80E+04	Tran or Rot	133	convex	weakly lithified, siltstone, sandslone and mudstone	Shale	b	y	N/A	25	open
CF		40.55335	-124.358	122	392	0.311	1.01E+05	Tran or Rot	247	convex	weakly lithified, siltstone, sandslone and mudstone	Shale	lf	n	N/A	15	open
CF		40.5613	-124.356	49	163	0.2992	3.80E+04	Tran or Rot	126	gentle	weakly lithified, siltstone, sandslone and mudstone	Shale	s	n	N/A	20	open
CF		40.56355	-124.355	61	188	0.3243	2.80E+04	Tran or Rot	122	convex	weakly lithified, siltstone, sandslone and mudstone	Shale	lf	n	N/A	25	open
CF		40.56638	-124.354	61	162	0.3763	2.60E+04	Tran or Rot	141	convex	weakly lithified, siltstone, sandslone and mudstone	Shale	s	n	N/A	20	open
CF		40.55397	-124.319	55	161	0.3408	1.50E+04	Tran or Rot	210	high	weakly lithified, siltstone, sandslone and mudstone	Shale	lf	n	N/A	35	open

Table B-2: Continued.

CF		40.55363	-124.315	49	154	0.3167	8.70E+03	Tran or Rot	346	high	weakly lithified, siltstone, sandslone and mudstone	Shale	lf	n	N/A	20	confined
CF		40.54815	-124.313	43	137	0.3115	6.80E+03	Tran or Rot	402	high	weakly lithified, siltstone, sandslone and mudstone	Shale	lf	n	N/A	20	open
CF		40.54427	-124.312	58	179	0.3235	1.40E+04	Tran or Rot	258	high	weakly lithified, siltstone, sandslone and mudstone	Shale	lf	n	N/A	20	open
CF		40.50565	-124.288	34	109	0.3076	3.70E+03	Tran or Rot	28	concave	folded argillite	Shale	lf	n	N/A	15	confined
CF		40.51283	-124.272	85	296	0.2883	2.30E+04	Tran or Rot	260	gentle	weakly lithified, siltstone, sandslone and mudstone	Shale	g	y	N/A	30	open
CF		40.51245	-124.263	49	153	0.3187	1.10E+04	Tran or Rot	151	low	diamicton	Clay	g	n	N/A	20	open
CF		40.56706	-124.271	64	227	0.282	9.50E+03	Tran or Rot	292	gentle	weakly lithified, siltstone, sandslone and mudstone	Shale	lf	n	N/A	20	confined
CR		38.78445	-120.446	122	303	0.4024	1.90E+04	Tran or Rot	1473	gentle	Qco	Granular	lf	n	N/A	20	open
CR		38.76916	-120.444	61	86	0.7088	9.60E+03	Tran or Rot	65	convex	Qls	Granular	b	n	N/A	20	wall
CR		38.77501	-120.447	101	317	0.3173	2.80E+04	Tran or Rot	446	concave	Qls	Granular	b	y	N/A	25	confined
CR		38.77004	-120.447	73	240	0.3048	1.10E+04	Tran or Rot	148	convex	Qls	Granular	lf	y	N/A	15	open
CR		38.7707	-120.442	165	500	0.3292	6.90E+04	Tran or Rot	252	gentle	Qls	Granular	b	y	N/A	20	wall
CR		38.77165	-120.442	55	144	0.381	4.70E+03	Tran or Rot	349	gentle	Qls	Granular	lf	y	N/A	25	confined
CR		38.77127	-120.44	82	278	0.296	1.30E+04	Tran or Rot	301	gentle	Qls	Granular	lf	y	N/A	20	confined
CR		38.7728	-120.436	27	80	0.3429	2.50E+03	Tran or Rot	335	gentle	Qls	Granular	b	n	N/A	20	confined
CR		38.77331	-120.434	30	94	0.3243	2.80E+03	Tran or Rot	288	gentle	Qls	Granular	s	n	N/A	20	confined
CR		38.77382	-120.429	58	131	0.4421	1.80E+04	Tran or Rot	90	gentle	granite	Hard Rock	s	n	N/A	25	wall
CR		38.76042	-120.434	64	125	0.5121	8.60E+03	Tran or Rot	1007	gentle	Qls	Granular	lf	n	N/A	30	wall
CR		38.75975	-120.433	64	148	0.4325	5.50E+03	Tran or Rot	1090	gentle	Qls	Granular	lf	n	N/A	30	confined
CR		38.77149	-120.424	207	350	0.5922	6.00E+04	Tran or Rot	216	gentle	Qls	Granular	lf	y	N/A	30	wall
CR		38.77194	-120.422	232	420	0.5515	6.40E+04	Tran or Rot	233	gentle	Qls	Granular	lf	y	N/A	30	wall
CR		38.77454	-120.425	70	185	0.3789	1.00E+04	Tran or Rot	88	gentle	Qls	Granular	s	n	N/A	20	wall
CR		38.77562	-120.423	91	228	0.4011	1.40E+04	Tran or Rot	105	gentle	Qls	Granular	s	n	N/A	20	wall
CR		38.78378	-120.425	40	114	0.3476	3.80E+03	Tran or Rot	1024	concave	Qls	Granular	b	n	N/A	25	confined
CR		38.78311	-120.423	49	121	0.403	3.80E+03	Tran or Rot	894	concave	Qls	Granular	s	n	N/A	25	confined
CR		38.78038	-120.416	64	118	0.5424	3.60E+03	Tran or Rot	612	convex	andesitic mudflow (lahar)	Shale	s	n	N/A	30	open
CR		38.77227	-120.418	79	131	0.6049	5.70E+03	Tran or Rot	248	gentle	Qls	Granular	s	n	N/A	40	confined
CR		38.7717	-120.415	49	83	0.5876	3.20E+03	Tran or Rot	346	gentle	Qls	Granular	b	n	N/A	30	open

Table B-2: Continued.

CR		38.76839	-120.411	82	164	0.5018	5.60E+03	Tran or Rot	761	gentle	Qls	Granular	lf	n	N/A	25	open
CR		38.77157	-120.408	55	147	0.3732	1.40E+04	Tran or Rot	437	gentle	Qls	Granular	b	n	N/A	25	open
CR		38.77191	-120.406	110	235	0.4669	1.40E+04	Tran or Rot	377	gentle	Qls	Granular	s	n	N/A	25	confined
CR		38.77048	-120.405	152	530	0.2875	3.50E+04	Tran or Rot	504	gentle	Qls	Granular	b	y	N/A	15	open
CR		38.77225	-120.401	70	197	0.3559	9.60E+03	Tran or Rot	179	gentle	Qls	Granular	s	n	N/A	20	confined
CR		38.77579	-120.41	37	102	0.3586	7.70E+03	Tran or Rot	78	gentle	Qls	Granular	b	y	N/A	20	wall
CR		38.7759	-120.408	67	194	0.3456	1.10E+04	Tran or Rot	82	gentle	Qls	Granular	s	y	N/A	20	wall
CR		38.77636	-120.409	98	274	0.356	2.30E+04	Tran or Rot	137	gentle	Qls	Granular	b	y	N/A	20	wall
CR		38.77607	-120.407	73	169	0.4329	1.60E+04	Tran or Rot	91	gentle	Qls	Granular	b	y	N/A	25	wall
CR		38.76909	-120.393	110	190	0.5775	7.60E+03	Tran or Rot	464	gentle	granite	Hard Rock	lf	n	N/A	30	open
CR		38.77971	-120.394	73	172	0.4253	1.50E+04	Tran or Rot	672	gentle	Qls	Granular	s	y	N/A	25	open
CR		38.77831	-120.393	85	154	0.5542	2.00E+04	Tran or Rot	508	gentle	Qls	Granular	s	y	N/A	30	open
CR		38.77261	-120.389	49	76	0.6417	4.20E+03	Tran or Rot	52	gentle	Qls	Granular	lf	n	N/A	35	wall
CR		38.77043	-120.389	232	565	0.41	7.50E+04	Tran or Rot	241	gentle	Qls	Granular	s	y	N/A	20	wall
CR		38.76865	-120.387	122	295	0.4133	5.40E+04	Tran or Rot	260	gentle	Qls	Granular	s	y	N/A	20	open
CR		38.75697	-120.382	146	349	0.4192	1.70E+04	Tran or Rot	521	concave	granite	Hard Rock	s	n	N/A	25	confined
CR		38.76785	-120.377	110	198	0.5542	1.00E+04	Tran or Rot	121	convex	granite	Hard Rock	s	n	N/A	30	open
CR		38.77185	-120.377	55	151	0.3633	4.60E+03	Tran or Rot	536	gentle	Qls	Granular	s	n	N/A	20	confined
CR		38.76704	-120.363	140	380	0.369	2.70E+04	Tran or Rot	302	concave	Qls	Granular	s	y	N/A	20	open
CS		38.76361	-104.779	18	120	0.1524	1.00E+04	Tran or Rot	54	gentle	shale	Shale	g	n	s	9	open
CS		38.75564	-104.817	12	100	0.1219	6.60E+03	Tran or Rot	163	low	shale	Shale	b	y	m	7	open
CS		38.75537	-104.823	24	134	0.182	1.90E+04	Tran or Rot	49	low	shale	Shale	s	y	m	10	wall
CS		38.75658	-104.821	20	70	0.283	2.50E+03	Tran or Rot	141	gentle	shale	Shale	s	y	m	20	open
CS		38.75664	-104.823	17	117	0.1433	9.30E+03	Tran or Rot	166	gentle	shale	Shale	s	y	m	20	open
CS		38.75808	-104.822	27	121	0.2267	1.20E+04	Tran or Rot	57	gentle	shale	Shale	s	y	m	20	open
CS		38.76168	-104.822	5	34	0.1345	8.40E+02	Tran or Rot	43	gentle	old landslide deposit	Granular	lf	n	m	7	open
CS		38.76394	-104.823	8	82	0.0929	7.60E+03	Tran or Rot	13	low	shale	Shale	lf	y	m	7	confined
CS		38.76326	-104.825	9	49	0.1866	4.20E+03	Tran or Rot	84	gentle	shale	Shale	s	n	s	20	confined
CS		38.76872	-104.82	5	75	0.061	2.80E+03	Tran or Rot	66	low	shale	Shale	b	n	s	4	open
CS		38.77064	-104.825	6	37	0.1648	1.80E+03	Tran or Rot	74	high	old landslide deposit	Granular	b	n	s	9	open
CS		38.7699	-104.826	12	57	0.2139	1.00E+03	Tran or Rot	70	gentle	shale	Shale	s	n	s	10	open
CS		38.77167	-104.826	30	230	0.1325	2.20E+04	Tran or Rot	194	gentle	shale	Shale	g	y	m	10	open
CS		38.77022	-104.842	143	1250	0.1146	9.50E+05	Tran or Rot	5	low	shale	Shale	g	y	d	6	open
CS		38.76117	-104.853	15	35	0.4354	5.10E+02	Tran or Rot	75	gentle	shale	Shale	lf	n	s	25	open
CS		38.76273	-104.854	9	15	0.6096	2.10E+02	Tran or Rot	107	convex	shale	Shale	lf	n	s	25	open
CS		38.76702	-104.864	18	49	0.3732	1.40E+03	Tran or Rot	650	high	granite/grus	Hard Rock	lf	n	s	20	open
CS		38.81232	-104.855	8	21	0.3629	7.20E+02	Tran or Rot	16	low	shale	Shale	s	n	s	20	open
CS		38.81311	-104.854	5	75	0.061	2.50E+03	Tran or Rot	20	low	shale	Shale	s	n	s	4	confined
CS		38.81554	-104.835	11	50	0.2134	8.70E+03	Tran or Rot	474	gentle	shale	Shale	g	n	s	10	open

Table B-2: Continued.

CS		38.81834	-104.838	23	120	0.1905	1.90E+04	Tran or Rot	385	gentle	shale	Shale	b	n	s	10	open
CS		38.85272	-104.852	12	27	0.4516	2.70E+03	Tran or Rot	914	gentle	shale	Shale	g	n	s	25	open
CS		38.85473	-104.854	15	48	0.3175	2.20E+03	Tran or Rot	900	high	shale	Shale	g	n	s	20	open
CS		38.85601	-104.854	8	19	0.4011	7.70E+02	Tran or Rot	857	gentle	shale	Shale	b	n	s	20	open
CS		38.85691	-104.853	8	35	0.2177	3.70E+03	Tran or Rot	695	convex	shale	Shale	b	n	s	10	open
CS		38.86561	-104.846	27	152	0.1805	1.00E+04	Tran or Rot	68	gentle	shale	Shale	g	n	s	10	open
CS		38.86281	-104.863	12	50	0.2438	2.50E+03	Tran or Rot	422	low	shale	Shale	g	n	s	15	open
CS		38.86944	-104.867	21	86	0.2481	3.90E+03	Tran or Rot	140	gentle	shale	Shale	g	n	s	15	open
CS		38.88258	-104.844	37	221	0.1655	1.80E+04	Tran or Rot	501	gentle	shale	Shale	g	n	s	10	open
CS		38.88886	-104.853	20	88	0.2251	6.50E+03	Tran or Rot	198	gentle	shale	Shale	g	y	m	30	open
CS		38.88881	-104.856	30	130	0.2345	7.50E+03	Tran or Rot	73	gentle	shale	Shale	g	y	m	15	open
CS		38.89253	-104.863	20	69	0.2871	1.20E+04	Tran or Rot	390	gentle	shale	Shale	g	n	s	15	open
CS		38.88365	-104.874	15	54	0.2822	3.20E+03	Tran or Rot	55	gentle	shale	Shale	g	y	m	15	open
CS		38.88732	-104.874	24	112	0.2177	1.60E+04	Tran or Rot	123	gentle	shale	Shale	g	y	m	10	open
CS		38.89117	-104.872	20	47	0.4215	2.50E+03	Tran or Rot	70	gentle	shale	Shale	s	y	m	25	open
CS		38.89243	-104.872	11	26	0.4103	6.50E+02	Tran or Rot	141	convex	shale	Shale	s	n	m	20	open
CS		38.89304	-104.874	12	33	0.3695	1.10E+03	Tran or Rot	263	convex	shale	Shale	s	n	m	20	open
CS		38.91729	-104.835	3	24	0.127	1.20E+03	Tran or Rot	68	gentle	sandy shale	Shale	g	n	s	7	open
CS		38.92022	-104.834	12	36	0.3387	1.20E+03	Tran or Rot	30	gentle	sandy shale	Shale	g	n	s	20	confined
CS		38.92179	-104.836	8	23	0.3313	9.00E+02	Tran or Rot	169	gentle	sandy shale	Shale	g	n	s	20	open
CS		38.92154	-104.837	15	51	0.2988	4.50E+03	Tran or Rot	100	gentle	sandy shale	Shale	g	n	s	20	confined
CS		38.89292	-104.864	10	37	0.2718	2.80E+03	Translational	448	gentle	shale	Shale	g	y	m	15	open
CS		38.88823	-104.874	12	44	0.2771	6.10E+02	Rotational	9	concave	shale	Shale	g	n	m	15	open
OR	5327	43.7428	-123.765	98	308	0.3167	3.70E+04	Translational	402	concave	basalt	Hard Rock	hf	y	N/A	20	confined
OR	5413	43.73039	-123.661	37	108	0.3387	3.30E+03	Translational	74	low	sandstone/siltstone	Sand/Siltstone	Ukn - hf	n	N/A	20	open
OR	5490	43.82617	-123.723	128	389	0.3291	5.70E+04	Translational	150	gentle	sandstone/siltstone	Sand/Siltstone	Ukn - hf	n	N/A	20	open
OR	5491	43.82606	-123.72	61	137	0.445	2.00E+04	Translational	188	high	sandstone/siltstone	Sand/Siltstone	Ukn - hf	n	N/A	20	open
OR	6022	43.63322	-123.803	58	269	0.2153	3.60E+04	Translational	185	gentle	basalt	Hard Rock	Ukn - hf	n	N/A	10	open
OR	6024	43.63883	-123.824	165	744	0.2212	2.00E+05	Translational	880	gentle	sandstone/siltstone	Sand/Siltstone	Ukn - hf	n	N/A	8	confined
OR	6040	43.67926	-123.792	61	186	0.3277	2.00E+04	Trans and Rot	544	convex	basalt	Hard Rock	Ukn - hf	y	N/A	20	wall
OR	6048	43.69304	-123.733	52	208	0.2491	2.10E+04	Rotational	239	gentle	basalt	Hard Rock	Ukn - hf	n	N/A	15	open
OR	6094	43.68889	-123.765	116	340	0.3407	3.90E+04	Translational	266	concave	basalt	Hard Rock	Ukn - hf	n	N/A	25	confined
OR	6096	43.65529	-123.793	49	159	0.3067	2.80E+04	Rotational	463	gentle	basalt	Hard Rock	Ukn - hf	y	N/A	15	open
OR	6103	43.69088	-123.777	49	112	0.4354	7.30E+03	Translational	305	high	basalt	Hard Rock	Ukn - hf	n	N/A	25	open
OR	6120	43.66264	-123.81	17	65	0.2579	5.00E+03	Rotational	260	low	sandstone/siltstone	Sand/Siltstone	Ukn - hf	n	N/A	15	open
OR	6178	43.64626	-123.775	55	256	0.2143	2.80E+04	Rotational	141	gentle	basalt	Hard Rock	Ukn - hf	n	N/A	15	confined
OR	6179	43.64721	-123.776	18	113	0.1618	7.80E+03	Rotational	161	gentle	basalt	Hard Rock	Ukn - hf	n	N/A	10	open
OR	6258	43.65998	-123.744	11	73	0.1461	5.70E+03	Translational	310	low	basalt	Hard Rock	Ukn - hf	n	N/A	15	open
OR	6259	43.66051	-123.742	9	45	0.2032	2.20E+03	Translational	204	low	basalt	Hard Rock	lf	n	N/A	10	confined

Table B-2: Continued.

OR	6262	43.6614	-123.739	14	73	0.1879	4.70E+03	Translational	117	low	basalt	Hard Rock	Ukn - hf	n	N/A	20	open
OR	6303	43.69552	-123.733	15	33	0.4618	7.70E+02	Rotational	28	low	basalt	Hard Rock	Ukn - hf	n	N/A	25	open
OR	6393	43.63487	-123.818	73	407	0.1797	6.60E+04	Rotational	499	gentle	sandstone/siltstone	Sand/Siltstone	Ukn - hf	n	N/A	15	confined
OR	6401	43.67058	-123.76	46	142	0.322	2.40E+04	Rotational	65	low	sandstone/siltstone	Sand/Siltstone	Ukn - hf	n	N/A	15	wall
OR	6409	43.64273	-123.754	113	301	0.3747	1.70E+04	Trans and Rot	310	convex	basalt	Hard Rock	Ukn - hf	n	N/A	25	open
OR	6438	43.65089	-123.842	50	115	0.4373	1.50E+04	Rotational	141	low	sandstone/siltstone	Sand/Siltstone	Ukn - hf	n	N/A	30	open
OR	6445	43.68407	-123.836	30	177	0.1722	6.70E+03	Rotational	32	concave	sandstone/siltstone	Sand/Siltstone	Ukn - hf	n	N/A	15	confined
OR	6466	43.63678	-123.811	73	372	0.1966	1.50E+05	Rotational	429	gentle	basalt	Hard Rock	Ukn - hf	n	N/A	15	open
OR	6479	43.67624	-123.789	15	35	0.4354	5.60E+02	Rotational	7	concave	basalt	Hard Rock	Ukn - hf	n	N/A	25	wall
OR	6487	43.65726	-123.8	43	221	0.1931	2.30E+04	Translational	141	low	basalt	Hard Rock	Ukn - hf	n	N/A	15	wall
OR	6515	43.63926	-123.764	43	96	0.4445	6.00E+03	Translational	67	convex	basalt	Hard Rock	Ukn - hf	n	N/A	25	wall
OR	6516	43.64087	-123.764	37	87	0.4204	5.30E+03	Translational	39	convex	basalt	Hard Rock	Ukn - hf	n	N/A	30	wall
OR	6525	43.6707	-123.749	27	68	0.4034	3.00E+03	Translational	50	low	sandstone/siltstone	Sand/Siltstone	Ukn - hf	n	N/A	25	wall
OR	6526	43.66981	-123.759	98	226	0.4316	3.40E+04	Translational	66	convex	sandstone/siltstone	Sand/Siltstone	Ukn - hf	n	N/A	25	wall
OR	6534	43.69186	-123.754	9	33	0.2771	8.40E+02	Translational	21	low	basalt	Hard Rock	Ukn - hf	n	N/A	15	open
OR	6535	43.6925	-123.755	9	28	0.3266	1.20E+03	Rotational	8	low	basalt	Hard Rock	Ukn - hf	n	N/A	20	wall
OR	6543	43.65311	-123.737	8	38	0.2005	7.30E+02	Rotational	425	concave	basalt	Hard Rock	Ukn - hf	n	N/A	10	confined
OR	6552	43.71239	-123.719	27	90	0.3048	6.60E+03	Rotational	53	low	Qal	Granular	Ukn - hf	n	N/A	20	wall
OR	6553	43.7136	-123.719	21	72	0.2963	7.00E+03	Rotational	50	low	Qal	Granular	Ukn - hf	n	N/A	20	wall
OR	6566	43.65455	-123.819	6	36	0.1693	1.30E+03	Rotational	176	low	basalt	Hard Rock	Ukn - hf	n	N/A	10	open
OR	6567	43.65538	-123.821	18	78	0.2345	6.90E+03	Rotational	189	low	sandstone/siltstone	Sand/Siltstone	Ukn - hf	n	N/A	15	open
OR	6581	43.65568	-123.857	73	138	0.5301	1.30E+04	Rotational	106	low	sandstone/siltstone	Sand/Siltstone	Ukn - hf	n	N/A	30	wall
OR	6586	43.65586	-123.871	35	44	0.7966	8.40E+02	Translational	71	low	sandstone/siltstone	Sand/Siltstone	Ukn - hf	n	N/A	40	open
OR	6588	43.64335	-123.753	88	241	0.3668	2.30E+04	Translational	231	convex	basalt	Hard Rock	Ukn - hf	n	N/A	20	confined
OR	6593	43.66185	-123.738	9	56	0.1633	3.30E+03	Translational	91	low	basalt	Hard Rock	Ukn - hf	n	N/A	15	open
OR	6598	43.84332	-123.571	43	126	0.3387	2.00E+04	Rotational	64	low	sandstone/siltstone	Sand/Siltstone	Ukn - hf	n	N/A	20	wall
OR	6667	43.83847	-123.671	85	201	0.4246	3.40E+04	Translational	136	gentle	sandstone/siltstone	Sand/Siltstone	Ukn - hf	n	N/A	25	wall
OR	6707	43.85645	-123.643	110	304	0.3609	7.30E+04	Rotational	131	concave	sandstone/siltstone	Sand/Siltstone	Ukn - hf	n	N/A	25	wall
OR	6749	43.82436	-123.605	61	159	0.3834	1.60E+04	Rotational	80	low	sandstone/siltstone	Sand/Siltstone	Ukn - hf	n	N/A	30	wall
OR	6753	43.80039	-123.592	158	643	0.2465	2.10E+05	Rotational	170	concave	sandstone/siltstone	Sand/Siltstone	Ukn - hf	n	N/A	20	confined
OR	6788	43.826	-123.583	61	196	0.311	4.70E+04	Rotational	63	low	sandstone/siltstone	Sand/Siltstone	Ukn - hf	y	N/A	15	open
OR	6792	43.81974	-123.585	61	229	0.2662	5.10E+04	Rotational	148	low	sandstone/siltstone	Sand/Siltstone	Ukn - hf	n	N/A	20	open
OR	6921	43.83174	-123.853	55	135	0.4064	8.80E+03	Rotational	169	convex	sandstone/siltstone	Sand/Siltstone	Ukn - hf	n	N/A	20	open
OR	6949	43.77315	-123.861	27	211	0.13	3.10E+04	Trans and Rot	115	low	sandstone/siltstone	Sand/Siltstone	Ukn - hf	n	N/A	10	open
OR	6959	43.82195	-123.863	110	221	0.4965	1.90E+04	Rotational	307	convex	sandstone/siltstone	Sand/Siltstone	Ukn - hf	n	N/A	30	open
OR	6965	43.78227	-123.867	37	144	0.254	2.00E+04	Rotational	75	low	sandstone/siltstone	Sand/Siltstone	Ukn - hf	n	N/A	15	open
OR	7177	43.71985	-123.804	34	236	0.1421	2.50E+04	Rotational	83	low	sandstone/siltstone	Sand/Siltstone	Ukn - hf	n	N/A	10	open
OR	7183	43.73158	-123.819	113	429	0.2629	1.10E+05	Rotational	131	gentle	sandstone/siltstone	Sand/Siltstone	Ukn - hf	n	N/A	15	open
OR	7184	43.7181	-123.798	73	253	0.2891	4.50E+04	Rotational	87	gentle	basalt	Hard Rock	Ukn - hf	n	N/A	20	open

Table B-2: Continued.

OR	7259	43.71786	-123.801	34	171	0.1961	3.20E+04	Rotational	101	low	basalt	Hard Rock	Ukn - hf	n	N/A	15	open
OR	7272	43.75848	-123.907	55	163	0.3366	8.00E+03	Translational	247	gentle	sandstone/siltstone	Sand/Siltstone	Ukn - hf	n	N/A	20	confined
OR	7352	43.70965	-123.798	61	268	0.2275	2.30E+04	Trans and Rot	420	convex	basalt	Hard Rock	Ukn - hf	y	N/A	15	wall
OR	7360	43.71626	-123.8	12	73	0.167	4.70E+03	Trans and Rot	36	low	basalt	Hard Rock	Ukn - hf	y	N/A	10	open
OR	7383	43.72985	-123.814	18	59	0.31	2.20E+03	Rotational	24	low	sandstone/siltstone	Sand/Siltstone	Ukn - hf	y	N/A	15	wall
OR	7390	43.72975	-123.808	30	105	0.2903	2.40E+03	Rotational	308	gentle	sandstone/siltstone	Sand/Siltstone	Ukn - hf	n	N/A	15	open
OR	7411	43.7478	-123.823	37	168	0.2177	1.70E+04	Trans and Rot	111	low	sandstone/siltstone	Sand/Siltstone	Ukn - hf	n	N/A	15	open
OR	7412	43.74742	-123.822	37	131	0.2792	4.10E+03	Rotational	76	low	sandstone/siltstone	Sand/Siltstone	Ukn - hf	n	N/A	20	open
OR	7426	43.73628	-123.801	27	110	0.2494	2.90E+04	Rotational	37	convex	sandstone/siltstone	Sand/Siltstone	Ukn - hf	n	N/A	15	confined
OR	7428	43.74564	-123.794	37	177	0.2066	5.80E+03	Trans and Rot	103	low	sandstone/siltstone	Sand/Siltstone	Ukn - hf	y	N/A	15	open
OR	7449	43.75	-123.792	37	273	0.134	6.30E+04	Rotational	81	low	sandstone/siltstone	Sand/Siltstone	Ukn - hf	y	N/A	8	confined
OR	7585	43.53243	-123.831	101	437	0.2302	1.20E+05	Translational	193	gentle	sandstone/siltstone	Sand/Siltstone	Ukn - hf	n	N/A	15	open
OR	7612	43.54383	-123.665	62	115	0.5433	1.10E+04	Translational	63	gentle	sandstone/siltstone	Sand/Siltstone	Ukn - hf	n	N/A	30	wall
OR	7750	43.56148	-123.737	18	81	0.2258	3.20E+03	Translational	387	high	basalt	Hard Rock	Ukn - hf	n	N/A	15	open
OR	7760	43.55835	-123.782	55	250	0.2195	2.50E+04	Translational	653	gentle	basalt	Hard Rock	Ukn - hf	n	N/A	20	confined
OR	7837	43.57197	-123.751	79	230	0.3446	1.90E+04	Translational	328	concave	basalt	Hard Rock	Ukn - hf	n	N/A	25	confined
OR	7915	43.60782	-123.877	219	609	0.3604	2.50E+05	Trans and Rot	323	convex	sandstone/siltstone	Sand/Siltstone	Ukn - hf	n	N/A	25	wall
OR	7916	43.61539	-123.864	85	184	0.4638	3.10E+04	Translational	151	gentle	sandstone/siltstone	Sand/Siltstone	lf	n	N/A	20	open
OR	7921	43.60568	-123.851	280	790	0.355	3.40E+05	Translational	603	convex	sandstone/siltstone	Sand/Siltstone	hf	n	N/A	20	wall
OR	8078	43.53511	-123.85	55	278	0.1974	3.50E+04	Translational	229	convex	basalt	Hard Rock	lf	n	N/A	10	open
OR	8105	43.53878	-123.806	116	319	0.3631	4.30E+04	Translational	731	high	basalt	Hard Rock	Ukn - hf	n	N/A	25	open
OR	8118	43.57017	-123.776	40	163	0.2431	1.90E+04	Translational	128	gentle	basalt	Hard Rock	Ukn - hf	n	N/A	20	open
OR	8146	43.58874	-123.755	49	118	0.4133	8.80E+03	Translational	540	gentle	basalt	Hard Rock	Ukn - hf	n	N/A	25	open
OR	8190	43.57882	-123.739	26	135	0.1919	1.60E+04	Translational	44	gentle	basalt	Hard Rock	Ukn - hf	n	N/A	15	wall
OR	8270	43.54395	-123.683	128	434	0.295	2.00E+05	Translational	240	convex	basalt	Hard Rock	Ukn - hf	n	N/A	25	wall
OR	8302	43.5773	-123.742	43	110	0.3879	6.10E+03	Translational	417	high	basalt	Hard Rock	Ukn - hf	n	N/A	20	open
OR	8304	43.58439	-123.717	67	162	0.4139	1.40E+04	Translational	300	convex	basalt	Hard Rock	Ukn - hf	n	N/A	25	confined
OR	8398	43.5543	-123.693	64	107	0.5982	8.60E+03	Translational	572	high	sandstone/siltstone	Sand/Siltstone	Ukn - hf	n	N/A	30	open
OR	8444	43.7971	-123.826	30	118	0.2583	2.70E+04	Translational	270	gentle	sandstone/siltstone	Sand/Siltstone	Ukn - hf	n	N/A	15	open
UN	4	39.51659	-111.212	18	70	0.2613	3.40E+03	Translational	44	concave	sandstone, siltstone and shale	Shale	b	n	N/A	15	wall
UN	80	39.52962	-111.088	17	75	0.2235	6.30E+03	Translational	474	high	mudstone, claystone, sandstone, and conglomerate	Shale	g	n	N/A	10	open
UN	97	39.61762	-111.089	37	120	0.3048	3.00E+03	Translational	365	convex	sandstone, siltstone and shale	Shale	b	n	N/A	20	open
UN	108	39.59281	-111.185	40	150	0.2642	5.80E+03	Translational	287	convex	sandstone, siltstone and shale	Shale	s	n	N/A	15	open

Table B-2: Continued.

UN	112	39.59033	-111.184	21	140	0.1524	4.00E+03	Translational	162	low	sandstone, siltstone and shale	Shale	g	y	N/A	9	confined
UN	114	39.60523	-111.175	15	80	0.1905	1.10E+03	Translational	503	concave	sandstone, siltstone and shale	Shale	lf	n	N/A	10	open
UN	116	39.57787	-111.173	98	330	0.2956	3.60E+04	Translational	195	gentle	sandstone, siltstone and shale	Shale	s	n	N/A	15	wall
UN	117	39.57708	-111.173	67	260	0.2579	7.70E+03	Translational	169	gentle	sandstone, siltstone and shale	Shale	s	n	N/A	15	wall
UN	118	39.57514	-111.176	101	380	0.2647	4.20E+04	Translational	224	convex	sandstone, siltstone and shale	Shale	s	n	N/A	25	wall
UN	119	39.57492	-111.177	73	320	0.2286	1.90E+04	Translational	170	convex	shale	Shale	s	n	N/A	15	wall
UN	121	39.5477	-111.137	8	40	0.1905	3.50E+03	Translational	15	low	sandstone, siltstone and shale	Shale	lf	n	N/A	15	wall
UN	122	39.54186	-111.136	12	45	0.2709	1.40E+03	Translational	28	low	sandstone, siltstone and shale	Shale	lf	n	N/A	15	wall
UN	127	39.57927	-111.122	12	60	0.2032	1.40E+03	Translational	480	high	sandstone, siltstone and shale	Shale	g	n	N/A	10	open
UN	129	39.59374	-111.127	18	60	0.3048	1.00E+03	Translational	409	high	sandstone, siltstone and shale	Shale	s	n	N/A	15	open
UN	133	39.53081	-111.193	49	190	0.2567	3.50E+03	Translational	247	concave	sandstone, siltstone and shale	Shale	g	n	N/A	15	open
UN	135	39.49949	-111.17	37	100	0.3658	2.00E+03	Translational	438	convex	sandstone, siltstone and shale	Shale	s	n	N/A	20	open
UN	141	39.50349	-111.172	24	60	0.4064	1.30E+03	Translational	124	low	sandstone, siltstone and shale	Shale	lf	n	N/A	20	confined
UN	144	39.50493	-111.173	6	25	0.2438	1.50E+03	Translational	10	low	sandstone, siltstone and shale	Shale	b	n	N/A	15	wall
UN	145	39.50602	-111.178	24	70	0.3483	1.20E+03	Translational	87	low	sandstone, siltstone and shale	Shale	s	n	N/A	20	open
UN	149	39.55223	-111.192	34	110	0.3048	2.90E+03	Translational	540	convex	sandstone, siltstone and shale	Shale	g	n	N/A	15	confined
UN	151	39.51941	-111.212	43	150	0.2845	2.50E+03	Translational	186	gentle	sandstone, siltstone and shale	Shale	lf	n	N/A	15	open
UN	153	39.50183	-111.16	30	80	0.381	1.30E+03	Translational	107	convex	sandstone, siltstone and shale	Shale	b	n	N/A	35	open
UN	154	39.57894	-111.17	15	140	0.1089	3.10E+03	Translational	88	concave	shale	Shale	s	n	N/A	6	wall
UN	156	39.54188	-111.14	37	110	0.3325	1.40E+03	Translational	243	convex	sandstone, siltstone and shale	Shale	s	n	N/A	20	open

Table B-2: Continued.

UN	157	39.57887	-111.181	40	130	0.3048	5.90E+03	Translational	451	gentle	sandstone, siltstone and shale	Shale	lf	n	N/A	15	confined
UN	158	39.51321	-111.112	9	55	0.1663	1.10E+03	Translational	51	concave	conglomerate, sandstone, minor shale	Shale	lf	n	N/A	10	wall
UN	161	39.54944	-111.158	37	120	0.3048	3.40E+03	Translational	330	convex	sandstone, siltstone and shale	Shale	lf	n	N/A	15	confined
UN	162	39.55121	-111.157	27	100	0.2743	1.90E+03	Translational	274	gentle	sandstone, siltstone and shale	Shale	lf	n	N/A	15	open
UN	164	39.54637	-111.157	18	60	0.3048	1.00E+03	Translational	703	convex	sandstone, siltstone and shale	Shale	lf	n	N/A	15	open
UN	167	39.56663	-111.175	37	110	0.3325	2.80E+03	Translational	306	gentle	sandstone, siltstone and shale	Shale	lf	n	N/A	20	confined
UN	168	39.61292	-111.13	9	40	0.2286	5.00E+02	Translational	340	concave	sandstone, siltstone and shale	Shale	lf	n	N/A	15	open
UN	174	39.52188	-111.203	67	180	0.3725	2.90E+03	Translational	153	convex	sandstone, siltstone and shale	Shale	lf	n	N/A	20	wall
UN	196	39.56082	-111.204	12	36	0.3387	6.70E+02	Translational	9	concave	sandstone, siltstone and shale	Shale	lf	n	N/A	25	wall
UN	197	39.56188	-111.199	49	170	0.2869	6.00E+03	Translational	282	gentle	sandstone, siltstone and shale	Shale	lf	n	N/A	15	open
UN	198	39.56211	-111.2	21	90	0.2371	1.70E+03	Translational	279	gentle	sandstone, siltstone and shale	Shale	lf	n	N/A	15	open
UN	199	39.5602	-111.201	21	100	0.2134	3.60E+03	Translational	44	concave	sandstone, siltstone and shale	Shale	lf	n	N/A	15	wall
UN	200	39.5679	-111.199	8	47	0.1621	2.50E+03	Translational	28	concave	sandstone, siltstone and shale	Shale	lf	n	N/A	15	open
US	203	39.11316	-111.477	256	870	0.29	1.10E+06	Translational	250	gentle	Qmw	Granular	g	n	s	35	open
US	205	39.11164	-111.482	18	340	0.05	4.40E+04	Translational	0	gentle	Qmw	Granular	g	y	d	10	open
US	207	39.09048	-111.459	201	1350	0.15	8.70E+05	Translational	447	gentle	Qmw	Granular	lf	y	d	10	wall
US	212	39.09345	-111.488	73	260	0.28	5.50E+04	Translational	136	gentle	limestone	Hard Rock	g	n	s	15	open
US	252	39.06352	-111.356	67	250	0.27	2.50E+04	Translational	96	gentle	Mudstone, claystone, sandstone, conglomerate	Shale	s	n	s	15	wall
US	268	39.09406	-111.464	219	1230	0.18	4.30E+05	Translational	706	gentle	Qmw	Granular	lf	y	d	10	open
US	323	39.10628	-111.471	73	140	0.52	4.00E+03	Translational	94	gentle	limestone	Hard Rock	g	n	m	35	open
US	331	39.11301	-111.407	15	90	0.17	1.00E+04	Translational	115	concave	Mudstone, claystone, sandstone, conglomerate	Shale	s	y	m	10	open

Table B-2: Continued.

US	413	39.11532	-111.43	98	290	0.34	2.50E+04	Translational	298	gentle	limestone	Hard Rock	g	n	s	20	confined
US	415	39.10095	-111.432	146	420	0.35	4.20E+04	Translational	606	convex	limestone	Hard Rock	lf	y	m	20	open
US	423	39.09939	-111.442	134	440	0.30	9.60E+04	Translational	743	high	limestone	Hard Rock	g	n	s	20	confined
US	434	39.08084	-111.447	52	360	0.14	2.20E+04	Translational	157	gentle	Qmw	Granular	lf	y	d	8	open
US	439	39.11329	-111.409	49	80	0.61	5.00E+03	Translational	247	concave	Mudstone, claystone, sandstone, conglomerate	Shale	b	n	s	30	open
US	505	39.10961	-111.377	110	650	0.17	1.50E+05	Translational	98	gentle	Qmw	Granular	lf	y	m	10	open
US	568	39.1514	-111.521	329	870	0.38	1.30E+05	Translational	1130	gentle	limestone	Hard Rock	g	n	s	20	open
US	607	39.12253	-111.61	110	390	0.28	1.00E+05	Translational	127	concave	Mudstone, claystone, sandstone, conglomerate	Shale	s	n	s	20	open
US	621	39.11071	-111.608	183	1030	0.18	5.10E+05	Translational	269	gentle	Mudstone, claystone, sandstone, conglomerate	Shale	s	n	s	10	wall
US	634	39.12098	-111.622	110	230	0.48	2.70E+04	Translational	229	gentle	Mudstone, claystone, sandstone, conglomerate	Shale	s	n	s	25	open
US	644	39.14818	-111.528	116	600	0.19	1.20E+05	Translational	348	gentle	Qmw	Granular	s	y	d	30	open
US	659	39.13952	-111.49	329	990	0.33	1.30E+05	Translational	674	gentle	Qmw	Granular	g	y	m	25	wall
US	731	39.08095	-111.629	98	210	0.46	1.30E+04	Translational	228	gentle	Mudstone, claystone, sandstone, conglomerate	Shale	s	n	s	25	confined
US	814	39.08911	-111.625	67	170	0.39	1.10E+04	Translational	196	gentle	Mudstone, claystone, sandstone, conglomerate	Shale	s	n	s	20	open
US	866	39.11467	-111.535	61	160	0.38	8.00E+03	Translational	394	gentle	Qmw	Granular	s	y	d	20	open
US	868	39.12819	-111.55	43	240	0.18	5.60E+04	Translational	172	concave	Mudstone, claystone, sandstone, conglomerate	Shale	s	n	s	10	open
US	871	39.12842	-111.537	61	380	0.16	5.10E+04	Translational	19	gentle	Qmw	Granular	s	y	d	10	open
US	872	39.13334	-111.537	98	560	0.17	8.10E+04	Translational	486	gentle	Qmw	Granular	s	y	d	10	open
US	1062	39.11398	-111.575	67	230	0.29	7.20E+04	Translational	551	gentle	conglomerate, sandstone with minor shale	Shale	s	n	d	20	open
US	1087	39.13045	-111.504	317	990	0.32	1.90E+05	Translational	956	high	limestone	Hard Rock	lf	n	s	35	open
US	1101	39.12602	-111.539	85	660	0.13	1.20E+05	Translational	372	gentle	Qmw	Granular	b	y	d	10	open
US	1116	39.13911	-111.634	305	990	0.31	1.60E+05	Translational	356	gentle	limestone	Hard Rock	s	n	s	35	confined

Table B-2: Continued.

US	1120	39.1669	-111.644	73	160	0.46	4.70E+04	Translational	707	gentle	limestone	Hard Rock	s	n	s	25	open
US	1132	39.19514	-111.642	107	170	0.63	1.20E+04	Translational	64	concave	Mudstone, claystone, sandstone, conglomerate	Shale	s	n	s	30	wall
US	1145	39.22053	-111.611	122	270	0.45	2.50E+04	Translational	269	gentle	Mudstone, claystone, sandstone, conglomerate	Shale	s	n	s	55	confined
US	1167	39.214	-111.585	134	300	0.45	1.10E+04	Translational	60	gentle	Mudstone, claystone, sandstone, conglomerate	Shale	s	n	s	25	confined
US	1189	39.18728	-111.587	207	390	0.53	2.00E+04	Translational	762	convex	limestone	Hard Rock	lf	n	s	40	confined
US	1254	39.21703	-111.53	165	340	0.48	2.00E+04	Translational	323	gentle	limestone	Hard Rock	g	n	s	25	confined
US	1266	39.21109	-111.509	58	140	0.41	3.00E+04	Translational	139	gentle	Qmw	Granular	g	y	d	20	open
US	1271	39.2068	-111.494	43	100	0.43	3.40E+03	Translational	42	concave	Qmw	Granular	g	y	d	25	wall
US	1288	39.20209	-111.526	61	71	0.86	3.40E+03	Translational	472	gentle	limestone	Hard Rock	g	n	s	40	open
US	1305	39.17781	-111.5	91	180	0.51	7.20E+03	Translational	308	gentle	Qmw	Granular	g	y	d	25	confined
US	1308	39.17245	-111.494	195	600	0.33	2.90E+04	Translational	89	gentle	Qmw	Granular	g	y	d	20	confined
US	1314	39.16539	-111.496	73	170	0.43	8.00E+03	Translational	450	convex	Qmw	Granular	lf	y	d	25	open
US	1329	39.17598	-111.513	219	460	0.48	3.90E+04	Translational	400	convex	limestone	Hard Rock	g	n	s	30	open
US	1337	39.21588	-111.539	241	480	0.50	2.60E+04	Translational	322	gentle	limestone	Hard Rock	g	n	s	30	wall
US	1439	39.19913	-111.523	183	290	0.63	2.50E+04	Translational	521	gentle	limestone	Hard Rock	g	n	s	40	open
US	1447	39.21668	-111.548	107	160	0.67	3.80E+03	Translational	440	gentle	limestone	Hard Rock	b	n	s	35	confined
US	1460	39.21538	-111.556	37	128	0.29	3.70E+03	Translational	474	gentle	Mudstone, claystone, sandstone, conglomerate	Shale	lf	n	s	25	open
US	1515	39.19111	-111.617	76	180	0.42	5.20E+03	Translational	128	gentle	limestone	Hard Rock	lf	n	s	25	open
US	1537	39.20558	-111.591	134	470	0.29	7.40E+04	Translational	157	concave	Mudstone, claystone, sandstone, conglomerate	Shale	s	y	m	25	confined
US	1572	39.17833	-111.499	73	130	0.56	4.30E+03	Translational	277	gentle	Qmw	Granular	s	y	d	25	open
US	1606	39.18945	-111.511	134	325	0.41	2.40E+04	Translational	300	convex	Qmw	Granular	g	y	d	20	open
WG		46.28113	-123.784	30	41	0.7434	1.20E+03	Translational	37	low	sandy silt	Granular	hf	n	N/A	20	open
WG		46.2828	-123.784	49	72	0.6773	3.00E+03	Translational	192	gentle	sandy silt	Granular	hf	n	N/A	20	open
WG		46.28095	-123.783	76	357	0.2134	3.00E+04	Tran or Rot	109	concave	sandy silt	Granular	lf	y	N/A	20	confined
WG		46.29082	-123.742	62	148	0.4222	1.10E+04	Tran or Rot	69	convex	silt	Granular	hf	n	N/A	25	open
WG		46.28212	-123.648	53	102	0.5229	6.90E+03	Tran or Rot	318	convex	sandy silt	Granular	lf	n	N/A	35	wall
WG		46.29638	-123.602	61	105	0.5806	9.60E+03	Tran or Rot	177	convex	silt	Granular	hf	n	N/A	20	wall
WG		46.29386	-123.596	91	120	0.762	2.00E+04	Tran or Rot	78	gentle	silt	Granular	hf	n	N/A	20	wall
WG		46.31101	-123.58	69	93	0.7374	2.20E+04	Tran or Rot	40	gentle	silt	Granular	hf	n	N/A	40	wall

Table B-2: Continued.

WG		46.32094	-123.731	61	324	0.1881	6.30E+04	Tran or Rot	172	gentle	sandy silt	Granular	hf	n	N/A	15	open
WG		46.31364	-123.651	38	118	0.3229	6.00E+03	Tran or Rot	82	concave	sandy silt	Granular	hf	n	N/A	25	wall
WG		46.32386	-123.598	61	281	0.2169	2.70E+04	Tran or Rot	466	concave	silt	Granular	hf	n	N/A	10	confined
WG		46.34347	-123.597	21	77	0.2771	5.00E+03	Tran or Rot	226	concave	silt	Granular	hf	n	N/A	15	open
WG		46.33907	-123.581	76	160	0.4763	9.80E+03	Tran or Rot	270	concave	silt	Granular	lf	n	N/A	30	confined
WG		46.34253	-123.56	94	339	0.2787	5.80E+04	Tran or Rot	219	concave	silt	Granular	hf	n	N/A	20	confined
WG		46.34319	-123.532	168	713	0.2351	2.40E+05	Tran or Rot	197	gentle	silt	Granular	hf	n	N/A	15	wall
WG		46.36077	-123.522	61	88	0.6927	5.60E+03	Tran or Rot	49	convex	silt	Granular	hf	n	N/A	40	wall
WG		46.35986	-123.486	30	115	0.265	6.60E+03	Tran or Rot	82	concave	silt	Granular	hf	n	N/A	15	wall
WG		46.38198	-123.586	82	275	0.2993	9.50E+04	Tran or Rot	133	concave	silt	Granular	hf	n	N/A	15	wall
WG		46.3926	-123.591	18	91	0.201	1.20E+04	Tran or Rot	56	gentle	sandy silt	Granular	hf	n	N/A	7	wall
WG		46.39598	-123.6	43	172	0.2481	1.00E+04	Tran or Rot	114	gentle	sandy silt	Granular	hf	n	N/A	10	open
WG		46.39513	-123.603	55	157	0.3495	1.00E+04	Tran or Rot	246	concave	silt	Granular	hf	n	N/A	25	open
WG		46.39593	-123.604	53	178	0.2997	1.60E+04	Tran or Rot	245	gentle	silt	Granular	hf	n	N/A	15	open
WG		46.39621	-123.606	49	155	0.3146	9.30E+03	Tran or Rot	287	gentle	silt	Granular	hf	n	N/A	20	open
WG		46.4066	-123.609	43	455	0.0938	6.30E+04	Tran or Rot	176	convex	sandy silt	Granular	hf	n	N/A	15	open
WG		46.40815	-123.61	27	121	0.2267	5.90E+03	Tran or Rot	65	gentle	sandy silt	Granular	hf	n	N/A	25	open
WG		46.40362	-123.581	37	125	0.2926	6.50E+03	Tran or Rot	222	concave	sandy silt	Granular	hf	n	N/A	20	wall
WG		46.40499	-123.586	30	113	0.2697	8.40E+03	Tran or Rot	561	concave	sandy silt	Granular	hf	n	N/A	15	open
WG		46.40915	-123.58	41	91	0.4522	5.00E+03	Tran or Rot	353	convex	sandy silt	Granular	hf	n	N/A	25	wall
WG		46.41824	-123.578	64	185	0.346	3.80E+04	Tran or Rot	155	convex	sandy silt	Granular	hf	n	N/A	25	open
WG		46.41799	-123.582	21	91	0.2345	7.50E+03	Tran or Rot	62	gentle	sandy silt	Granular	hf	n	N/A	20	open
WG		46.4211	-123.59	76	179	0.4257	1.60E+04	Tran or Rot	103	convex	sandy silt	Granular	hf	n	N/A	25	wall
WP		47.97459	-122.223	27	43	0.638	5.50E+03	Translational	226	gentle	clay,silt, fine sand	Clay	lf	n	N/A	45	open
WP		47.97364	-122.225	35	39	0.8988	3.20E+03	Translational	260	gentle	clay,silt, fine sand	Clay	hf	n	N/A	45	open
WP		47.9724	-122.226	38	102	0.3735	9.00E+03	Translational	17	concave	clay,silt, fine sand	Clay	lf	n	N/A	30	confined
WP		47.97166	-122.227	43	64	0.6668	2.70E+03	Translational	210	gentle	clay,silt, fine sand	Clay	lf	n	N/A	30	open
WP		47.97146	-122.227	27	28	0.9797	4.80E+02	Translational	111	gentle	clay,silt, fine sand	Clay	hf	n	N/A	40	open
WP		47.97128	-122.228	27	26	1.0551	4.60E+02	Translational	87	gentle	clay,silt, fine sand	Clay	hf	n	N/A	40	open
WP		47.96922	-122.229	30	82	0.3717	2.40E+03	Translational	63	concave	clay,silt, fine sand	Clay	hf	n	N/A	25	wall
WP		47.96678	-122.228	34	54	0.6209	9.40E+02	Translational	63	concave	gravelly sand	Granular	hf	n	N/A	50	open
WP		47.96481	-122.23	29	60	0.4826	8.30E+02	Translational	211	concave	diamicton	Clay	hf	n	N/A	30	open
WP		47.969	-122.232	41	43	0.9569	5.10E+02	Translational	65	convex	sand	Granular	hf	n	N/A	45	open
WP		47.96813	-122.232	11	53	0.2013	1.10E+03	Translational	110	concave	clay,silt, fine sand	Clay	hf	n	N/A	30	wall
WP		47.96802	-122.233	43	41	1.0408	5.20E+02	Translational	65	gentle	sand	Granular	hf	n	N/A	30	open
WP		47.96196	-122.243	27	44	0.6235	7.40E+02	Translational	66	gentle	clay,silt, fine sand	Clay	hf	n	N/A	50	open
WP		47.96176	-122.243	32	49	0.6531	7.00E+02	Translational	69	gentle	clay,silt, fine sand	Clay	hf	n	N/A	45	open
WP		47.9615	-122.244	35	51	0.6873	7.70E+02	Translational	68	gentle	clay,silt, fine sand	Clay	hf	n	N/A	40	open
WP		47.9569	-122.266	26	47	0.5512	1.20E+03	Translational	72	gentle	sand	Granular	hf	n	N/A	30	open

Table B-2: Continued.

WP		47.95624	-122.27	26	46	0.5632	6.40E+02	Translational	93	gentle	clay,silt, fine sand	Clay	hf	n	N/A	25	open
WP		47.95621	-122.27	37	74	0.4943	6.20E+03	Translational	102	gentle	clay,silt, fine sand	Clay	hf	n	N/A	30	open
WP		47.95509	-122.272	21	56	0.381	4.50E+03	Translational	58	concave	clay,silt, fine sand	Clay	hf	n	N/A	30	wall
WP		47.95433	-122.271	23	68	0.3362	1.50E+03	Translational	70	concave	clay,silt, fine sand	Clay	hf	n	N/A	25	wall
WP		47.95083	-122.284	27	65	0.422	5.10E+03	Translational	40	concave	clay,silt, sand, gravel	Clay	lf	n	N/A	20	wall
WP		47.94975	-122.283	14	41	0.3345	1.10E+03	Translational	35	concave	clay,silt, sand, gravel	Clay	lf	n	N/A	15	open
WP		47.94942	-122.283	12	35	0.3483	3.00E+02	Translational	25	concave	clay,silt, sand, gravel	Clay	hf	n	N/A	30	open
WP		47.95113	-122.287	23	40	0.5715	7.90E+02	Translational	53	concave	clay,silt, sand, gravel	Clay	hf	n	N/A	25	open
WP		47.93687	-122.31	56	80	0.7049	3.30E+03	Translational	91	gentle	clay,silt, fine sand	Clay	hf	n	N/A	45	open
WP		47.93563	-122.309	64	103	0.6214	5.50E+03	Translational	110	gentle	clay,silt, fine sand	Clay	hf	n	N/A	40	open
WP		47.93298	-122.309	41	76	0.5414	6.30E+03	Translational	83	gentle	sand	Granular	hf	n	N/A	35	open
WP		47.93138	-122.309	41	67	0.6141	1.20E+04	Translational	77	gentle	sand	Granular	hf	y	N/A	40	open
WP		47.92758	-122.309	27	75	0.3658	4.50E+03	Translational	86	gentle	sand	Granular	hf	n	N/A	25	open
WP		47.92692	-122.307	30	62	0.4916	3.20E+03	Translational	207	convex	diamicton	Clay	lf	n	N/A	25	open
WP		47.9266	-122.304	46	82	0.5576	2.20E+03	Translational	180	concave	diamicton	Clay	hf	n	N/A	50	wall
WP		47.92506	-122.308	96	138	0.6957	5.70E+03	Translational	150	gentle	clay,silt, fine sand	Clay	hf	n	N/A	50	open
WP		47.91739	-122.313	35	168	0.2086	1.00E+04	Translational	112	concave	gravelly sand	Granular	hf	y	N/A	25	wall
WP		47.91649	-122.311	38	99	0.3848	8.40E+03	Translational	62	concave	diamicton	Clay	hf	n	N/A	20	wall
WP		47.90918	-122.31	29	79	0.3665	1.80E+03	Translational	54	concave	sand	Granular	hf	n	N/A	20	wall
WP		47.90844	-122.311	23	77	0.2969	2.40E+03	Translational	42	concave	gravelly sand	Granular	hf	n	N/A	30	wall
WP		47.90009	-122.326	29	95	0.3048	3.00E+03	Translational	73	concave	sand	Granular	hf	n	N/A	40	open
WP		47.88724	-122.328	107	246	0.4337	1.40E+04	Translational	205	gentle	gravelly sand	Granular	hf	n	N/A	25	open
WP		47.87777	-122.328	34	61	0.5496	2.00E+03	Translational	273	convex	gravelly sand	Granular	hf	n	N/A	30	open
WP		47.88911	-122.329	32	92	0.3479	4.10E+03	Translational	79	gentle	sand	Granular	g	y	N/A	25	open